Study of magnetic oxyborates with ludwigite and hulsite structures

Cynthia Paola Contreras Medrano

Niterói

September 2017

C764 Contreras Medrano, Cynthia Paola.
Study of magnetic oxyborates with ludwigite and hulsite structures / Cynthia Paola Contreras Medrano ; orientador: Dalber Ruben Sanchez Candela. -- Niterói, 2017.
131 p. : il.

Tese (Doutorado) – Universidade Federal Fluminense, Instituto de Física, Niterói, 2017.
Bibliografia: p. 124-131.

1. LUDWIGITA. 2. HULSITA. 3. OXIBORATO. 4. MAGNETISMO. I. Sanchez Candela, Dalber Ruben, Orientador. II.Universidade Federal Fluminense. Instituto de Física, Instituição responsável. III.Título.

CDD 538.44

CYNTHIA PAOLA CONTRERAS MEDRANO

Study of magnetic oxyborates with ludwigite and hulsite structures

This dissertation is submitted to the graduate program in Physics of Universidade Federal Fluminense, in partial fulfilment of the requirements for the degree Doctor in Physics.

Advisor: Prof. Dalber R. Sánchez Candela

Niterói

September 2017

Acknowledgements

My sincere thanks to my advisor, Dalber R. S. Candela for his patience and dedication at work, for his concern with my academic and personal growth, and for his support and friendship.

To Mucio Continentino and Daniele Freitas, who made the leading research on the topic, for give me the opportunity to learn and discuss in many meetings different aspects of this work.

To Joao Carlos Fernandes for the guidance on the synthesis of the samples.

To Renato Guimarães and Daniele Freitas, for the advices and guidance at LDRX-UFF on powder x-ray measurements and refinements.

To Daniele Freitas, Jackson Resende, Carlos Pinheiro on the single crystal x-ray measurements and refinements. And, Maria Clara Ramalho for the introductory lecture.

To Daniele Freitas for the Neutron Diffraction Spectroscopy measurements and refinement presented on this dissertation.

To Elisa Baggio Saitovitch for give me the opportunity to measure different magnetic and thermodynamic properties with the Dynacool PPMS at CBPF.

To Mariella Alzamora for the ^{119}Sn Mössbauer Spectroscopy measurements at CBPF.

To Edson Passamani for the ac-susceptibility measurements of different systems.

To Rafael Garcia for the assistance on the magnetic measurements of the ludwigite $Ni_5Sn(O_2BO_3)_2$ at UFSCAR.

To Luis Ghivelder and Gabriel Eslava for the magnetic and thermodinamic measurements of the ludwigite $Co_5Sn(O_2BO_3)_2$.

To all the professors at IF-UFF for the lectures. Especially Mario Reis, for the different lectures on magnetism.

To Richard, Vanesa, Raquel, and Daniele for their support and sincere friendship. Richard and Vanesa special thanks for the happy and healthly environment, inside and outside the IF, especially during my pregnancy period.

To Giovana, Enrique and family in Peru for helping me and support my dream.

To my beloved Rosa Sofia, Evelyn and Carlos Enrique, for give me a home full of love and for brace me up during these years.

To the brazillian agencies CAPES and CNPq for the financial support.

Abstract

This dissertation presents the study of five oxyborates single crystals, being four with ludwigite structure: $Co_3O_2BO_3$, $Co_5Sn(O_2BO_3)_2$, $Co_{4.76}Al_{1.24}(O_2BO_3)_2$, and $Ni_5Sn(O_2BO_3)_2$, and one with hulsite structure: $Ni_{5.14}Sn_{0.86}(O_2BO_3)_2$. Those compounds have been synthesized and characterized by different techniques including x-ray diffraction, ac susceptibility, magnetization, Mössbauer spectroscopy, specific heat and neutron diffraction. The main results are:

1. Neutron diffraction studies in $Co_3O_2BO_3$ show a charge stability of Co^{3+} with low spin state (S=0) that confers to this compound a two-dimensional magnetic character.

2. Nonmagnetic dilution of $Co_3O_2BO_3$ with Sn and Al has shown an unexpected increase of the magnetic ordering temperature. This increase can be explained by the absence of double exchange interactions and by the presence of high spin Co^{2+} connecting magnetic layers. These compounds have shown unusual properties for oxyborates as magnetocaloric effect and metamagnetic transitions.

3. The ludwigite $Ni_5Sn(O_2BO_3)_2$ was synthesized for the first time. A partial ordering of the Ni^{2+} (S=1) take place at ~80 K, and at ~6 K a second magnetic order appear. These properties are completely different of that shown by their counterpart $Co_5Sn(O_2BO_3)_2$ (where the Co^{2+} are in the HS state with S=3/2) which shows only one transition of the whole system at 82 K. These results indicate that the spin size of the involved ions plays an essential role in determining the magnetic properties of ludwigites.

4. We synthesized a novel hulsite $Ni_{5.14}Sn_{0.86}(O_2BO_3)_2$ compound, and the results point to a complex magnetic behavior consistent with two magnetic subsystems. The subsystem formed by Ni ions located in a plane with a quadrangular arrangement (2–3 layer) order magnetically at 180 K (one of the highest magnetic transitions among the oxyborates). On the other hand, the other subsystem formed by Ni atoms located in a two-dimensional triangular lattice (1–4 layer) does not order at temperatures as low as 3 K indicating magnetic frustration. The experimental results suggest a spin liquid behavior for this subsystem. The two magnetic subsystems coexist at low temperatures.

Resumo

Nessa dissertação é apresentado o estudo de 5 oxiboratos, sendo 4 ludwigitas: $Co_3O_2BO_3$, $Co_5Sn(O_2BO_3)_2$, $Co_{4.76}Al_{1.24}(O_2BO_3)_2$, e $Ni_5Sn(O_2BO_3)_2$, e uma hulsita: $Ni_{5.14}Sn_{0.86}$ $(O_2BO_3)_2$. Esses compostos foram sintetizados e caracterizados com diferentes técnicas, incluindo a difração de raios X, susceptibilidade ac, magnetização, calor específico, espectroscopia Mössbauer e difração de nêutrons. Os principais resultados são:

1. Os estudos de difração de nêutrons em $Co_3O_2BO_3$ sugerem uma estado de baixo spin (S=0) para os íons de Co^{3+} conferindo um comportamento magnético bidimensional para este composto.

2. A diluição não magnética da ludwigita $Co_3O_2BO_3$ com Sn e Al mostraram um aumento inesperado da temperatura de ordenamento magnético. Isto pode ser explicado pela ausência de interações de dupla troca e pela presença de íons de Co^{2+} em estado de alto spin ligando camadas magnéticas e fortalecendo o magnetismo. Estes compostos mostraram também propriedades não usuais em oxiboratos como efeito magnetocalórico e transições metamagneticas.

3. A ludwigita $Ni_5Sn(O_2BO_3)_2$ foi sintetizado pela primeira vez. Um ordenamento magnético parcial dos íons de Ni^{2+} ($S = 1$) acontece a 80 K e em aproximadamente 6 K uma segunda ordem magnética parece acontecer. Estas propriedades são completamente diferentes daquelas mostradas pelo seu homólogo $Co_5Sn(O_2BO_3)_2$ (onde os ions de Co^{2+} estão no estado HS com $S = 3/2$) onde apenas uma transição magnética de todo o sistema acontece a 82 K. Estes resultados mostram

que o tamanho dos spins envolvidos desempenha um papel essencial nas propriedades magnéticas das ludwigitas.

4. A hulsita $Ni_{5.14}Sn_{0.86}(O_2BO_3)_2$ também foi sintetizada pela primeira vez e os resultados apontam para um comportamento magnético complexo consistente com dois subsistemas magnéticos. O subsistema formado por íons de Ni numa rede quadrangular bidimensional (camada 2–3) se ordena magneticamente a 180 K (uma das maiores temperaturas de transição magnética encontrada nos oxiboratos). Por outro lado, o outro subsistema é formado por íons de Ni localizados em uma rede triangular bidimensional (camada 1–4), não apresenta ordem magnética até temperaturas tão baixas quanto 3 K indicando uma possível frustração magnética. Os resultados experimentais sugerem também um comportamento tipo liquido quântico de spin para este subsistema. Os dois subsistemas coexistem a baixas temperaturas.

Summary

Tables list

Figures list

Chapter 1. General introduction

Borates are commonly minerals with complex chemistry and structure mainly due to the fact that boron is a small ion of trivalent nature, see Figure 1-1, which allows the formation of isolated chains, layers or multiple groups structures. Mineralogists have identified many minerals with boron, but most are rarely found in nature.

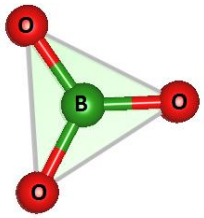

Figure 1-1: Scheme of the coordination of boron with three oxygens. This figure was generated by Vesta 3.1.1 software[1]

Anhydrous borates, where boron forms an orthoborate $(BO_3)^{-3}$ anionic groups, are called oxyborates. The oxyborates are characterized by their high structural anisotropy which is revealed by the morphology of the crystals that grow as needles or platelets. The name oxyborate is because they have one or two oxygen ions per chemical formula, which are not bounded to boron.

In recent years very interesting physical properties have been observed in the oxyborates with warwickite, ludwigite and hulsite structures. The chemical formulas associated with these structures are generally: $M^{2+}M'^{3+}OBO_3$ for warwickites and $M_2^{2+}M'^{3+}O_2BO_3$ for the ludwigites and $M_{6-x}^{2+}M'^{5+}_x(O_2BO_3)_2$ for hulsites, where M and M' represent metal ions, if M = M' the oxyborate is called homometallic, but if M≠ M' the oxyborate is called heterometallic. In those species the metal ions M and M 'are located at the center of the oxygen octahedron, as shown in Figure 1-2. These metallic ions are generally transition metals 3*d* which gives to them interesting physical properties such as: charge density and spin wave, disordered magnetic chains, coexistence of paramagnetism and magnetic order, charge ordering, unconventional magnetism, among others.

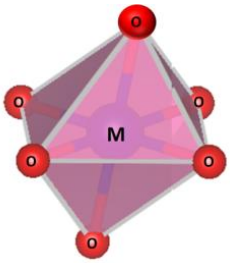

Figure 1-2: Schematic representation of the metal ion, blue sphere, in the center of the octahedron. Oxygen ions are represented by the red spheres. This figure was generated by Vesta 3.1.1 software[1].

In this way, oxyborates are known by their complex magnetic behavior related to low dimensional magnetic order, structural instabilities, and to the competition between three types of magnetic interactions: direct exchange, superexchange, and double exchange. In an effort to simplify the magnetic interactions and better understand the complex magnetic behavior in oxyborates type ludwigite and hulsite, we doped them with a nonmagnetic ion (Sn and Al). In this thesis we preferentially used the nonmagnetic Sn atom as a dopant because it is a Mössbauer probe and relevant local information on the magnetic state of the compound can be obtained. This study has shown that substitution of the $3d$ transition metal by nonmagnetic ions reduce the number of competing exchange interactions, giving place to unusual physical phenomena observed for the first time in these oxyborates.

In the next chapters are presented a study of each compound separately. This study was performed using experimental techniques such as x-ray diffraction, ac susceptibility, magnetization, specific heat, neutron diffraction and Mössbauer spectroscopy. The last two techniques gave relevant information about the local magnetic structure of these compounds.

In chapter 2 is studied the magnetic structure of the homometallic ludwigite $Co_3O_2BO_3$. The objective was to get information about the spin state and arrangement of the Co ions in $Co_3O_2BO_3$ through neutron powder diffraction (NPD) experiments and compare with that of the only other known homometallic ludwigite $Fe_3O_2BO_3$ so as to allow a better understanding of the origin of their different physical properties. The results show a charge stability of Co^{3+} with low spin state (S=0) that confers to $Co_3O_2BO_3$ a two-dimensional magnetic arrangement. These results are in contrast to the charge instability and one-dimensional magnetic order in $Fe_3O_2BO_3$.

In chapter 3 we studied the effect of the Sn doping in the magnetic properties of $Co_3O_2BO_3$. The objective was to reduce the magnetic frustration in $Co_3O_2BO_3$ by eliminating the double exchange interaction that competes with super exchange and direct exchange. This can be done through doping the $Co_3O_2BO_3$ with nonmagnetic Sn^{4+} which leads to the disappearance of the Co^{3+} ions. We verified the enhancement of the magnetism through Sn doping, rising the magnetic transition temperature from 42 K in $Co_3O_2BO_3$ to 82 K in $Co_5Sn(O_2BO_3)_2$.

In chapter 4 we studied the effect of the nonmagnetic Al doping in the magnetic properties of $Co_3O_2BO_3$. In addition to the increase of the magnetic ordering temperature from 42 K in $Co_3O_2BO_3$ to 57 K in $Co_{4.76}Al_{1.24}(O_2BO_3)2$, the compound shows unusual features for oxyborates as magnetocaloric and metamagnetic properties.

In chapter 5 we studied the structural and magnetic properties of the ludwigite $Ni_5Sn(O_2BO_3)_2$. The aim is to compare their magnetic properties with that of the previously studied $Co_5Sn(O_2BO_3)_2$. Due that both compounds have the same crystalline structure similar magnetic behaviors are expected. However, preliminary results shown a more complex magnetic behavior for $Ni_5Sn(O_2BO_3)_2$, with partial magnetic ordering at 80K and a second magnetic order at ~6 K..

In chapter 6 was studied the structural and magnetic properties of the hulsite $Ni_{5.14}Sn_{0.86}(O_2BO_3)_2$. This is the first time that a Mössbauer local probe was used to study this compound. The structure of the hulsite is formed by two planar substructures, one with a quadrangular arrangement of the Ni and the other with a triangular arrangement. From a geometrical point of view, if antiferromagnetic interactions are considered, a magnetic order is expected for the quadrangular arrangement while a magnetic frustration is expected for the triangular arrangement of the Ni atoms. We verified, combining macroscopic and local experimental techniques, the coexistence of two magnetic subsystems. The results show that one subsystem order magnetically at 180 K while the other subsystem do not order magnetically down to 3K, suggesting a quantum spin liquid (QSL) behavior.

In chapter 7 are presented the general and specific conclusions. Two short appendix topics are shown at the end of the thesis.

Chapter 2. Neutron powder diffraction study of Ludwigite $Co_3O_2BO_3$

This chapter presents results of neutron powder diffraction (NPD) studies that follow references [2] and [3]. A new perspective of the magnetic structure is presented.

2.1 Introduction

The ludwigites have a crystal structure with a space group *Pbam* (N°55), where $a \approx 9$ Å, $b \approx 12$ Å, $c \approx 3$ Å e $\alpha = \beta = \gamma = 90°$. The structure presents four nonequivalent crystallographic sites corresponding to the metallic ions located in the center of the oxygen octahedron. The metal ions are arranged to form zigzag walls that extend along the *c* axis, the walls are joined by boron ions in trigonal coordination with oxygen, so that each boron links 2 adjacent walls, see Figure 2-1.

A short distance between the metallic ions at sites 2 and 4 (approximately 2.8 Å) is characteristic of this structure (Figure 2-1). All other intermetallic distances are greater than 3 Å. The main physical properties observed in these materials are attributed to this short distance between sites 2 and 4, so the ludwigites are also represented by two substructures formed by triads of octahedra at the sites 4-2-4 and 3-1-3, respectively. The triads extend along the *c* axis and are called three-legged ladders (3LLs). This representation is shown in Figure 2-2.

There are only two known homometallic ludwigites in the literature, $Fe_3O_2BO_3$ and $Co_3O_2BO_3$. Both are represented by the same space group *Pbam* at room temperature with rather similar lattice parameters and contain one trivalent and two divalent ions per formula unit (f.u.). Moreover, the transition metals Co and Fe are neighbors in the periodic table, with comparable magnetic moments. However, in spite of all the similarities, the structural and magnetic properties of $Fe_3O_2BO_3$ and $Co_3O_2BO_3$ are different. Their properties will be presented to emphasize the differences between them.

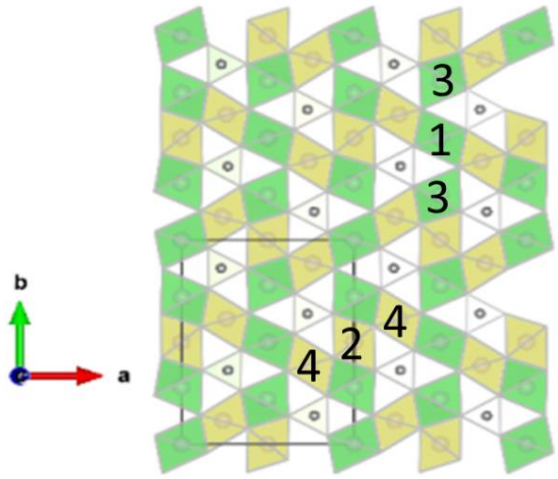

Figure 2-1: The schematic structure of the ludwigites projected along the *c* axis. The oxygen octahedra centered on the metal ions are shown. The numbers indicate nonequivalent crystallographic metallic sites and the vectors indicate the *a* and *b* axes of the unit cell. The subunits formed by the octahedra at sites 4-2-4 and 3-1-3 are emphasized by different colors. The boron ions (gray spheres) have trigonal coordination. This figure was generated by Vesta 3.1.1 software[1].

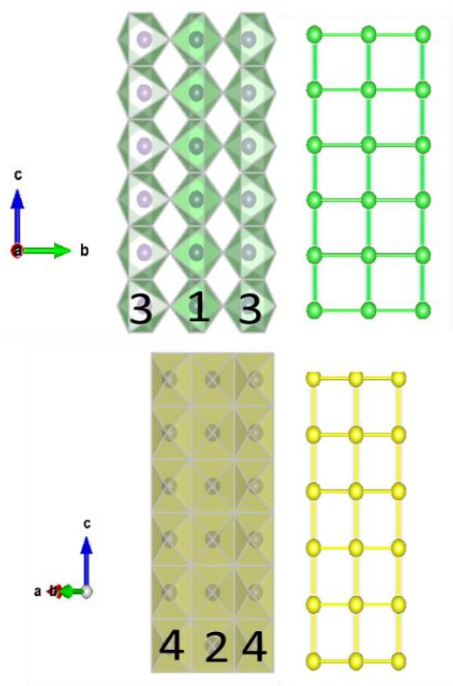

Figure 2-2: The schematic structure of the 3 leg ladders (3LLs) extended along the *c* axis. The 3LL formed by metallic sites 1 and 3 in green (top) and sites 2 and 4 in yellow (bottom). Intermetallic coordination (right) and inside oxygen octahedra (left).

The homometallic ludwigite $Fe_3O_2BO_3$ presents unconventional one dimensional (1D) structural and magnetic properties. For this reason, the three-dimensional (3D)

crystalline structure of the ludwigites is usually described by two one-dimensional (1D) substructures, see Figure 2-1 and Figure 2-2.

The $Fe_3O_2BO_3$ presents a 1D structural property related to $4-2-4$ ladder, which is responsible for charge density wave (CDW) observed below 283 K [4]. Figure 2-3 shows the schematic representations of the $4-2-4$ ladder above and below the CDW. The CDW produces a structural transition that double the *c* parameter of the unit cell. The new structure is represented by the space group *Pbnm*. In the CDW the distance between sites 2 and 4 become shorter or longer following a charge sharing process. For the shorter distance (2.62 Å) between site 2 and 4a, the charge sharing confers to them a 2.5 oxidation number. For the longer distance (2.94 Å) between site 2 and site 4b, the Fe ions on site 4b have the oxidation number 3. The position of shorter and longer distance is alternate along the ladder, giving rise to the duplication of the *c* parameter.

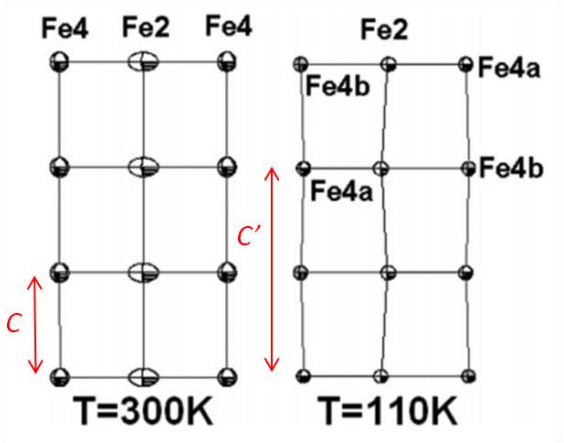

Figure 2-3: Schematic structure of the 4-2-4 ladder above and below 283 K [5].

The 1D magnetic properties of the ladders rely on the differentiated intralattice interactions and magnetic order temperature (Figure 2-4). Figure 2-4 left shows the magnetic structure at 82 K, where ladder 4-2-4 order in the *b* axis direction while ladder 3-1-3 remains paramagnetic. Figure 2-4 right shows the magnetic structure at 10 K, where ladder 3-1-3 gets order along the *a* axis direction and the whole structure order magnetically. The authors in reference [6] suggest that the 1D magnetic properties of this compound are evidence of weak magnetic interactions between the ladders with the prevalence of intraladder interactions. On the other hand,

magnetization measurements on oriented crystals determine that *a* axis is the easy axis of magnetization of this compound [6].

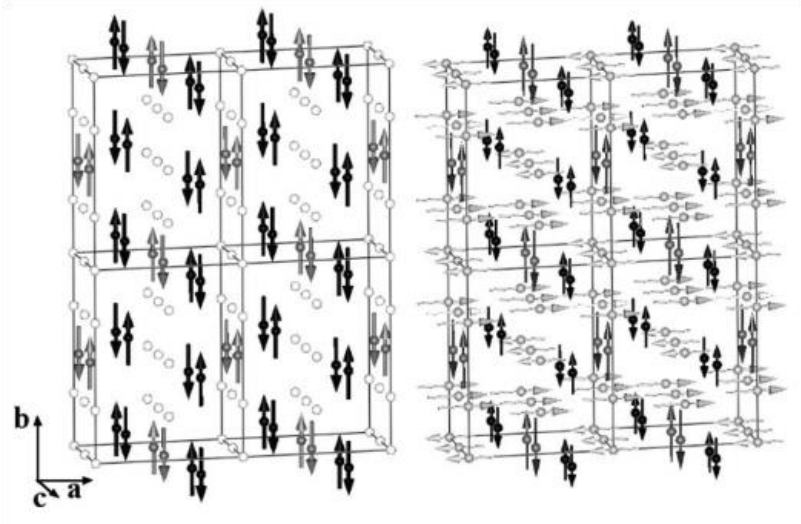

Figure 2-4: $Fe_3O_2BO_3$ magnetic structure at 82 K (left) and 10 K (right) [5]. Only the Fe atoms are shown. At 82 K: Fe1 and Fe3: white (no moment); Fe2: gray, Fe4a, Fe4b: black. At 10 K: Fe1 and Fe3: light gray; Fe2: dark gray, Fe4a, Fe4b: black [5].

On the other hand the homometallic ludwigite $Co_3O_2BO_3$ seemed to be a conventional compound, without signs of structural transitions or charge ordering. The calculus of the oxidation number in reference [7] indicates that site 4 is occupied by Co^{3+} and the other sites by Co^{2+} without charge sharing (at least down to 110 K) as in $Fe_3O_2BO_3$. The whole system get order at 42 K. Figure 2-5 (left) shows the low temperature magnetization of the $Co_3O_2BO_3$. The magnetization at 5 T is $\sim 45\ emu/g$ for $Co_3O_2BO_3$ [7], a large value when compared with the value of $\sim 4 emu/g$ for $Fe_3O_2BO_3$ [6, 8] (Figure 2-5, right) indicating that ferromagnetic interactions are more important in $Co_3O_2BO_3$ system [7]. Magnetization measurements on oriented crystals determine that *b* axis is the easy axis in $Co_3O_2BO_3$ [6, 9].

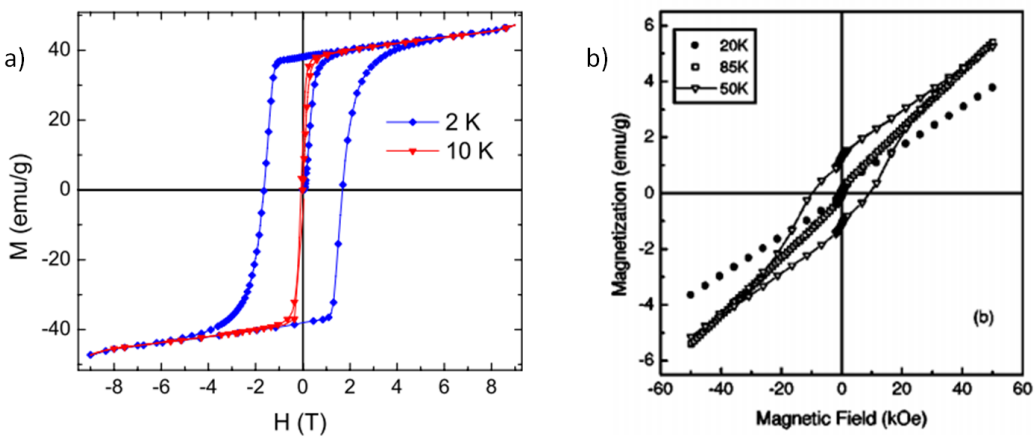

Figure 2-5: Low temperature hysteresis cycles for powder samples of $Co_3O_2BO_3$ (left) [7] and $Fe_3O_2BO_3$ (right) [8].

The unexpected different properties observed in $Co_3O_2BO_3$ and $Fe_3O_2BO_3$ homometallic ludwigites has motivated different studies on this two systems [5, 6]. We have summarized the main properties of $Co_3O_2BO_3$ and $Fe_3O_2BO_3$ in Table 2-1. It also motivated studies of ludwigites of $Co_3O_2BO_3$ doped with Fe ions, in an effort to identify why the bulk properties of these two homomentallic ludwigites are different [6, 9, 10, 11]. As an example we could mention a partial magnetic order on ludwigite $Co_2FeO_2BO_3$, the magnetic order of this compound is 117 K, close to the magnetic order temperature of the $Fe_3O_2BO_3$ than to the $Co_3O_2BO_3$, despite the fact that there are less Fe than Co atoms per formula unit. These results increase the interest to study these systems. Since the magnetic structure of $Co_3O_2BO_3$ remained unknown, neutron diffraction experiments were projected to better understand the magnetic properties of this compound and, in general, of the ludwigites.

Table 2-1: Summarized structural and magnetic properties of homometallic ludwigites.

Propriedade	**$Fe_3O_2BO_3$***	**$Co_3O_2BO_3$****
Ordenamento de carga	300 K	?
Transição estrutural	283 K	Não
Ordenamento magnético (T_N)	110 K, parcial 74 K, total	42 K
Eixo de fácil magnetização	*a*	*b*

2.2 NPD studies in $Co_3O_2BO_3$

2.2.1 Synthesis and previous characterizations

The syntheses of 3g of black-needle crystals of $Co_3O_2BO_3$ were performed at the Instituto de Física da Universidade Federal Fluminense (IF-UFF), following the recipe of reference [7]. X-ray powder diffraction and magnetic measurements confirmed the purity of the samples. Figure 2-6 shows the x-ray powder diffraction measurements performed at the Laboratório de Difração de Raios X (LDRX) at IF-UFF. Figure 2-7 shows the magnetic measurements, in units of μ_B/Co atom, the magnetic values are in agreement with previous measurements [6, 7]. The characterized samples were ground and sent to NPD experiments.

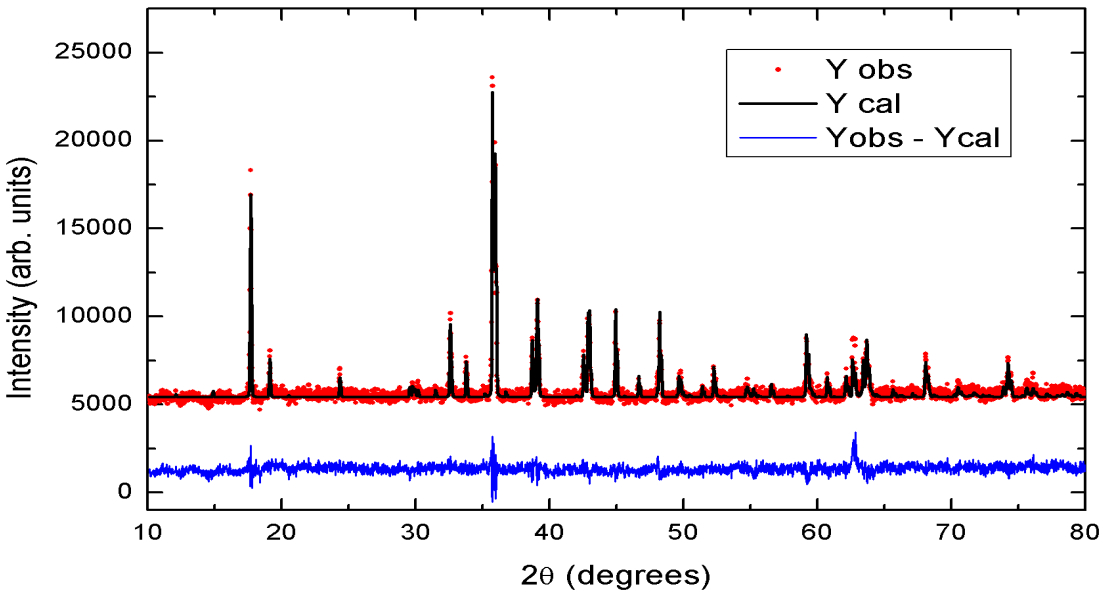

Figure 2-6: Rietveld fit with the *Pbam* space group to the room temperature x-ray diffraction data of $Co_3O_2BO_3$.

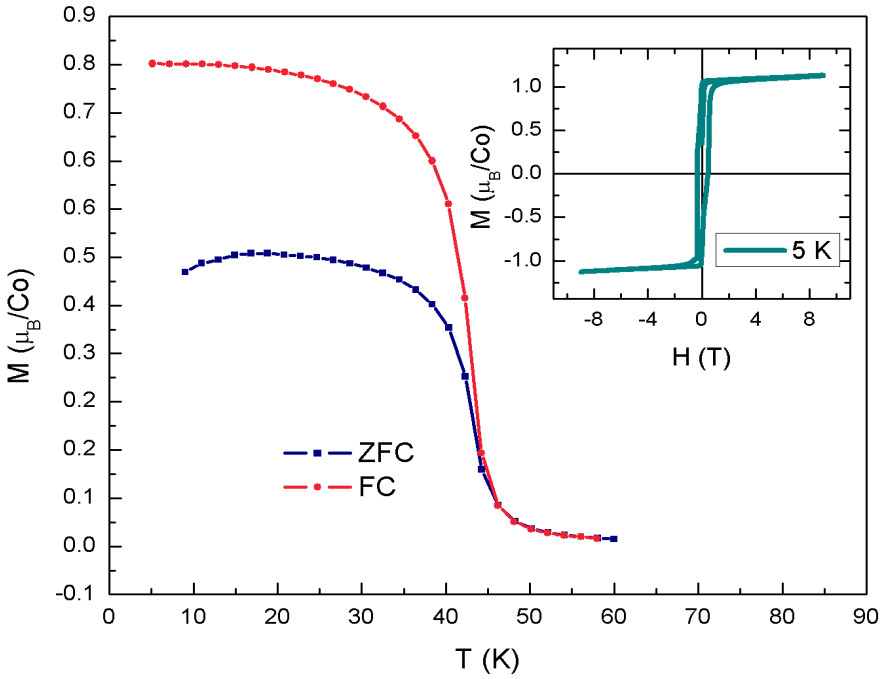

Figure 2-7: Magnetization versus temperature for powder sample of $Co_3O_2BO_3$ under an applied magnetic field of 1000 Oe. $Co_3O_2BO_3$ sample has a magnetic order at 42 K as in reference [7]. Inset: Hysteresis loop at 5K.

2.2.2 NPD experiments

NPD measurements were performed at the D1B instrument at Institut Laue-Langevin (ILL) in Grenoble by J. A. Rodríguez-Velamazan. The data were refined and analyzed by Daniele Freitas. Measurements and refinement details are in reference [2].

The magnetic transition at 42 K was confirmed and no structural transitions were observed. Table 2-2 shows the results of the magnetic refinements at 2K. The magnetic structure has the periodicity of one unit cell. Figure 2-8 shows the magnetic structure of $Co_3O_2BO_3$ represented with the two 3LL.

Table 2-2: $Co_3O_2BO_3$ magnetic moments at 2 K in μ_B units. M represents the modulus of the magnetic moment vector [2].

Atom (Wyckoff positions)	$M\,x$	$M\,y$	$M\,z$	M
Co4 (4*h*)	-0.5(1)	-0.1(1)	0	0.5
Co3 (4*g*)	1.7(1)	3.38(8)	0	3.8
Co2 (2*d*)	0.4(2)	3.06(9)	0	3.1
Co1 (2*a*)	1.2(1)	-3.4(1)	0	3.6

The magnetic moments of the majority of the Co ions are in agreement with high spin (HS) Co^{2+} (Table 2-2), however the moment of the Co^{3+} atom at site 4 is rather small suggesting a low spin (LS) state ($S = 0$) for the Co at this site. Figure 2-8 shows the magnetic structure of a unit cell according to Table 2-2. The moments on Co sites 1, 2 and 3 are nearly parallel to the b axis, with a ferromagnetic coupling along the c axis. The coupling of site 1 with sites 2 and 3 is antiferromagnetic, and between sites 2 and 3 is ferromagnetic. Then, there is a predominance of ferromagnetic couplings in this compound. This result is consistent with previous magnetic measurements as shown in Figure 2-7 and references [6, 7], in which a predominance of ferromagnetic couplings is observed.

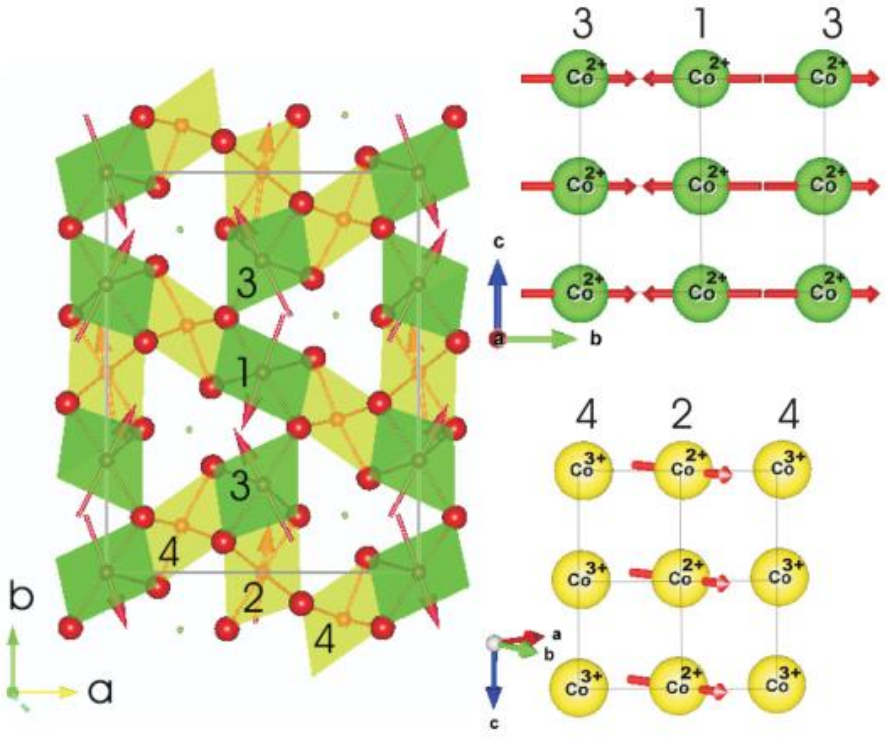

Figure 2-8: Magnetic structure proposed for $Co_3O_2BO_3$ by NPD. The two subunits in the form of 3LL are shown. The numbers indicate the crystallographic sites. Magnetic moments are ferromagnetically aligned along the c axis [2].

2.3 Discussion

The spin state of Co^{3+} ions in an octahedral environment is determined by a competition between intra-atomic exchange energy (Hund's rule) and crystal field energy [12, 13, 14]. The exchange energy favors the high spin (HS) state ($t_{2g}^4 e_g^2$, S = 2) while the crystal

field favors the low spin state (LS) ($t_{2g}^6 e_g^0$, $S = 0$). For Co^{3+} and Fe^{2+} very often these states are close in energy and include also the possibility of an intermediate spin state (IS) with the configuration ($t_{2g}^5 e_g^1$, $S = 1$). Among the Co oxides, $LaCoO_3$ and $GdCoO_3$ exhibit a thermal transition from low spin to high spin, probably with an intervening IS [12, 13, 15]. The Co_2O_3 exhibits a low spin to high spin transition with decreasing pressure [16].

The electron count in a rung of the 4-2-4 ladder corresponds to a background of three Co^{3+} ions with an extra *itinerant* electron per rung [4, 17]. The magnetic configuration obtained by neutrons implies a localization, or charge ordering, of this extra electron on site 2 of the rung, leaving two low spin Co^{3+} ions in the two outer sites 4 of the rung and a Co^{2+} on the center. Since site 2 is a symmetric site, this charge ordering is not necessarily accompanied by a structural transition as in the case of the Fe homometallic ludwigite.

We now compare the properties and magnetic structures of the two homometallic ludwigites after the neutron scattering experiments. First, the magnetic ordering in the $Co_3O_2BO_3$ is a single step phenomenon in which the magnetic moments in the two different ladders order simultaneously. This is in contrast to $Fe_3O_2BO_3$ where 4-2-4 ladders order at 110 K and the 3-1-3 ladders order at lower temperature (70 K). Concerning the magnetic structures, the moments in the ladders are coupled in different ways in the two compounds. In the $Fe_3O_2BO_3$ system the magnetic moments in a rung of the 4-2-4 ladders couple *ferromagnetically*, pointing along the *b* axis [5]. The coupling between the magnetic moments in consecutive rungs of these ladders along the *c* axis is *antiferromagnetic*. Notice that due to the staggered CDW ordering at ≈ 283 K one should distinguish between sites 4*a* and 4*b* in the 4-2-4 ladders of $Fe_3O_2BO_3$. However, the moments in these sites were found to be nearly the same [5]. $Co_3O_2BO_3$ has a ferromagnetic spin configuration in the rungs of the 4-2-4, but along the *c* axis the moments are ferromagnetically aligned. In $Fe_3O_2BO_3$, the magnetic moments in the 3-1-3 ladders have a ferrimagnetic coupling along a rung with the moments pointing into the *a* direction (see Figure 2-8). These in turn are ferromagnetically coupled along the *c* axis [5]. The $Co_3O_2BO_3$ has a ferrimagnetic configuration and the moments are all pointing almost into the *b* direction.

In both homometallic ludwigites, ferromagnetic ordering between the moments in a rung of the 4-2-4 ladders favors delocalization of this extra electron that gains kinetic energy. Since there is no structural transition in $Co_3O_2BO_3$, this delocalized electron could partially Kondo screen the moments in the rung of this ladder. This mechanism, however, is not sufficient to explain the small value of the magnetic moments found in the neutron experiments and especially why this occurs for the moments on sites 4 and not for that on site 2. Also in the oxyborates there are many competing magnetic interactions. The moments at site 4 are connected through different superexchange paths to several other magnetic ions in the structure. This results in conflicting information with a cost in energy for the system. A nonmagnetic, LS Co^{3+} occupying this site avoids the system to have to account for this energy cost.

In an effort to clarify the mechanism responsible for the coexistence of high and low spin states in the Co ludwigite, we calculated the Vzz component of the electric field gradient (EFG) on the different Co sites surrounded by oxygen octahedra. This parameter is a measure of the deviation of the environment from symmetric octahedra. Following Ivanova et al. [9] and taking the z axis along the main axis of the oxygen octahedra, we calculated Vzz for all the Co sites using the equation:

$$V_{zz} = \sum \frac{2e(3cos^2\theta - 1)}{r^3}$$

where e is the electron charge, θ is the angle between the main axis of the oxygen octahedron and the direction to the neighboring oxygen ion and r the distance to the oxygen atom. Table 2-3 shows the Vzz values for each Co site.

Table 2-3: Main component of the EFG for Co sites at different temperatures in units of e/Å.

	Site 1	Site 2	Site 3	Site 4
2K	0.384	0.166	0.138	0.014
30K	0.375	0.170	0.149	0.015
50K	0.267	0.151	0.230	0.031
300K	0.288	0.159	0.202	0.032

We find that site 4 has the smallest Vzz, showing that this is the most symmetric site in the compound. For lower temperatures the Vzz parameter for site 4 decreases, going from 0.0322 e/Å^3 at room temperature to 0.0145 e/Å^3 at 2 K, indicating that the oxygen octahedra surrounding site 4 become even more symmetric at low temperatures. It should be noted that in $LaCoO_3$, an archetypical compound with Co^{3+} ions in the LS state at low temperatures, Vzz = 0.00244 e/Å^3 at 5 K [15, 18]. In a more recent study of trivalent Co ions in sites with octahedral symmetry (Vzz = 0.0117 e/Å^3), Chen et al. [19] have shown a close relation between the spin states and the Co-O distances in the octahedra (see Figure 2-9).

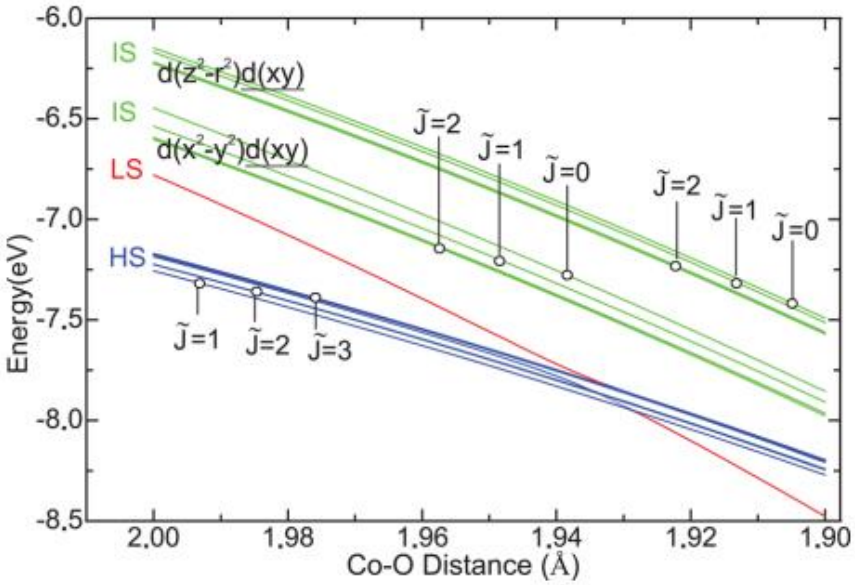

Figure 2-9: Energy level of a Co^{3+} in oxygen octahedra as a function of Co-O distance [19].

The intermediate spin (IS) states are always higher in energy, but the HS and LS states exchange stability at a distance of ~1.932 Å, the latter becoming more stable at shorter distances. As we can see in Figure 2-10, Co-O distances below this limit are observed only for site 4, yielding in this case a favorable condition for a low spin state. Notice that site 4 is the one with shorter weighted average distances.

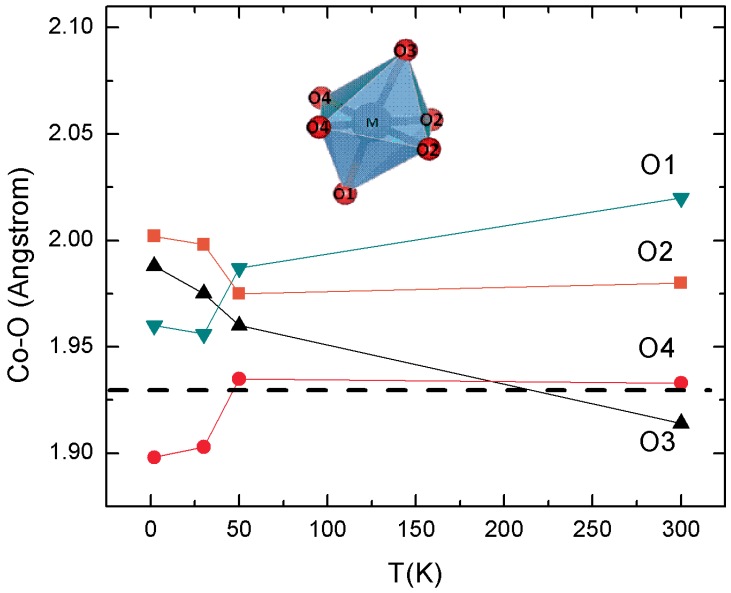

Figure 2-10: Co-O distances of the octahedra in site 4 of $Co_3O_2BO_3$ obtained by NPD measurements. The dashed line shows the threshold distance obtained for a CoO_6 cluster by Chen at al. [19], where HS and LS exchange instability.

To better understand the magnetic properties shown it is appropriate to view this compound as consisting of magnetic planes separated by nonmagnetic ions. The magnetic plane is parallel to b–c plane and formed by rectangular coordination between sites 1 and 3 ($d_{1-3} = 3.33$ Å) and triangular coordination between sites 2 and 3 ($d_{2-3} = 3.03$ Å) (see Figure 2-12 and Figure 2-13). These layers are separated by the (nonmagnetic) LS Co^{3+} at sites 4.

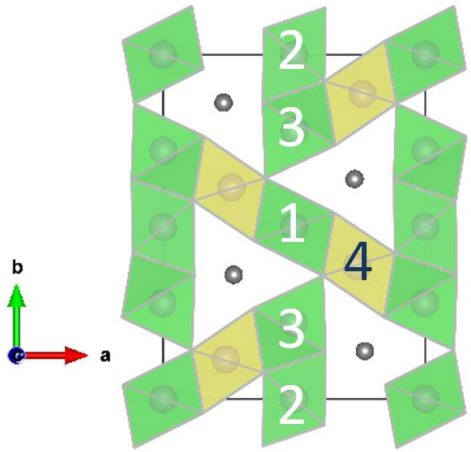

Figure 2-11: Schematic structure of $Co_3O_2BO_3$ showing the magnetic sites obtained by NPD in green and the nonmagnetic site in yellow. The gray circles represent the boron atoms.

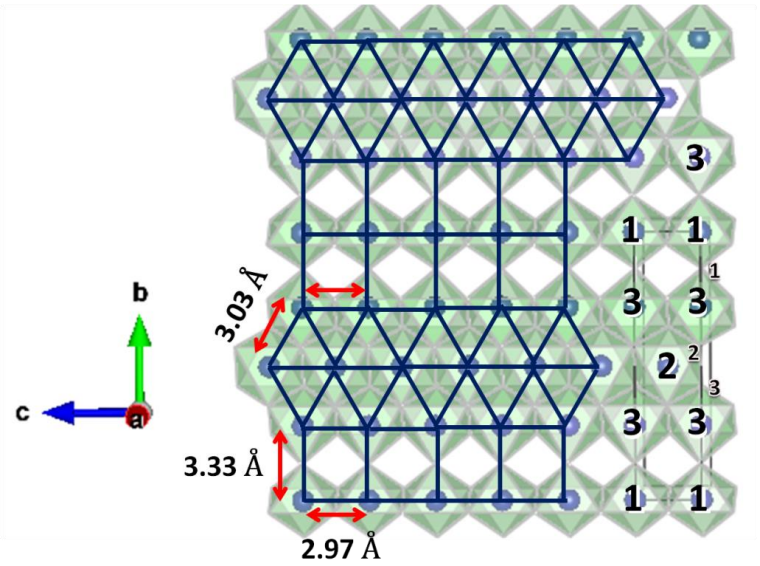

Figure 2-12: Schematic structure of the plane formed by magnetic sites 1, 2 and 3 parallel to *b* and *c* axis. Numbers indicate the metallic sites of Co ions. Black lines enclose the unitary cell. Blue lines show the intermetallic coordinations. Sites 2 and 3 have triangular coordinations and sites 1 and 3 rectangular coordination. The arrows show intermetallic distances.

In this way we can see that the magnetic structure in the *b*–*c* plane is formed by ferromagnetic regions (Co moments at sites 2 and 3) separated by Co moments at sites 1 coupled antiferromagnetically (see Figure 2-13). Then, the singularly small magnetic moment of the Co^{3+} at site 4, confers to $Co_3O_2BO_3$ a 2D magnetic character rather than a 1D as displayed by $Fe_3O_2BO_3$.

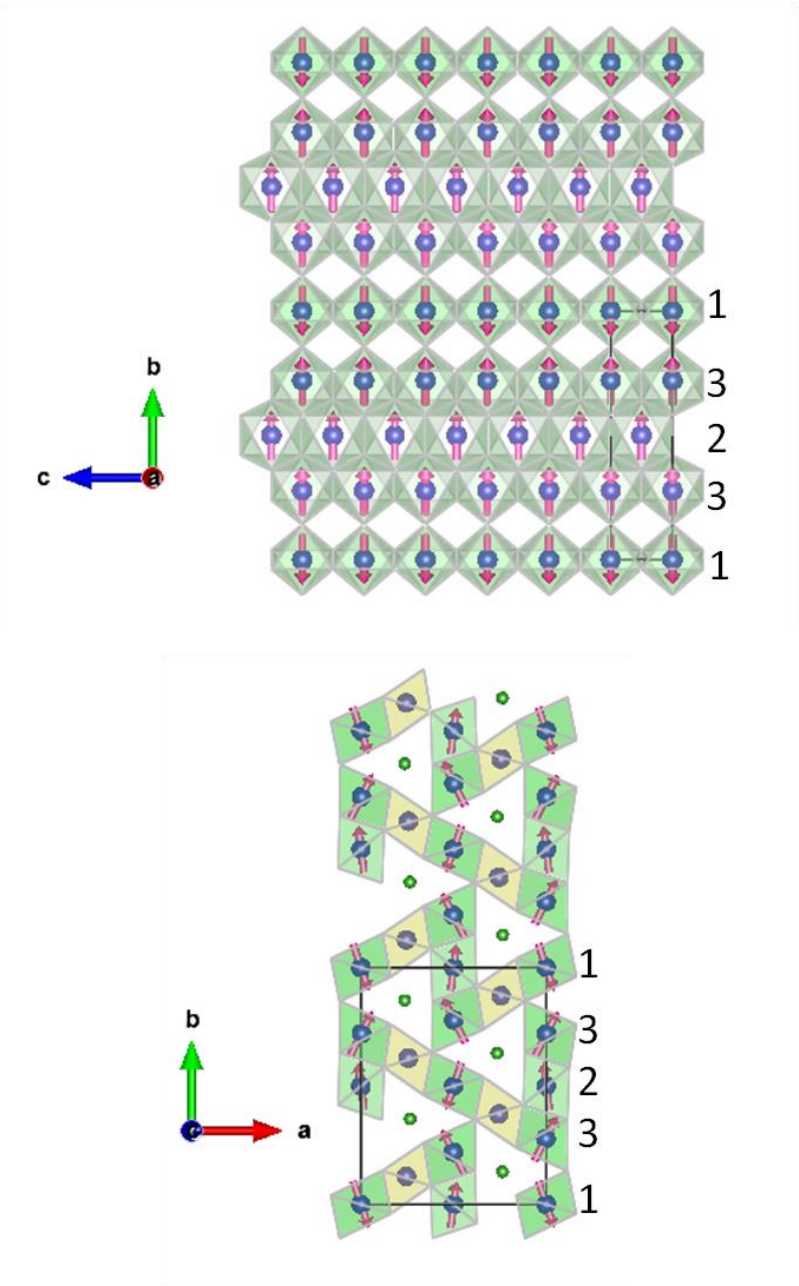

Figure 2-13: Magnetic structure of $Co_3O_2BO_3$, oxygen octahedra of sites 1, 2 and 3 in green, site 4 in yellow. Boron represented by little green circles. A black line enclose a unit cell. Top, layer formed by sites 1, 2 and 3, in which each site form a line along the *c* axis. Bottom, projection on the *ab* plane.

Two dimensional (2D) antiferromagnetic structures usually show a T^2 dependence on the low-temperature specific heat related to two-dimensional magnons, as seen in the hulsite $Co_5Sb(O_2BO_3)_2$, an oxyborate with a 2D structure. Revisiting the low-temperature specific heat of $Co_3O_2BO_3$, a fit including a T^2 dependence could be done on data of reference [7]. It shows a predominance of the T^2 dependence (see Figure 2-14).

This result should be analyzed together with the results shown by the other ludwigites studied until now.

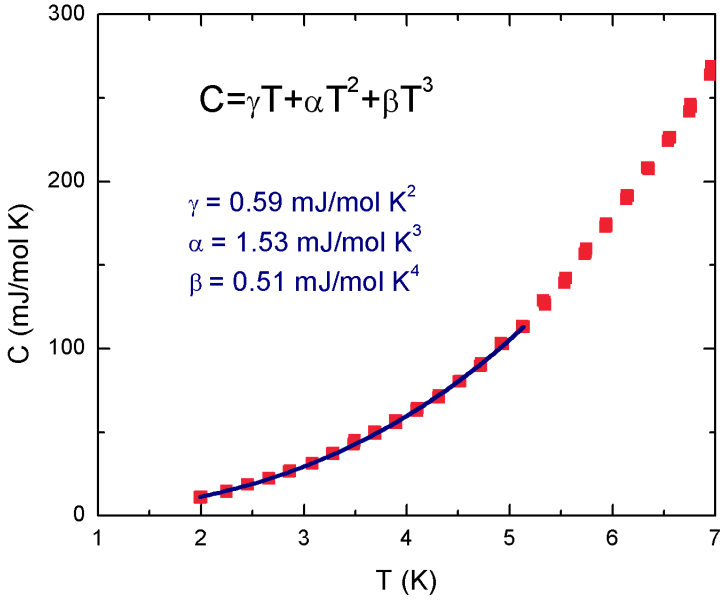

Figure 2-14: Fitting of the low-temperature specific heat of $Co_3O_2BO_3$ with the equation $C = \gamma T + \alpha T^2 + \beta T^3$. The T^2 term is dominant.

Another thing that called our attention is the fact that sites 2 and 3 are forming a two dimensional triangular network (Figure 2-12) that could give place to geometric frustration if antiferromagnetic interactions are considered. As we will see in chapter 4, geometric frustration seems to play an important role in the magnetic properties shown by $Co_5Al(O_2BO_3)_2$.

Chapter 3. Structural and magnetic properties of ludwigite $Co_5Sn(O_2BO_3)_2$

The content of this chapter is largely the same in reference [20].

3.1 Introduction

Nonmagnetic doping of Co ludwigite has been done with the purpose of get more information about the mechanisms involved in the magnetic properties shown by the ludwigites. The first Co ludwigite diluted with a nonmagnetic ion was the $Co_5Ti(O_2BO_3)_2$ [21]. Magnetic and thermodynamic properties were studied in this compound. The $Co_5Ti(O_2BO_3)_2$ do not show long-range magnetic order at low temperatures, instead a spin-glass state is established at 19 K. The Curie-Weiss temperature of the ludwigite $Co_5Ti(O_2BO_3)_2$ is $\theta_{cw} = -1.4$ K. The real part of the ac susceptibility show a wide peak that moves to higher temperatures as the frequency of the applied magnetic field increases (see Figure 3-1 – a). In the specific heat measurements no peaks were observed at this temperature, indicating the absence of phase magnetic transitions (see Figure 3-1 – c).

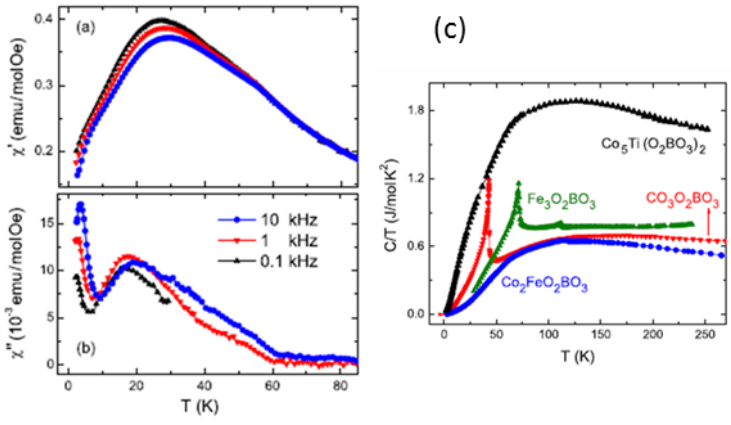

Figure 3-1: Magnetic and specific heat measurements of ludwigite $Co_5Ti(O_2BO_3)_2$. (a) real part of the ac susceptibility, (b) imaginary part of the susceptibility, (c) specific heat measurements of different ludwigites, (d) M (H) measurements [21].

The next nonmagnetic diluted Co ludwigite studied was the $CoMgGaO_2BO_3$ [22]. In this case the purpose was to introduce nonmagnetic ions into each crystallographic site. The authors proposed that all Co^{3+} ions were replaced by Ga^{3+} ions and part of the Co^{2+} ions replaced by Mg^{2+} ions leaving the remaining Co with a configuration d^7 and spin S = 3/2. On the other hand, the results of the X-ray measurements and the metal occupancies in each crystallographic site were not shown. The authors proposed a spin-glass ground state for this ludwigite. The peak of the ac susceptibility varies with frequency, characteristic of a spin-glass state.

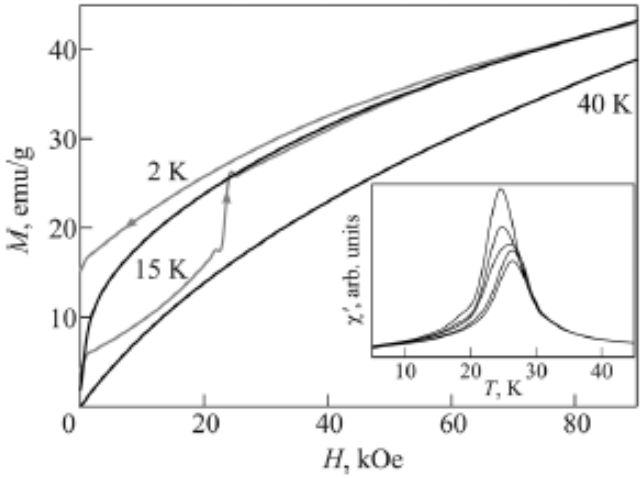

Figure 3-2: Magnetization as a function of temperature for powder sample of $CoMgGaO_2BO_3$. Inset: Real part of the ac susceptibility [22].

The last Co ludwigite doped with nonmagnetic ions studied was the $Co_{2.4}Ga_{0.6}O_2BO_3$ [23]. In this case, Ga ions enter in sites 4 and 2 occupying 54% and 15.5% of each site respectively. The introduction of Ga in the structure weakens the magnetic interactions, reducing the magnetic transition temperature to 37 K.

The study of $Co_5Ti(O_2BO_3)_2$ [21], $CoMgGaO_2BO_3$ [22] and $Co_{2.4}Ga_{0.6}O_2BO_3$ [23] showed that the nonmagnetic ions substitutes Co atoms in two or more crystallographic sites weakens the magnetic interactions and decrease the magnetic ordering temperature. In this context, we synthesized $Co_5Sn(O_2BO_3)_2$, and to our surprise the results have shown that the nonmagnetic Sn ion occupy only one site (4) and that the magnetic ordering temperature raised drastically reaching 82 K, the highest T_N observed among the Co ludwigites.

In this chapter we will show the results of x-ray diffraction, ac susceptibility, magnetization, ^{119}Sn Mössbauer spectroscopy, specific heat and NPD experiments performed in $Co_5Sn(O_2BO_3)_2$.

3.2 Experimental

3.2.1 Synthesis

The syntheses were performed at the laboratories of the IF-UFF. Black needle crystals of $Co_5Sn(O_2BO_3)_2$ were obtained from a mixture of $CoO : SnO_2 : H_3BO_3 : Na_2B_4O_7$ in 5:1:2:10 molar proportions respectively. The mixture was heated for 24 hours at 1100 °C and cooled down to 600 °C for 48 hours. Then the oven was turned off. The result was dissolved in hot water and the crystals cleaned in an ultrasonic bath at 50 ◦C. The presence of tin in the crystals was confirmed by ^{119}Sn Mössbauer Spectroscopy.

3.2.2 Structural Characterization

Powder x-ray diffraction (XRD) measurements were performed at LDRX – UFF laboratory. The initial XRD pattern consist of two phases, $Co_5Sn(O_2BO_3)_2$ and less than 10 % of SnO_2. SnO_2 is a nonmagnetic oxide with a rhombohedral morphology. Needle crystals of $Co_5Sn(O_2BO_3)_2$ were separated with tweezers and ground.

Single crystal x-ray diffraction measurements and initial structure refinement were conducted at LabCri-UFMG laboratory by Carlos Pinheiro. Final refinements and tables were made by Daniele Freitas. Table 3-1 summarizes the crystal data for the measurement performed at 110 K.

Table 3-1: Crystal data of $Co_5Sn(O_2BO_3)_2$.

Empirical Formula	$Co_{5.07}Sn_{0.93}B_2O_{10}$
Formula weight	591.08 g/mol
Wave length	0.717073 Å
Crystal Size	$0.4567 \times 0.1511 \times 0.0550$ mm^3

Temperature	110 K
Crystal system	Orthorhombic
Space group	*Pbam*
Unit cell dimension *a*=	9.4216(3) Å
b=	12.3281(2) Å
c=	3.10109(1) Å
Volume	360.194(2) Å^3
Z	2

The structure was solved in analogous experimental conditions at 293 K and 110 K in order to observe any eventual conformational change with temperature. No evidence for any phase transition was found above 110 K. Figure 3-3 shows a schematic structure of the ludwigites projected along the *c* axis together with the polyhedra centered at metal ions. The green sites 1, 2, and 3 are exclusively occupied by Co atoms. The yellow site 4 is occupied randomly by Sn and Co ions in a proportion of 0.46:0.54. The purity of the samples after selection was confirmed by powder x-ray diffraction and the presence of the Sn in the compound by energy-dispersive x-ray spectroscopy (EDS) (not shown). Despite having almost the same proportion we did not see additional peaks indicating some kind of long-range order from the Sn and Co ions in this site. Contrary to the other nonmagnetic ions in the cobalt heterometallic structures, the Sn occupies only one site of the lattice. So the chemical composition of our sample, obtained from x-ray analysis, is $Co_{5.07}Sn_{0.93}(O_2BO_3)_2$. Table 3-2 shows the fractional coordinates, the site occupancy factor (SOF) and the normalized occupancy (Occ.).

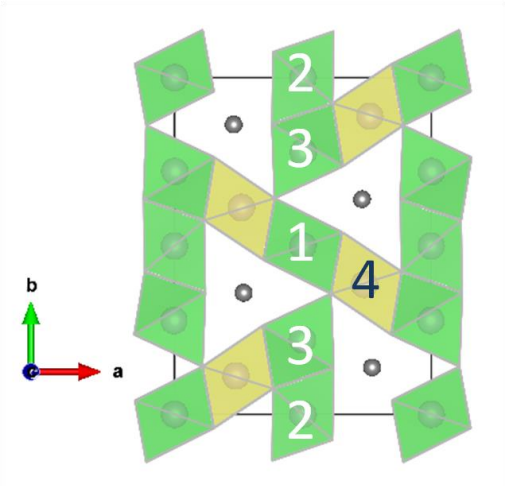

Figure 3-3: Schematic structure of $Co_5Sn(O_2BO_3)2$ showing the metallic sites in octahedral coordination. The green sites 1, 2, and 3 are exclusively occupied by Co atoms. The yellow site 4 is occupied randomly by Sn and Co ions in a proportion of 0.46:0.54.The gray circles represent the boron atoms. This figure was generated by Vesta 3.1.1 software [1].

As described in chapter 2, we calculate the V_{ZZ} values for the four Co sites, the results are presented in Table 3-3. It shows that site 4 is the most symmetric site, this is a common characteristic of ludwigite compounds and seems to be related to the preferential occupation of this site. Table 3-3 also shows the oxidation numbers Z_j for Co ion on site *j,* these oxidation numbers were calculated applying the formula given by Wood and Palenik [24],

$$Z_j = \sum_i (R_0 - r_{ij})/b,$$

with r_{ij} being the distance to the nearest-neighbour oxygen ions. R_0 and b are parameters given in reference [24] for inorganic cobalt compounds. The oxidation numbers Z_j show that we can nominally ascribe oxidation number 2+ for all the Co ions.

Table 3-2: Fractional coordinates, site occupation factor (SOF), the normalized occupancy (Occ.) per site and the equivalent isotropic displacement parameters ($Å^2 \times 10^3$) for $Co_5Sn(O_2BO_3)_2$. U(eq) is defined as one-third of the trace of the orthogonalized Uij tensor. The Occ. is the occupancy of atoms per site, normalized by the SOF. The SOF values must be multiplied by the factor 8 to obtain the number of atoms in the unit cell [25].

site	x/a	y/b	z/c	SOF	Occ.	U(eq)
Co(1)	0	0	0.5	0.25	1	6(1)
Co(2)	0	0.5	0	0.25	1	9(1)
Co(3)	0.0015(1)	0.2810(1)	0.5	0.5	1	6(1)
Co(4)	0.2397(1)	0.1151(1)	0	0.267	0.46	4(1)
Sn(4)	0.2405(1)	0.1161(1)	0	0.233	0.54	4(1)
O(1)	0.1520(1)	-0.0420(1)	0	0.5		7(1)
O(2)	0.1045(2)	0.1429(1)	0.5	0.5		7(1)
O(3)	0.1258(2)	0.3599(1)	0	0.5		7(1)

O(4)	- 0.1143(2)	0.4210(1)	0.5	0.5	9(1)
O(5)	- 0.1528(1)	0.2356(2)	0	0.5	7(1)
B	0.2723(2)	0.3618(2)	0	0.5	7(1)

Table 3-3: Oxidation numbers Z_j for Co ions on site j and the and the V_{ZZ} component of the EFG, see text for details.

Site	Z_j	V_{ZZ} (e/Å)
Co1	1.806	0.220
Co2	1.806	0.059
Co3	1.818	0.269
Co4	1.956	0.015

3.2.3 Magnetic measurements

The magnetic measurements of powdered samples of $Co_5Sn(O_2BO_3)_2$ were performed in the Laboratório de Baixas Temperatures of the IF-UFRJ, by Gabriel Eslava and Luis Ghivelder using a commercial PPMS platform from Quantum Design. Magnetic measurements on oriented single crystals were performed at CBPF using a commercial Versalab platform from Quantum Design. The results of the magnetic measurements are shown from Figure 3-4 to Figure 3-7.

Figure 3-4 shows the magnetization versus temperature curves for field-cooled (FC) and zero-field-cooled (ZFC) measurements with applied fields of 0.1 and 1T from powder samples. Below 82 K the curves show an abrupt change of derivative and then the ZFC and FC curves separate. From the linear fit of the inverse dc susceptibility (FC-1T) above 120 K, we obtained the Curie-Weiss temperature $\theta_{CW} = -32.5$ K and the Curie constant, $C = 26.06 \times 10^{-3}$ emu.K/g.Oe. The negative value of θ_{CW} indicates the predominance of antiferromagnetic interactions in this systems. From the Curie constant we determine the effective moment per formula unit (f.u.) $p_{eff} = 11.09\,\mu_B$.

The spin only moment per f.u. of $Co_5Sn(O_2BO_3)_2$ gives $p = \sqrt{5 \times 3/2 \times (3/2 + 1)} = 8.6\ \mu_B$. In most of the 3d transition metals, the magnetism is due mainly to the spin magnetic moment, with a little or null orbital contribution. An exception seems to be Co^{2+}, as pointed out by J.M.D. Coey in reference [26]. The value of the effective moment per f.u., 11.09 μ_B, is considerably higher than an expected spin only moment, 8.6 μ_B, showing that the orbital contribution is not quenched. This is consistent with experimental observations for Co^{2+} ions [26].

Figure 3-5 shows the real part of the ac-susceptibility measurements for different frequencies as a function of temperature from powder samples. The sharp peak at the temperature $T_C = 82$ K sets the order temperature of this material. The variation of T_C with frequency for two decades is smaller than 0.2 K, consistent with a long range magnetic transition as confirmed by specific-heat results to be shown later. We remark that this temperature is almost two times higher than that obtained for $Co_3O_2BO_3$ [7], 42 K.

The magnetization curves from powder samples as functions of applied fields for different temperatures are shown in Figure 3-6. At 100 K the magnetization exhibits a paramagnetic behavior. Below T_N the magnetization versus field curves present hysteresis cycles down to the lowest reached temperatures. Below 10 K these curves present small jumps at low fields and, near 2 K, a sharp one at 3.8 T. This behavior was also found in $Co_5Ti(O_2BO_3)_2$ [21] and in this case is related to a spin-glass phase [27]. However, contrary to the $Co_5Ti(O_2BO_3)_2$ system, for which the specific heat as a function of temperature does not present any feature, here it has a narrow peak characteristic of a well-defined thermodynamic transition. This excludes a spin-glass transition in the present system, differently from what was found in the former. Figure 3-7 shows magnetization measurements in oriented single crystals with the applied magnetic field along ($\parallel c$) and perpendicular ($\perp c$) to the c axis. The results are compatible with a highly anisotropic compound with the easy magnetization direction on the *ab* plane.

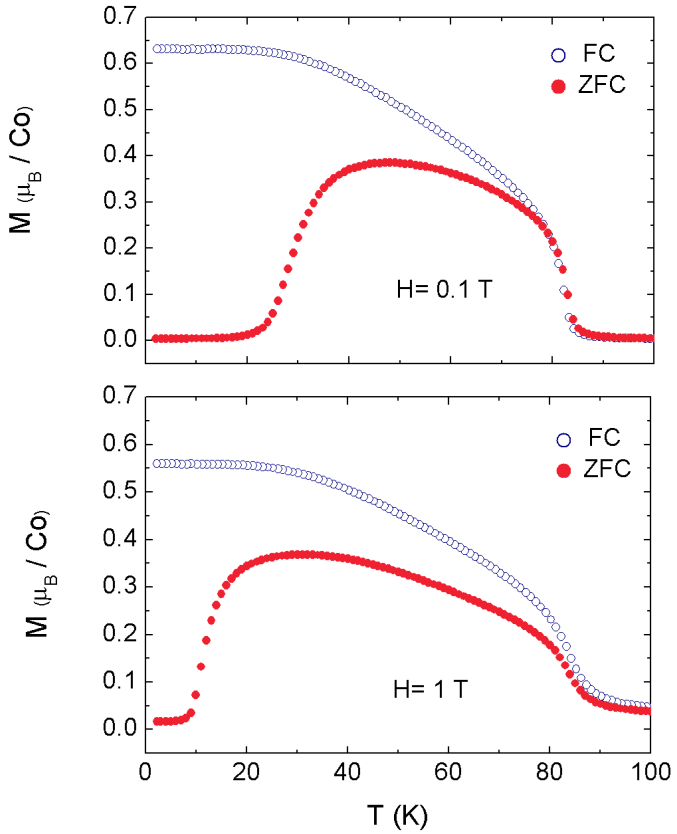

Figure 3-4: Magnetization versus temperature for powder sample of $Co_5Sn(O_2BO_3)_2$ under an applied fields of 0.1 and 1 T in both regimes: field cooled (FC) and zero field cooled (ZFC).

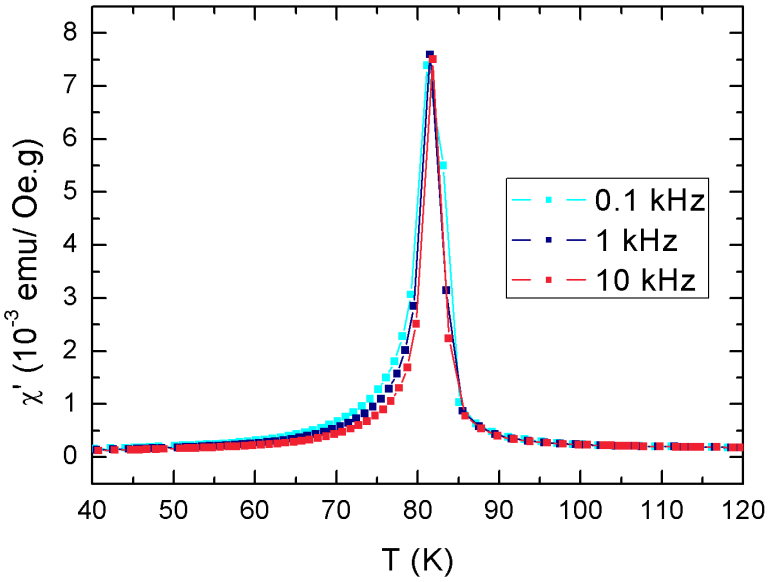

Figure 3-5: Real (χ') part of $Co_5Sn(O_2BO_3)_2$ ac magnetic susceptibility on powder sample as functions of temperature for 0.1 kHz, 1 kHz, and 10 kHz. The amplitude of the oscillating magnetic field is 1 Oe.

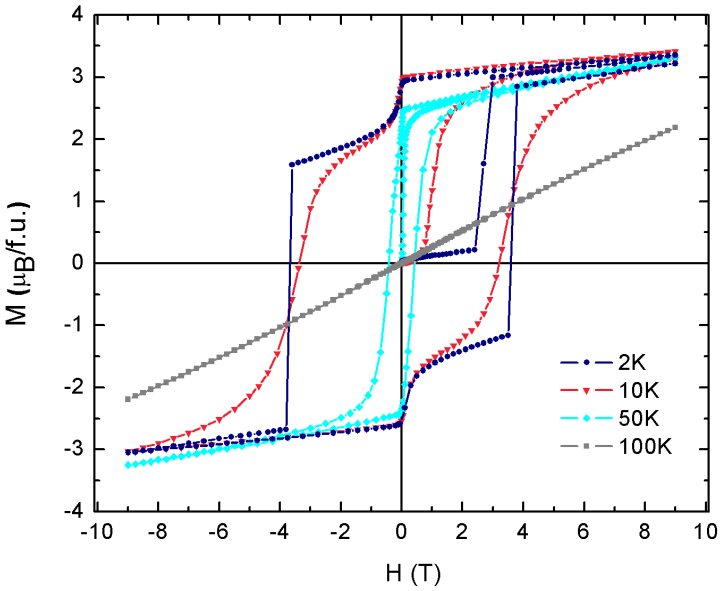

Figure 3-6: $Co_5Sn(O_2BO_3)_2$ magnetization versus applied magnetic field loops at 2, 10, 50, and 100 K on powder sample.

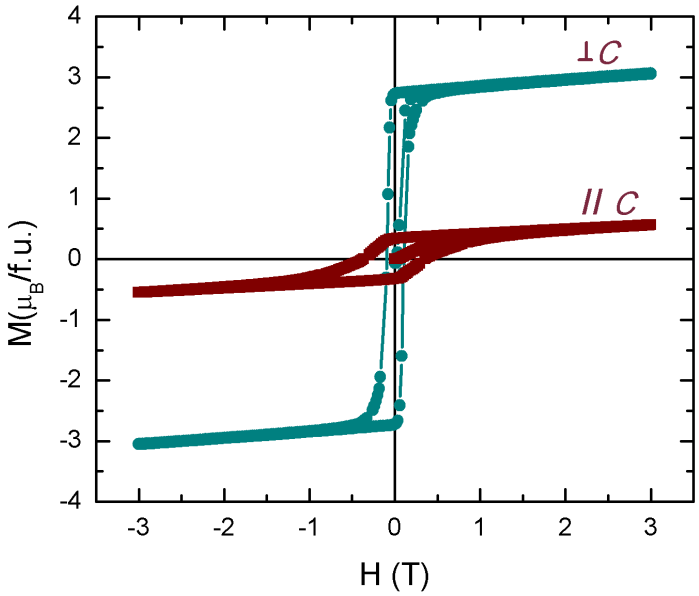

Figure 3-7: Hysteresis loops for oriented crystals parallel (∥) and perpendicular (⊥) to the *c* axis at 50 K.

3.2.4 Specific heat measurements

Specific-heat measurements of $Co_5Sn(O_2BO_3)_2$ were performed in the Laboratório de Baixas Temperatures of the IF-UFRJ, by Gabriel Eslava and Prof. Luis Ghivelder using a commercial PPMS platform from Quantum Design. The measurements were performed employing 11.3 mg of randomly oriented needle crystals. Results are shown in Figure 3-8 and Figure 3-9.

Figure 3-8 shows the specific-heat curves plotted as *C/T* versus *T* for different ludwigites with equivalent formula units: $Co_{2.5}Sn_{0.5}(O_2BO_3)_2$, $Co_{2.5}Ti_{0.5}(O_2BO_3)_2$ [21], $Co_3O_2BO_3$ [7], and $Fe_3O_2BO_3$ [28]. The two homometallic ludwigites $Co_3O_2BO_3$ and $Fe_3O_2BO_3$ present sharp peaks at 42 K and 70 K, respectively, showing the magnetic order of the whole system. $Fe_3O_2BO_3$ has still another small peak at 110 K due to a partial magnetic order of the ladder 4-2-4 [28]. Co ludwigites doped by nonmagnetic ions have the magnetic order diminished or suppressed as in $Co_5Ti(O_2BO_3)_2$.

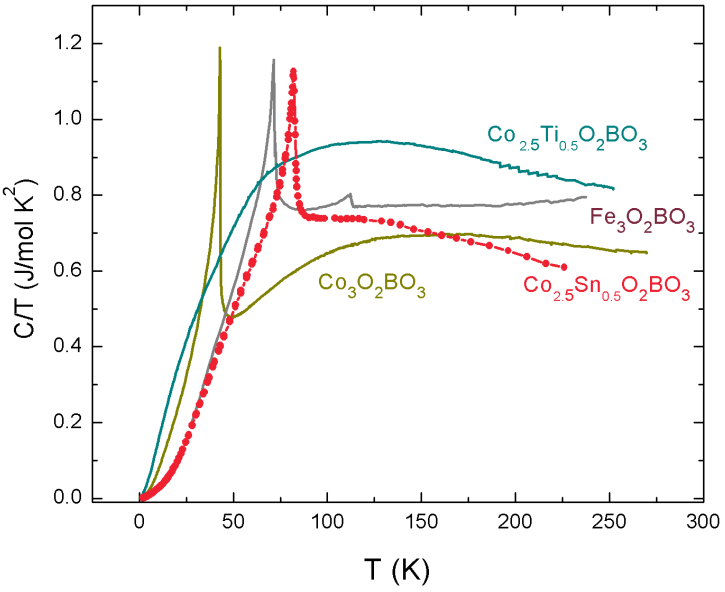

Figure 3-8: Specific heat of ludwigites, plotted a C/T vs T, compared with equivalent formula units: $Co_{2.5}Sn_{0.5}(O_2BO_3)_2$, $Co_{2.5}Ti_{0.5}(O_2BO_3)_2$ [21], $Co_3O_2BO_3$ [7], and $Fe_3O_2BO_3$ [28].

The $Co_5Sn(O_2BO_3)_2$ system has a sharp peak at 81.5 K similar to that observed in the homometallic ludwigites. This peak together with the results of the magnetic measurements suggests that this compound has a ferrimagnetic transition near 82 K. Contrary to other Co ludwigites doped with nonmagnetic ions, Sn doping enhances the magnetic order, reaching a magnetic order in $Co_5Sn(O_2BO_3)_2$ at a temperature even higher than that of the homometallic compound. Figure 3-9 shows the specific-heat curves of $Co_5Sn(O_2BO_3)_2$, plotted as C/T versus T, with applied magnetic fields of 0, 1 and 9 T. We notice that the peak at 82 K smooths down but does not shift with the applied magnetic fields. Similar behavior with applied magnetic fields is observed in the $Co_3O_2BO_3$ [7] and indicates a type of magnetic order more complex than that of a conventional antiferromagnet. It is possible that the field polarizes the spins on both sides of the transition reducing the variation of entropy. This also reinforces the ferrimagnetic nature of the sample. The inset of Figure 3-9 shows the fitting of the low-temperature specific heat with a $C/T = \gamma + \beta T^2$. This yields the parameters shown in Table 3-4.

The T^3 term in solids is generally due to lattice excitations and we can extract the Debye temperature θ_D using the formula $\theta_D^3 = 234\, R/\beta$, where R is the universal gas constant [29]. The θ_D of $Co_5Sn(O_2BO_3)_2$ is of the same order of magnitude as that obtained for $Co_3O_2BO_3$, while the γ parameter is much smaller than in the other ludwigites. This linear term is usually attributed to charge carriers, as free electrons in a Fermi liquid. The oxyborates are generally semiconductors at low temperatures but, in principle, this term could arise from itinerant electrons in the three-leg ladders in the mixed-valent ludwigites [5]. A linear temperature dependent specific heat is also observed in spin glasses [27], which have magnetic frustration, such as $Co_5Ti(O_2BO_3)_2$. In this case, values of γ can also be high and present strong magnetic field dependence. For the present $Co_5Sn(O_2BO_3)_2$ system, the linear contribution to the specific heat turns out to be very small as can be seen in Table 3-4. According to our x-ray and Mössbauer data (see below) the $Co_5Sn(O_2BO_3)_2$ only has Co^{2+} ions. Then, since this system has no mixed-valency, we can expect the electronic contribution to the linear specific heat to be negligible. On the other hand the experimental finding of negligible γ shows that the present material has fewer competing interactions and consequently a smaller degree

of frustration when compared to the other ludwigites. This is consistent with the existence of long-range magnetic order (as opposed to spin-glass ordering) and the observed enhancement of the ordering temperature of this system.

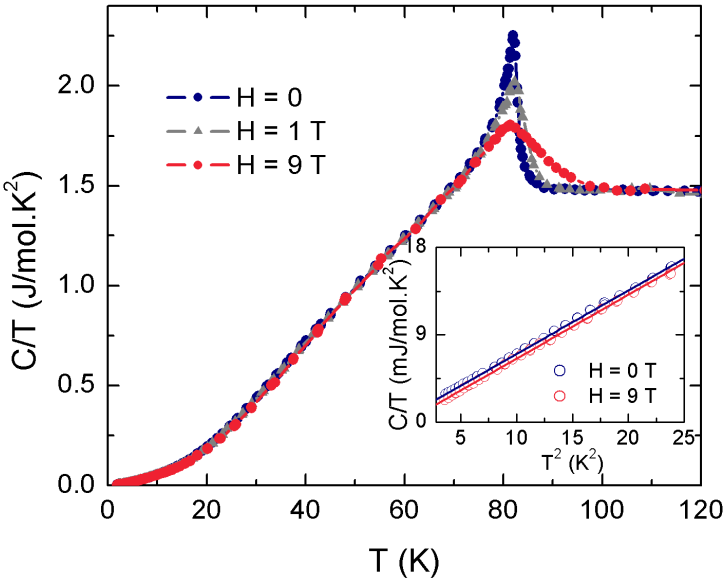

Figure 3-9: $Co_5Sn(O_2BO_3)_2$ specific heat as C/T vs T for applied fields of 0, 1 and 9 T. The inset shows the low temperature of C/T versus T^2 curve for applied fields of 0 and 9 T, with a linear fitting by the equation $C/T = \gamma + \beta T^2$.

Table 3-4: Fitting coefficients of the low-temperature specific heat (see text).

	H (T)	γ (mJ/mol K^2)	β (mJ/mol K^4)	θ_D (K)	ref.
$Co_5Ti(O_2BO_3)_2$	0	15.03	3.94	79	[21]
$Co_5Ti(O_2BO_3)_2$	3	6.88	2.78	89	[21]
$Co_5Ti(O_2BO_3)_2$	9	3.61	2.76	89	[21]
$Co_5Sn(O_2BO_3)_2$	0	0.54	0.650	144	[20]
$Co_5Sn(O_2BO_3)_2$	9	0.00	0.656	143	[20]

3.2.5 Mössbauer spectroscopy

The Mössbauer spectroscopy of ^{119}Sn was performed at CBPF. The measurements were made between 4.2 K and 300 K in transmission geometry. The spectra were taken with the $^{119m}Sn : CaSnO_3$ source. The spectra were least-squares fitted using the NORMOS program and the isomer shift values are in relation to $BaSnO_3$. The Mössbauer spectra of

^{119}Sn of $Co_5Sn(O_2BO_3)_2$ and the hyperfine parameters for different temperatures are shown in Figure 3-10 and Table 3-5.

For the fit of the paramagnetic spectra (300 K and 84 K) only one doublet was used. The observed linewidth of $\Gamma = 0.85$ mm/s is in reasonable agreement with the theoretical value of 0.64 mm/s (Ref. [30]), indicating that Sn ions occupy only one type of site, in agreement with the x-ray data presented above. The isomer shift value δ = 0.2 mm/s is consistent with an oxidation state of 4+ for Sn [30]. As is evident from the ^{119}Sn Mössbauer spectra shown in Figure 3-10, below 82 K the spectra begin to broaden magnetically indicating the onset of the magnetic transition according to the transition temperature obtained by the magnetic and transport measurements.

Below 82 K the spectra were fitted with two magnetic components. The quadrupole splitting E_Q, isomer shift δ, sign of V_{ZZ} (main component of the electrical field gradient tensor), hyperfine magnetic field B_{hf}, and angle θ between the directions of B_{hf} and V_{ZZ} were the free fitting parameters. Between $82 \geq T \geq 80$ the main component corresponds to the ions in a static magnetic state (blue line) and the minor one to the ions in a magnetic relaxation state, due to a short-range interaction near the transition temperature, or to a state with a not well defined direction (cyan line).

Below 80 K only the static magnetic components survive. Since Sn is not a transition element, it does not have a magnetic hyperfine field in the nucleus created by the unfilled 3*d* orbitals in its own electronic layer. So the magnetic hyperfine field on the Sn nucleus is a transferred magnetic field due to the magnetic moments of the neighbor Co ions. At 60 K the B_{hf} almost reach the saturation value (see Table 3-5) and below this temperature the spectra were fitted with two magnetic subspectra.

Table 3-5: Mossbauer hyperfine parameter of $Co_5Sn(O_2BO_3)_2$ for temperatures between 300 and 4.2 K. The parameters are the temperature T, isomer shift δ, quadrupole splitting ΔE_Q, linewidth Γ, hyperfine magnetic field B_{hf}, angle θ between the B_{hf} and the principal axis of the electrical gradient field V_{zz}, and the absorption area A.

T(K)	δ (mm/s)	ΔE_Q (mm/s)	Γ (mm/s)	B_{hf} (T)	θ(°)	A(%)
300	0.21	0.97	0.85	-	-	100
87	0.20	1.01	1.00	-	-	100
84	0.21	1.02	1.18	-	-	100

82	0.18	0.97	1.30	5.15	16.2	67.4
	0.22	-1.01	2.20	1.01	55.0	32.6
80	0.20	-1.06	1.18	6.44	11.2	79.5
	0.22	-0.94	1.30	3.88	27.1	20.5
60	0.17	-0.97	1.20	8.72	10.0	92.4
	0.17	-0.91	1.30	9.94	0	7.6
40	0.20	-0.94	1.28	9.00	0	92.4
	0.18	-0.92	1.30	11.00	0	7.6
20	0.18	-0.94	1.24	9.05	0	92.4
	0.20	-0.94	1.30	11.07	0	7.6
4.2	0.20	-0.91	1.20	9.08	0	92.4
	0.20	-0.90	1.20	10.83	0	7.6

The sextet with an absorption area of 92.6% is attributed to the Sn in the site 4. The other subspectra, corresponding to a 7.6% of the total area, can be due to the Sn at the site 4 in a special configuration, like clusters, or due to a small percentage of Sn at site 2. This small fraction of Sn is not observed in the paramagnetic spectra (where only electric interactions take place) probably due the crystallographic similarity of sites 2 and 4 which can generate almost the same quadrupole splitting.

The presence of practically a single magnetic component (93%) indicates a relatively simple magnetic structure. Due to the transferred character of the B_{hf} at the ^{119}Sn nuclei, the direction of the B_{hf} follows the effective direction of the magnetic moments around. Then, from the fitting at low temperatures, we can infer the direction of the magnetic moments of the Co ions. The metal ions occupy the center of oxygen octahedra and through symmetry arguments is inferred that the direction of the V_{ZZ} (main component of the electric field gradient tensor (EFG) is along the main axis of the octahedra. The direction of the main axis of the octahedra for each site is indicated with red lines in Figure 3-11 and can be seen that this direction is almost along the b axis. The fitting at low temperatures show that the angle between the V_{ZZ} and the B_{hf} is

$\theta \approx 0°$ (see Figure 3-11). This indicates that the magnetic moment of the Co ions around Sn at site 4 are parallel to the main axis of the octahedra, or nearly along the b axis (see Figure 3-11). This conclusion is compatible with the direction of the Co spins in the Co homometallic ludwigite (see Figure 2-13) and with the magnetic asymmetry observed in magnetic measurements of oriented crystals (Figure 3-7).

With the aim of obtaining information about magnetic arrangement of the spins and taking into account that B_{hf} is proportional to the magnetization, we have plotted the normalized B_{hf} vs T/T_C together with a normalized Brillouin function corresponding to a ferromagnetic order [29] (Figure 3-12) with J=1/2 and J=2. However, the Brillouin functions do not fit the experimental data, indicating that the magnetic order in $Co_5Sn(O_2BO_3)_2$ do not correspond to a classical ferromagnet. There are also antiferromagnetic interactions involved as indicated by the negative Curie Weis temperature. In Figure 3-12 we also compared the normalized hyperfine magnetic field in $Co_5Sn(O_2BO_3)_2$ with that corresponding to the 3-1-3 ladder of the homometallic $Fe_3O_2BO_3$ ludwigite, where the spins have an antiferromagnetic coupling along the b axis (considering the orientation in Figure 3-11) and a ferromagnetic coupling along the c axis (see Figure 2-4). The magnetization curves of these two systems almost overlap (see Figure 3-12) and the little difference could be related to the spin of the involved magnetic ions, S=2 in the 3-1-3 ladder of $Fe_3O_2BO_3$ and S=3/2 in $Co_5Sn(O_2BO_3)_2$. This results indicate that ferromagnetic and antiferromagnetic couplings could take place in $Co_5Sn(O_2BO_3)_2$.

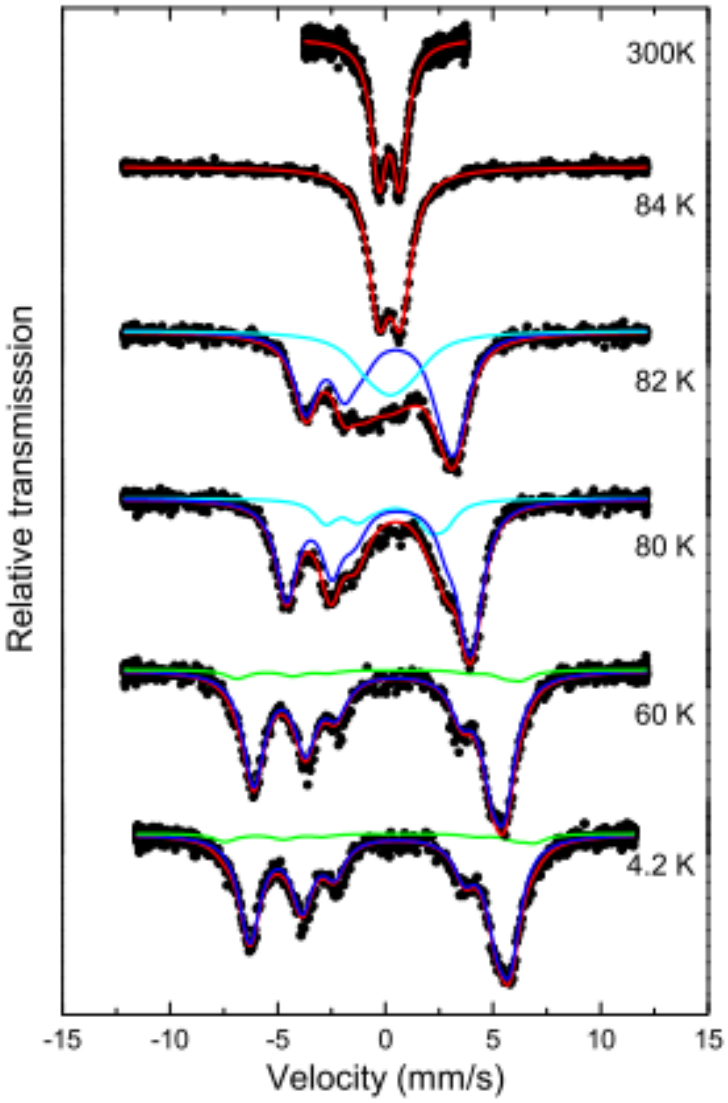

Figure 3-10: Some ^{119}Sn Mossbauer spectra of $Co_5Sn(O_2BO_3)_2$ in the temperature range of $300 \geq T \geq 4.2$ K. Between $300 \geq T \geq 84$ K only one doublet was used to fit the spectra. Below 82 K all the spectra were fitted with two magnetic subspectra.

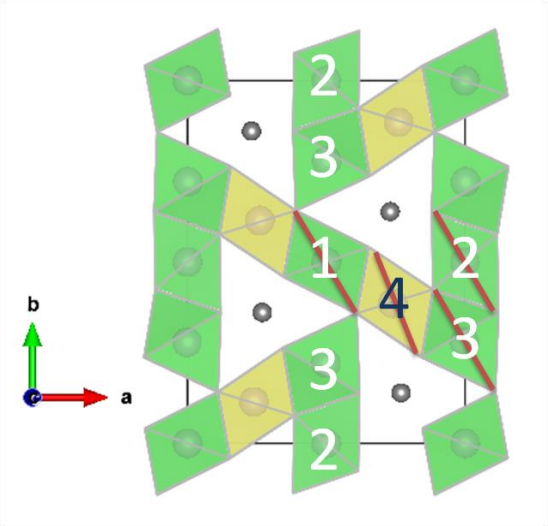

Figure 3-11: Schematic structure of the $Co_5Sn(O_2BO_2)_2$. Metallic sites 1, 2, and 3 in green are exclusively occupied by Co ions; site 4 is randomly occupied by 46% of Co and 54% of Sn ions. The red lines indicate the direction of the main axis of the octahedra.

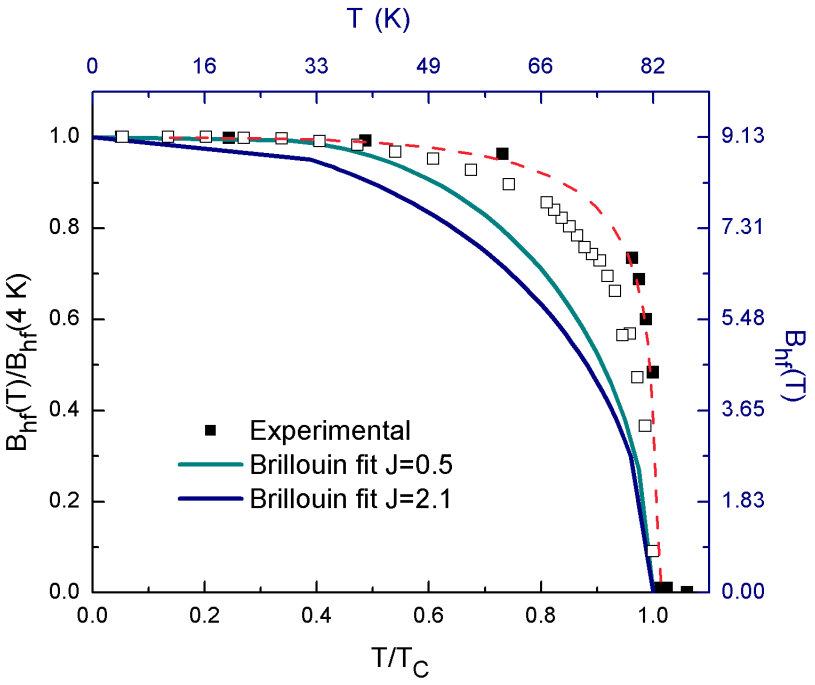

Figure 3-12: Normalized hyperfine magnetic field ($B_{hf}(T)/B_{hf}(4K)$) as a function of reduce temperature. Close square corresponds to $Co_5Sn(O_2BO_3)_2$, open square $Fe_3O_2BO_3$. Solid lines correspond to Brillouin fitting, the dashed line is a guide to the eye. Top and right axis correspond only to $Co_5Sn(O_2BO_3)_2$ data.

3.2.6 NPD experiments

Three grams of black-needle crystals of $Co_5Sn(O_2BO_3)_2$ were necessary to perform NPD experiments. The sample was synthesized at the laboratories of the IF-UFF following the method used in reference [20]. X-ray powder diffraction experiments showed the presence of a small amount of SnO_2 impurity phase (~10%). Due to the large amount of sample it was difficult to separate 3 grams of needles with tweezers and we believe that a small amount of the impurity SnO_2 phase was present in the sample when NPD experiments were performed. The sample was characterized magnetically and the results corresponded to the magnetic properties of the $Co_5Sn(O_2BO_3)_2$.

NPD experiments were performed by J. A. Rodríguez-Velamazan in the D1B instrument at Institut Laue-Langevin (ILL) in Grenoble. A wavelength of 1.28 Å from Ge (311) monochromator reflection was used to reduce boron absorption.

The sample was cooled down to 2 K and diffraction patterns covering the angular range 0.8 – 128.8 deg. were collected for 3 h at temperatures of 2, 60, 100, and 300 K. Figure 3-13 shows the small angle part of the NPD pattern of $Co_5Sn(O_2BO_3)_2$. It is observed that the diffractograms below 82 K, i. e. for 60 and 2 K, present a reduced background and new peaks indicating ferrimagnetic transitions. However, the difractogram pattern at 100 K, for medium angles (Figure 3-14) shows peaks that are not observed at 300 K. Those peaks were not expected since the magnetic transition is below 82 K and x-ray diffraction at 110 K do not show structural transitions. Rietveld refinement shows 2% of SnO_2, but to the best of our knowledge, there are neither structural transitions below 300 K nor magnetic order in SnO_2 that could justify those peaks. The analysis of the NPD data is in progress.

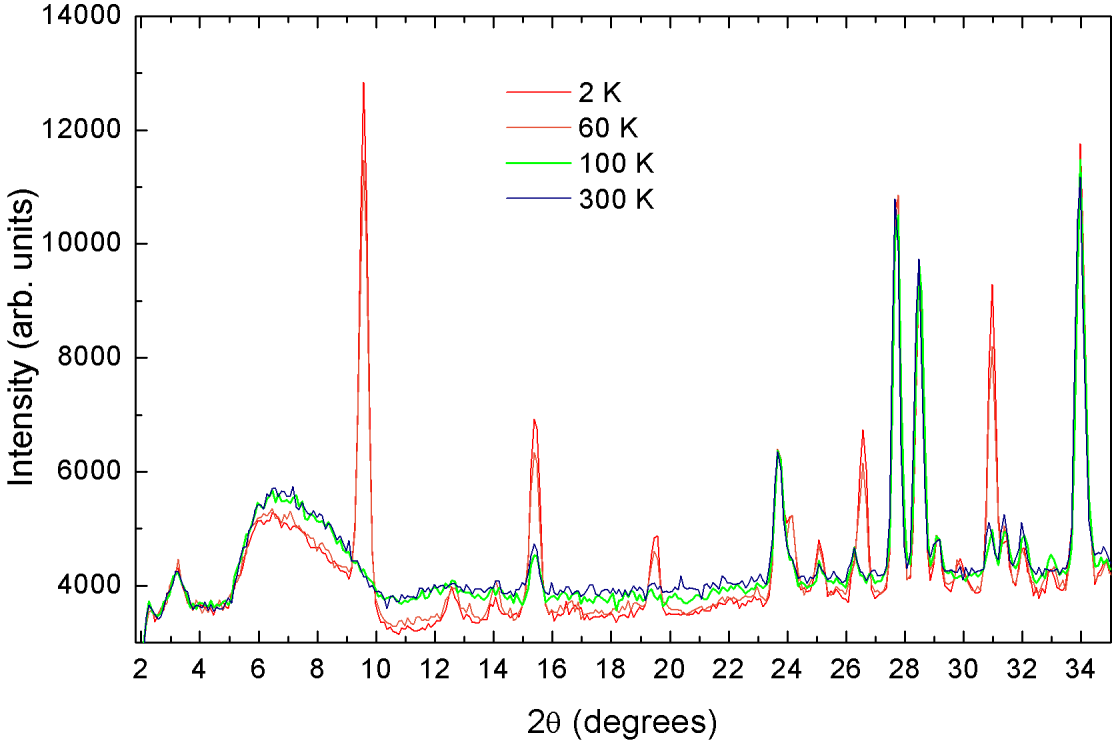

Figure 3-13: Small angle part of neutron diffractograms for $Co_5Sn(O_2BO_3)_2$ at 300, 100, 60, and 2 K.

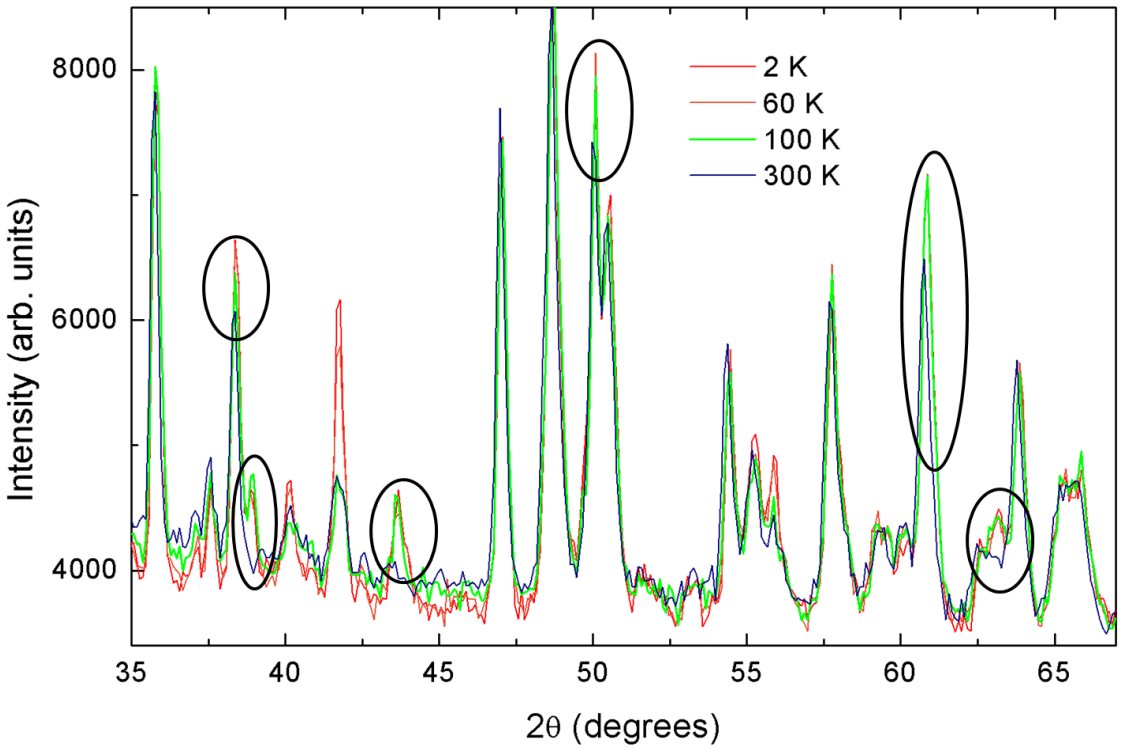

Figure 3-14: Medium angle part of neutron diffractograms for $Co_5Sn(O_2BO_3)_2$ at 300, 100, 60, and 2 K.

3.3 Discussion

In this chapter, we presented the synthesis and an extensive characterization of the system $Co_5Sn(O_2BO_3)_2$ using x-ray diffraction, Mössbauer spectroscopy, magnetization, specific-heat and NPD measurements. The Sn ions replace the Co ions only in the site 4 of the ludwigite structure (Figure 3-11) in almost equal proportion, as indicated by the x-ray diffraction and Mössbauer spectroscopy. By using the x-ray data we calculated the valence 2+ for all the Co ions using the bond valence sum method, and this was confirmed by charge balance. The Mössbauer spectroscopy of ^{119}Sn confirms the oxidation state 4+ obtained for Sn. On average, it keeps the site 4 with valence 3+; this seems to be a characteristic of all the ludwigites. We did not find any evidence for a structural transition to temperatures as low as 110 K. The presence of nonmagnetic ions in other cobalt ludwigites diminishes the magnetic interactions as evidenced by the smaller transition temperatures, as in $Co_{3-x}Ga_xO_2BO_3$ [23] ($T_0 = 37$ K), or destroys completely the order in favor of a spin-glass state like in $Co_5Ti(O_2BO_3)_2$ [21] ($T_{sg} = 19$ K) and $CoMgGaO_2BO_3$ [22] ($T_{sg} = 25$ K).

The $Co_5Sn(O_2BO_3)_2$ system has long-range magnetic order below $T_N \approx 82$ K as shown by narrow peaks in the specific-heat and susceptibility measurements (see Figure 3-5 and Figure 3-8). Surprisingly the magnetic interactions are strengthened by the introduction of nonmagnetic ions and the transition temperature of the whole system is the highest found among the ludwigites. On the other hand, the strength of the magnetic anisotropy can be gauged by the low-temperature coercive field, $H_{coercive} \approx 4$ T, obtained by magnetization measurements shown in Figure 3-6. The coercive field found in $Co_3O_2BO_3$ is near 2 T [7], almost half the value of the present system, as is also the case for the transition temperature, 42 K. In the ludwigites there is a competition between three types of magnetic interactions: direct exchange, superexchange, and double exchange. In $Co_5Sn(O_2BO_3)_2$ the latter should not be present since the magnetic ions do not have mixed valence in this material. Direct exchange is usually possible in the 4-2-4 ladders which have the smallest intermetallic distances. For $Co_5Sn(O_2BO_3)_2$ this distance is 2.8338(1) Å that is higher compared to the homometallic compounds, 2.7510(4) Å for $Co_3O_2BO_3$ [7] and 2.786(1) Å for $Fe_3O_2BO_3$ [4] at room temperature. Thus the magnetism of this system shall be governed essentially by superexchange interactions. This seems to reduce competition and reinforce long-range magnetic

order. The small γ parameter which vanishes in an applied magnetic field (see Table 3-4) corroborates the absence of frustration and a feeble competition between the magnetic interactions. Although the compound has θ_{CW} negative, which indicates the predominance of antiferromagnetic interactions, the ground state is not a conventional antiferromagnet. This is shown by the effect of the external magnetic field in the peak of the specific heat that is not shifted to low temperatures as would be expected. There are ferromagnetic interactions, as we can see by the magnetization curves in Figure 3-4 and also by the hysteresis below T_C in Figure 3-6. These figures are very similar to those of $Co_3O_2BO_3$, with the exception of the discontinuities found in the magnetization versus field curves of $Co_5Sn(O_2BO_3)_2$ below 10 K. It reveals the ferrimagnetic nature of both compounds.

The ^{119}Sn Mössbauer spectroscopy and magnetization measurements in oriented crystals show high magnetic anisotropy for $Co_5Sn(O_2BO_3)_2$ with the spins oriented almost along the b axis. In addition, the saturation of the magnetic moment at 9 T, $M_S = gS \simeq 3.3\,\mu_B/f.u.$ give $S \approx 3/2$ that correspond to the moment of one Co^{2+} spin per formula unit. These experimental results are in agreement with an antiferromagnetic coupling of the Co atoms in the ab plane and a ferromagnetic coupling along the c axis. In this way, the coupling of the 5 Co atoms in a unit formula is such that it results in a unique spin pointing in the b direction (↑↓↑↓↑). A confirmation of these magnetic couplings is expected after the analysis of the NPD data.

Chapter 4. Structural and magnetic studies of ludwigite $Co_{4.76}Al_{1.24}(O_2BO_3)_2$

The content of this chapter is closely the same in reference [3].

4.1 Introduction

Motivated by the unexpected differences between Co and Fe homometallic ludwigites described in chapter 2, many other heterometallic ludwigites were synthesized [6, 9, 10, 31]. The study of these latter compounds show that the magnetic interactions between different types of magnetic ions are more complex and lead to a spin-glass freezing or to a reduction of the effective magnetic moments [21, 22, 23]. With the aim of simplifying the magnetic complexity, $Co_3O_2BO_3$ was diluted diamagnetically by substituting Co with Ti [21], Mg-Ga [22], Ga [23], and Sn (chapter 3) ions. As shown in these works, nonmagnetic Ti, Mg, and Ga ions can reduce or even destroy long-range magnetic order. On the other hand, Sn drastically raised the magnetic ordering (chapter 3).

Aiming to simplify the magnetic interactions and better understand the complex magnetic behavior in ludwigites, in this chapter we study the $Co_{4.76}Al_{1.24}(O_2BO_3)_2$ and their results are compared with that of the $Co_3O_2BO_3$ and $Co_5Sn(O_2BO_3)_2$. This compound showed interesting magnetic properties never seen before in other ludwigite: Metamagnetic transitions with moderate applied magnetic fields of first and second order, the magnetocaloric effect, and the T^2 dependence of the specific heat at low temperatures attributed to magnon and phonon planar excitations. In addition, an increase of the magnetic order temperature is observed as in $Co_5Sn(O_2BO_3)_2$. These results open the question about the role of the spin state of metallic site 4 in this kind of compounds.

4.2 Experimental

4.2.1 Synthesis

The syntheses were performed at the laboratories of the IF-UFF. The crystals were synthesized from a 5: 1: 2 molar mixture of Co_3O_4: Al_2O_3: H_3BO_3 with an excess of borax.

The mixture was heated at 1160 °C for 24 hours and cooled down to 600 °C for 48 hours. Then the oven was turned off. The bath was dissolved in hot water and the crystals washed in diluted hydrochloric acid. Needle-shape black crystals up to 5 mm length were obtained. The purity of the sample was confirmed by x-ray powder diffraction.

4.2.2 Structural Characterization

Single crystal X-ray diffraction measurements were conducted at LDRX – UFF laboratory by Jackson Resende and Daniele Freitas. Due to the unconventional reflections presented by $Co_{4.76}Al_{1.24}(O_2BO_3)_2$, the sample was also measured by Carlos Pinheiro (LabCri-UFMG).

The structure was solved in analogous experimental conditions at 270 K and 120 K in order to observe any eventual change with temperature, and no evidence for any phase transition was found in this temperature range. Crystal data for the measurement performed at 120 K are summarized in Table 4-1.

Table 4-1: Crystal data of $Co_{6-x}Al_x(O_2BO_3)_2$.

Empirical formula	$Co_{4.76}\ Al_{1.24}\ B_2\ O_{10}$
Formula weight	495.42 g/mol
Temperature	120(2) K
Wavelength	0.71073 Å
Crystal size	$0.145 \times 0.075 \times 0.05\ mm^3$
Crystal system	Orthorhombic
Space group	$P\ b\ a\ m$
Unit cell dimensions a =	9.1959(4) Å
b =	12.0434(5) Å
c =	3.00010(10) Å
Volume	$332.26(2)\ Å^3$
Z	2

To compare the measurements at different temperatures, Table 4-2 shows selected bond length at 270 and 120 K and the difference. They do not have significant

differences. For the analysis of the magnetic part, the structural parameters at 120 K will be used.

Table 4-2: Selected bond lengths in Å for $Co_{4.76}Al_{1.24}(O_2BO_3)_2$ at two temperatures and the difference.

Bonds	120 K	270 K	Δ(dist) (Å)
O1-B	1.372(3)	1.374(3)	0.002
O1-Al1	2.1015(12)	2.1074(12)	0.006
O1-Co1	2.1015(12)	2.1074(12)	0.006
O2-Al4	1.926(11)	1.932(10)	0.006
O2-Co4	1.941(4)	1.941(3)	0.000
O3-Co3	2.1376(12)	2.1344(12)	-0.003
O4-Al2	2.0384(12)	2.0432(12)	0.005
O4-Co2	2.0384(12)	2.0432(12)	0.005
O4-Co4	2.072(4)	2.069(3)	-0.003
O4-Al4	2.097(12)	2.088(10)	-0.009
O5-B	1.384(3)	1.387(3)	0.003
O5-Al4	1.933(14)	1.919(11)	-0.014
O5-Co4	2.032(5)	2.036(3)	0.004
O5-Co3	2.1329(13)	2.1324(12)	0.000

Table 4-3 shows the fractional coordinates, site occupancy factor (SOF), normalized site occupancy (Occ.), and equivalent isotropic displacement parameters (Ueq.). Co atoms exclusively occupy the site 3. The sites 1, 2 and 4 are occupied randomly by Al and Co ions. The oxygen atoms on sites O4 and O2, which are not bonded to boron, showed unusual large atomic displacement parameters (Ueq.), see Table 4-3. This particular feature could suggest a modulated structure as a function of the Co/Al substitution ratio whose occurrence is being investigated and will be published in the future.

Table 4-3: Fractional coordinates, SOF, occupation, and equivalent isotropic displacement parameters Ueq. ($Å^2$ x 10^3) for $Co_{4.76}Al_{1.24}(O_2BO_3)_2$. The Occ. is the occupancy of atoms per site, normalized by the SOF. *U*(eq) is defined as

one-third of the trace of the orthogonalized U_{ij} tensor. The SOF values must be multiplied by the factor 8 to obtain the number of atoms in the unit cell [25].

Site	x/a	y/b	z/c	SOF	Occ.	U(eq)
Co1	0	0	0	0.221	0.882	4(1)
Al1	0	0	0	0.029	0.118	4(1)
Co2	0	0.5	-0.5	0.168	0.672	5(1)
Al2	0	0.5	-0.5	0.082	0.328	5(1)
Co3	-0.0020(1)	0.2787(1)	0	0.5	1	4(1)
Co4	0.2378(4)	0.1116(2)	-0.5	0.301	0.601	4(1)
Al4	0.2398(16)	0.1218(9)	-0.5	0.199	0.399	4(1)
B	0.2703(3)	0.3620(2)	-0.5	0.5	1	5(1)
O1	0.1516(2)	-0.0409(1)	-0.5	0.5	1	8(1)
O2	0.1101(2)	0.1419(1)	0	0.5	1	10(1)
O3	0.1204(2)	0.3631(1)	-0.5	0.5	1	7(1)
O4	-0.1155(2)	0.4262(1)	0	0.5	1	18(1)
O5	-0.1584(2)	0.2393(1)	-0.5	0.5	1	7(1)

Table 4-4 shows the oxidation numbers and the V_{ZZ} component of the EFG of the four Co sites, those values were calculated as described in Chapter 3. The oxidation numbers Z_j for Co ion on site j in Table 4-4 show that we can nominally ascribe valence 2+ for the Co ions in sites 1 and 3 and a valence number between 2+ and 3+ for Co ions on sites 2 and 4. Table 4-4 also shows that site 4 has the lowest V_{ZZ} values, similar behavior was observed in several other doped Co ludwigite (Sn (section 3.2.2), Fe[9, 11], Ga[23], Mn[31], and Cu[32]), in which site 4 has a preferential occupation. However, that do not apply for the present sample, as shown in Table 4-3, site 2 as well as site 4 have comparable amounts of Al, the doped ion.

Table 4-4: Oxidation numbers Z_j for Co ions on site j and the and the V_{ZZ} component of the EFG, see text for details.

Site	Z_j	$V_{ZZ}(e/\text{Å})$
Co1	2.088	0.209
Co2	2.320	0.095
Co3	1.980	0.227
Co4	2.535	0.019

4.2.3 Magnetic Measurements

The DC magnetization measurements of $Co_{4.76}Al_{1.24}(O_2BO_3)_2$ were performed on both powder and oriented single crystals using a commercial Quantum Design PPMS at CBPF.

Figure 4-1, shows the temperature dependence of the DC magnetization for field cooled (FC) and zero field cooled (ZFC) procedures, for an applied field of 100 Oe. Cooling down, the magnetization values increases until a maximum value of 0.08 emu/g at 57 K and decreases for lower temperatures. The magnetization values of this compound are lower than those corresponding to $Co_3O_2B_2O_3$ with 2 emu/g at $T_N = 42$ K [7], which are two orders of magnitude larger. The inset shows the inverse of the magnetization at 1 T as a function of temperature. The paramagnetic region, above 180 K follows the Curie-Weiss law, with $C = 31.37 \times 10^{-3}$ emu K g^{-1} Oe^{-1} and Curie-Weiss temperature $\theta_{CW} = -4.81$ K, which indicates antiferromagnetic interactions. However, the small θ_{CW}/T_C ratio shows competing FM and AFM interactions at high temperatures. From the Curie constant, the effective moment per Co atom is $p_{eff} = 5.2\mu_B$, which yields J = 2.16 considering g = 2. In $Co_{4.76}Al_{1.24}(O_2BO_3)_2$, charge balance leaves 4 atoms of Co^{2+} and 0.76 atoms of Co^{3+}. The spin only moment per Co atom could be calculated following reference [31] as:

$$p = g\,\frac{\sqrt{n_{Co^{2+}} \times S_{Co^{2+}} \times (S_{Co^{2+}} + 1)) + n_{Co^{3+}} \times S_{Co^{3+}} \times (S_{Co^{3+}} + 1)}}{\sqrt{n}}$$

Where n is the total number of magnetic ions per f.u. If all the Co ions are in high spin state (HS), then $S_{Co^{2+}} = 3/2$ and $S_{Co^{3+}} = 2$, which leaves $p = 4.05\mu_B$. A configuration with Co^{2+} in HS and Co^{3+} in LS, it is $S_{Co^{3+}} = 0$, gives $p = 3.55\mu_B$. Then, in any case, there

is a reasonable orbital contribution to the total magnetic moment, characteristic of Co^{2+} magnetic ions as observed previously in $Co_3O_2BO_3$ [7] and $Co_5Sn(O_2BO_3)_2$ (section 3.2.3).

Edson Pasamani of the PPGFis UFES made the ac magnetic measurements with a Quantum Design PPMS. Figure 4-2 shows the measurements for different frequencies as a function of temperature. A peak is observed at 57 K in χ'_{ac} whose position does not change for three decades of frequency variation; this is typical of a long-range magnetic ordering. It is a well-defined thermodynamic transition, as established by specific heat results also, as will be shown below.

Figure 4-3 shows the magnetization curves as a function of applied magnetic fields for different temperatures. At 100 K the magnetization exhibits a linear behavior, characteristic of the paramagnetic state. For fixed temperatures below the zero magnetic field T_C temperature, the magnetization presents an inflection point at a critical field H_C. This is better seen in the inset of Figure 4-3 where it appears as a maximum in the derivative $\partial M/\partial H$. This field and the temperature at which it occurs define a metamagnetic transition at (T_C, H_C) in the compound. As the temperature is further reduced, the M (H) curves become hysteretic down to the lowest temperatures as can be seen in Figure 4-3.

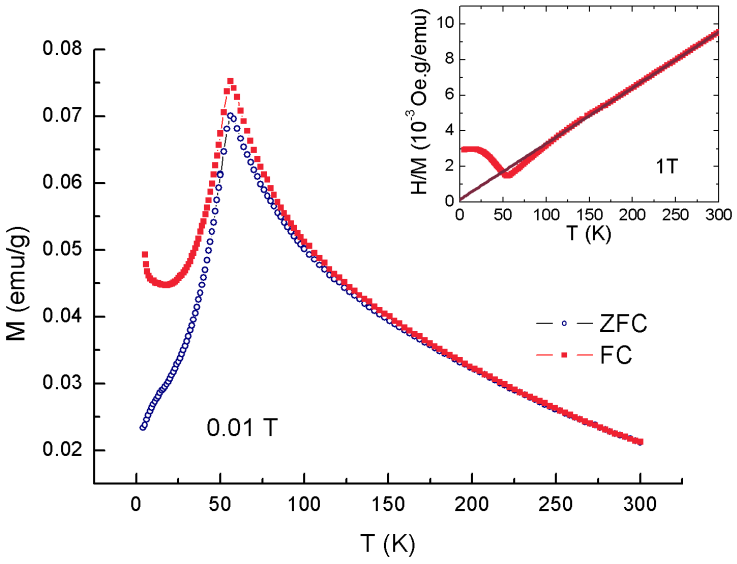

Figure 4-1: Magnetization versus temperature for powder sample of $Co_{4.76}Al_{1.24}(O_2BO_3)_2$ under an applied field of 100 Oe in both regimes: field cooled (FC closed symbol) and zero field cooled(ZFC open symbol). The inset shows the inverse of the FC magnetization curve for an applied magnetic field of 1 T and the linear fit of the paramagnetic region.

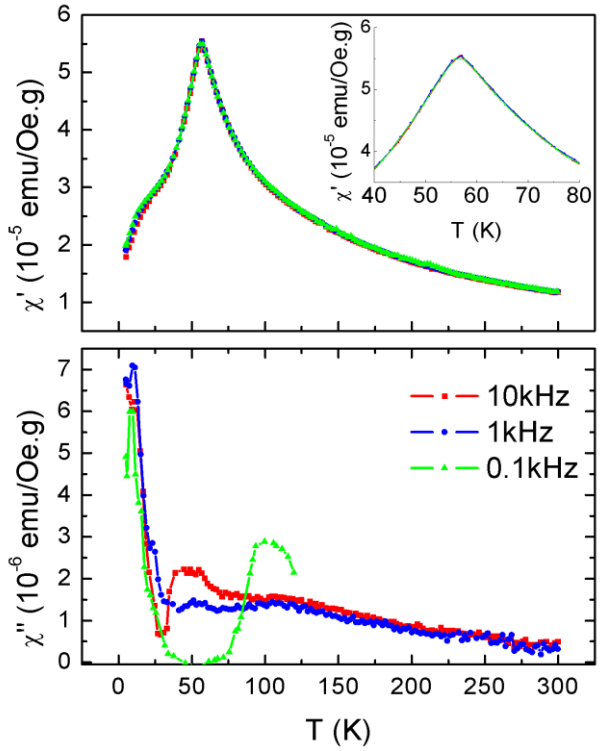

Figure 4-2: ac magnetic susceptibility for powder sample of $Co_{4.76}Al_{1.24}(O_2BO_3)_2$ as functions of temperature for 100 Hz,1 kHz and 10 kHz. Top: Real part, the inset shows a zoom of the region close to the peak. Bottom: Imaginary part.

Figure 4-4 shows magnetic measurements in oriented single crystals with the applied magnetic field along and perpendicular to *c*-axis. The magnetic measurements are compatible with a highly anisotropic compound, with the easy magnetization direction in the *ab* plane. The small remnant magnetization ($\sim 0.07\,\mu_B/Co$) observed in the hysteresis curves taken with an applied field perpendicular to *c*-axis could be related with a non-compensated AFM structure resulting in a very small FM component. Then, the magnetic configuration that better describe the low-temperature, low-field magnetic structure is a ferrimagnetic order (FIM), in agreement with the specific heat results presented below.

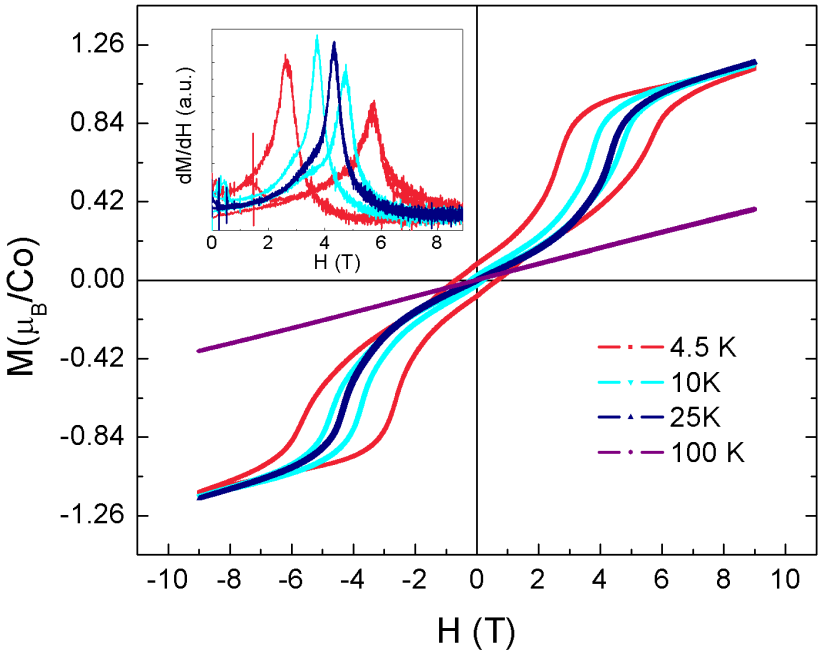

Figure 4-3: Magnetization as a function of applied magnetic fields for powder sample of $Co_{4.76}Al_{1.24}(O_2BO_3)_2$ at 4.5, 10, 25 and 100 K. The inset shows the derivative of the curves.

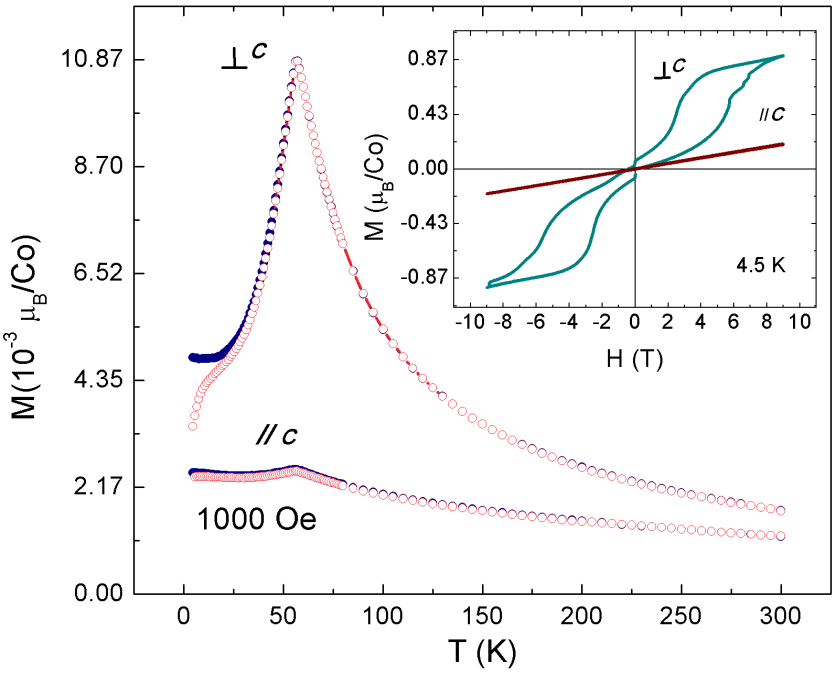

Figure 4-4: $Co_{4.76}Al_{1.24}(O_2BO_3)_2$ magnetization versus temperature under an applied field of 1000 Oe in both regimes: field cooled (FC, closed symbol) and zero field cooled (ZFC, open symbol) for oriented crystals. The inset shows the hysteresis loops for oriented crystals at 4.5 K.

4.2.4 Specific Heat Measurements

Specific heat measurements as a function of temperature and magnetic field were performed in 3 mg of randomly oriented needles crystals using a commercial Quantum Design PPMS at CBPF. Figure 4-5 and Figure 4-6 show the results.

Figure 4-5 shows the specific heat curves plotted as C/T versus T, with applied magnetic fields of 9, 5, 3 and 0 T. The specific heat at 0 T has a peak at $T_C = 57$ K that shifts to lower temperatures with increasing applied magnetic fields and eventually disappears. This behavior is observed for the first time in Co ludwigites and is characteristic of systems with FIM coupling. For sufficiently high magnetic fields there is no sign of FIM transitions. The specific heat is substantially reduced in the large field, which points out to a contribution from magnetic excitations that are quenched by the 9 T magnetic field.

The inset of Figure 4-5 shows the low-temperature specific heat for 0 and 9 T applied magnetic fields. A T^2 power law can fit the data in both cases. This contribution can arise due to gapless excitations with a linear dispersion relation, $\hbar\omega = vk$ in two-dimensional (2D) systems. A calculation presented in Appendix A in this case yields,

$$C = 14.4R(T/T^*)^2 = aT^2 \quad (1)$$

where R is the universal gas constant and the characteristic temperature T^* is related to a cut-off wave-vector k_C by $k_B T^* = vk_C$. It seems that in an applied magnetic field of 9 T, for the low temperatures, the magnetic excitations are quenched due to the Zeeman gap. In this case, we attribute the specific heat entirely to the excitation of 2D acoustic phonons with linear dispersion. Using the fitting coefficient $\alpha\,(9\,T) = 0.00194\,J/mol$ K^3 obtained from the inset of Figure 4-5 and replacing it in eq. (1) one gets the characteristic elastic temperature, $T_E{}^* = 252$ K. This is of the order of magnitude of the Debye temperature obtained for other ludwigites [10, 7, 20, 21]. In zero applied magnetic fields it is natural to assume that the T^2 term arises due to the contribution of both, 2D phonons and 2D FIM magnons with linear dispersion, given by the relation

$$C = 14.4R\left(\frac{1}{T_E^{*2}} + \frac{1}{T_M^{*2}}\right)T^2 = \alpha T^2. \quad (2)$$

Since the experiments yield $\alpha\,(0\,T) = 0.00295\,J/mol\cdot$K^3, using $T_E{}^* = 252$ K in eq. (2) we obtain $T_M{}^* = 344$ K. This is to be compared with the Curie-Weiss temperature or the magnetic ordering temperature. Then, our assumption that the low-temperature specific heat of $Co_{4.76}Al_{1.24}(O_2BO_3)_2$ ludwigite is due to linear dispersing elastic and magnetic excitations in planes gives a consistent description of the thermodynamic properties of this system at low temperatures.

Figure 4-6 shows the entropy as a function of temperature obtained from the specific heat curves of $Co_{4.76}Al_{1.24}(O_2BO_3)_2$ at applied fields of 0, 3, 5 and 9 T. Notice that the curve for the 3 T magnetic field presents *the inverse magnetocaloric effect* since the entropy at this field is larger than that in zero field for a given range of temperature ($23 \lesssim T \lesssim 54$ K). Similar behaviors have been observed in other ferromagnetic systems at low temperatures and applied magnetic fields [33, 34]. The sensitivity of the variation in magnetic entropy as a function of temperature for different magnetic fields ($-\Delta S = 7.5$J kg^{-1} K^{-1} at 80 K for $\Delta H = 9$) makes this compound likely for application in magnetic refrigeration.

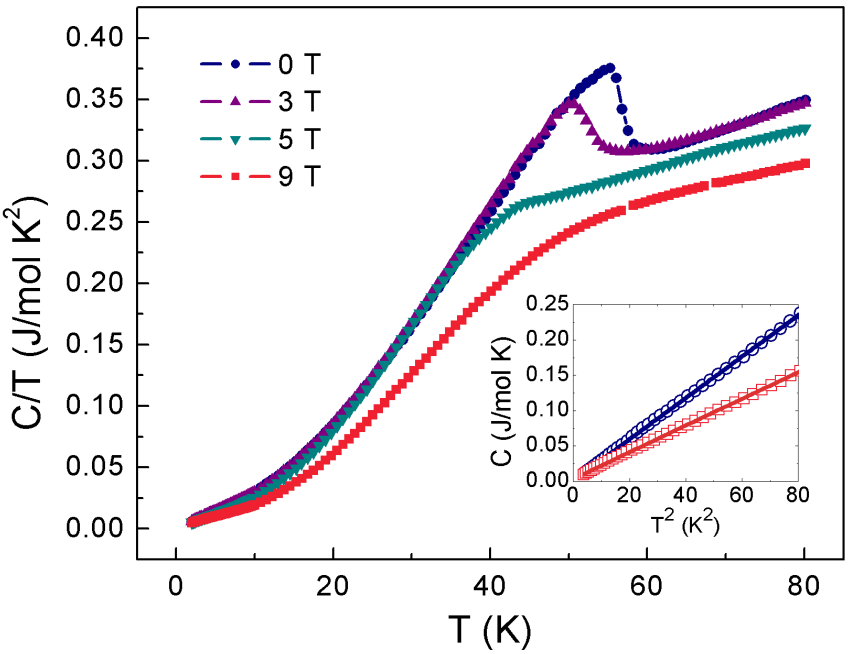

Figure 4-5: $Co_{4.76}Al_{1.24}(O_2BO_3)_2$ specific heat as C/T vs. T for applied magnetic fields of 0 to 9 T. Inset: Low-temperature specific heat versus temperature square for 0 and 9 T. The lines are fittings to a power law, $C = aT^2$ (see text).

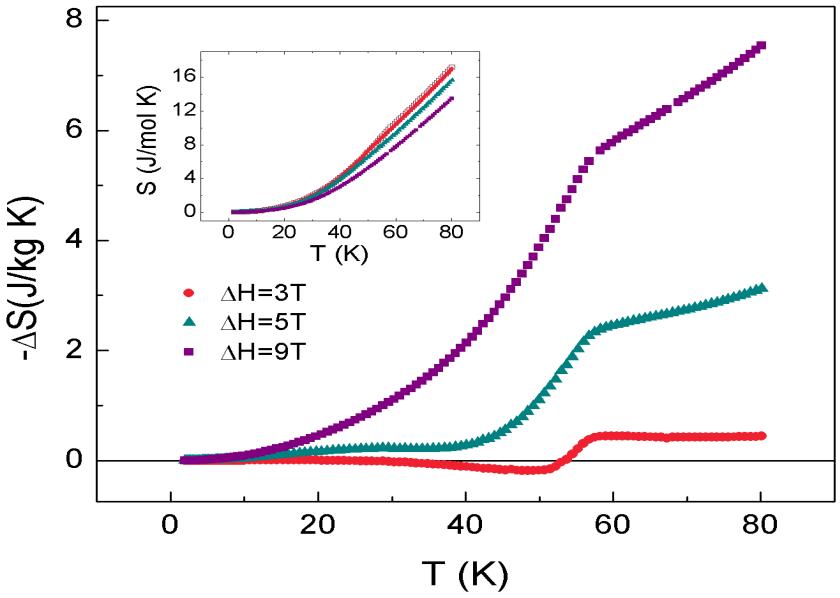

Figure 4-6: Isothermal magnetic entropy change ($-\Delta S = S(H = 0) - S(H \neq 0)$) of $Co_{4.76}Al_{1.24}(O_2BO_3)_2$ as a function of temperature for magnetic field changes up to 9 T. Inset: Entropy as a function of temperature obtained from the specific heat curves for the $Co_{4.76}Al_{1.24}(O_2BO_3)_2$ at applied fields of 0, 3, 5 and 9 T.

4.3 Discussion

In this chapter, we reported the synthesis and an extensive characterization by x-ray diffraction, magnetization, and specific-heat experiments of the new ludwigite $Co_{4.76}Al_{1.24}(O_2BO_3)_2$.

In $Co_3O_2BO_3$ ions with charge 3+ occupy sites 4 leaving sites 1, 2, and 3 to be occupied by ions with charge 2+ [7]. Single-crystal x-ray experiments in $Co_{4.76}Al_{1.24}(O_2BO_3)_2$ have shown that Al^{3+} enters mainly in site 4 and in a minor proportion in sites 2 and 1 (see Table 4-3). Here it is important to point out that the presence of Al^{3+} at different sites in $Co_{4.76}Al_{1.24}(O_2BO_3)_2$ forces a fraction of Co ions at site 4 (at least ~20%) to adopt the valence 2+, in order to preserve charge balance.

Site 4 is the metallic site with the most symmetric oxygen environment, as shows the lowest V_{ZZ} value (see Table 4-4). Similar characteristic is found in other ludwigites [9, 23, 11, 31, 32]. It was speculated, in reference [32], that it could be the reason for the preferential occupation of site 4 regardless the type of metal ion as observed in several doped Co ludwigites [9, 23, 11, 31, 32]. However, different from the other Co ludwigites, in $Co_{4.76}Al_{1.24}(O_2BO_3)_2$ sites 4 and 2 have a comparable amount of Al, see Table 4-3.

The structural characteristics of $Co_{4.76}Al_{1.24}(O_2BO_3)_2$ could be related to the proximity of the effective ionic radii of Al (0.535 Å) to that of LS Co^{3+} (0.545 Å), that could be present in this compound as it is in $Co_3O_2BO_3$ (see Chapter 2). Just for comparison, the effective ionic radii of the HS Co^{3+} (0.61 Å) is larger and could be absent.

The dc-magnetization results show the presence of a long-range magnetic ordering below $T_C = 57$ K in $Co_{4.76}Al_{1.24}(O_2BO_3)_2$. This is confirmed by ac-susceptibility and specific heat measurements. The Curie Weiss temperature is small compared to T_C indicating competition between interactions with different signs and that frustration is important in this system.

The hysteresis loops in Figure 4-3 with sigmoidal shapes below the magnetic transition is unusual for ludwigites. The appearance of hysteresis for $T < T_t$, $H > H_t$ sets the existence of a tricritical point at (T_t, H_t) in the $T_C(H_C)$ phase diagram, such that, for $T < T_t$ and $H > H_t$ the FIM to PM transition becomes first order. The two maxima in

the $\partial M/\partial H$ curves point the limits of stability of these different phases coexisting at the first order line.

The phase diagram obtained from the $\chi'(T)$, $C(T)$ and $M(H)$ measurements is presented in Figure 4-7. This metamagnetic transition is related to magnetic ions in a frustrated state, which are flipped at moderate critical fields increasing the magnetization abruptly. Geometrical frustration is found in the 1 - 2- 3 magnetic layers ($b-c$ plane), in which site 2 is in a triangular coordination (see Figure 2-12). Hence, the HS Co^{2+} ions in site 2 are potential candidates to be in an unstable spin state due to geometrical frustration with an antiferromagnetic coupling. On the other hand, at the highest field measured on powder sample, Figure 4-3, the magnetic moment is $M_S \simeq 1.2\,\mu_B/Co \equiv 5.8\,\mu_B/f.u.$ The high value of magnetic moment at 9 T could be explained considering 4 magnetic ions (in sites 1, 2 and 3) per formula unit in a (non-compensated) AFM structure with soft magnetically frustrated ions, probably located in site 2. In zero applied magnetic fields the moments are almost compensated with two spin up and two spin down (↑↓↑↓) giving a small magnetization signal as observed in Figure 4-3. As the applied magnetic field increases, the metamagnetic transition take place and the frustrated spins establish a structure with three spin up and one down (↑↑↑↓) whose value for the magnetic moment is expected to be $M = gS \simeq 6\,\mu_B/f.u.$, if a spin only (S = 3/2) system is considered. These results are consistent with the presence of frustrated magnetic spins. A confirmation of these magnetic couplings is expected with other experimental technique such NPD.

Specific heat results indicate ferrimagnetic ordering too, as the peak is suppressed and shifted to lower temperatures with increasing applied magnetic fields. This behavior is unusual in Co ludwigites. Applied magnetic fields on specific heat measurements usually smooth down the peak without shifting in temperature as seen in CoO_2BO_3 [7] and $Co_5Sn(O_2BO_3)_2$ [20]. For sufficiently strong magnetic fields there is no sign of FIM transitions in agreement with the magnetic phase diagram shown in Figure 4-7. The fit at low temperatures shows a dominant T^2 contribution either in zero applied magnetic fields or under a 9 Tesla field. This suggests the presence of magnetic excitations and elastic excitations with a linear dispersion and essentially two-dimensional character. This contribution was also observed in two-dimensional compounds, as in the hulsite $Co_5Sb(O_2BO_3)_2$ formed by two families of parallel sheets [35]. It is interesting that from

the point of view of the elastic properties the present system also presents two-dimensional character. A possible scenario for the magnetic structure of $Co_{4.76}Al_{1.24}(O_2BO_3)_2$ consist of magnetic planes composed by Co^{2+} in sites 1, 2, and 3 (1-2-3 planes), those separated by nonmagnetic ions (Al^{3+} and LS Co^{3+}). A similar scenario that $Co_3O_2B_2O_3$ (section 2.4) presents, where LS Co^{3+} occupies site 4 (see Figure 2-12). This scenario is also compatible with frustration of the magnetic ions at sites 2 due to a planar triangular coordination and that is increased by the presence of nonmagnetic Al ions in this site [36]. As a consequence of the softly frustrated site 2, metamagnetic transitions could take place.

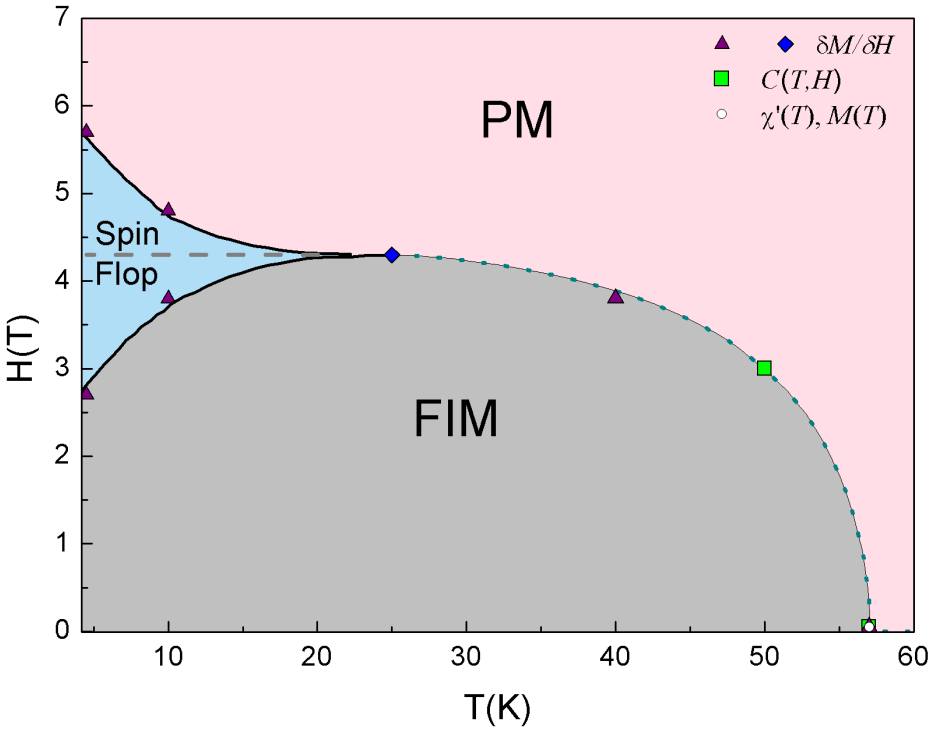

Figure 4-7: Phase diagram of the $Co_{4.76}Al_{1.24}(O_2BO_3)_2$. Phase boundaries were determined as follows: White circle is data obtained from the magnetic susceptibility $\chi(T)$ and magnetization $M(T)$. Green squares from specific heat $C(T; H)$ and purple triangles are from $\partial M/\partial H$. A tricritical point separating the lines of second and first order transitions appears at (H_t= 4.2 T, T_t= 25 K), indicated by a blue diamond symbol. The *spin flop* phases are in fact metastable phases where FIM and PM phases coexist.

On the other hand, $Co_6(O_2BO_3)_2$ and $Co_{4.76}Al_{1.24}(O_2BO_3)_2$ are characterized by a small entropy release at *Tc,* see Figure 4-8. For comparison Table 4-5 shows the total entropy (S) released at T_C and the magnetic entropy (S_M) for $Co_6(O_2BO_3)_2$, $Co_{4.76}Al_{1.24}(O_2BO_3)_2$

and $Co_5Sn(O_2BO_3)_2$. The magnetic entropy was calculated using $S_M = n \times R \times Ln(2S + 1)$, where n is the number of magnetic ions per f.u., R the universal gas constant, and S the spin moment. The total entropy released at T_C for $Co_6(O_2BO_3)_2$ and $Co_{4.76}Al_{1.24}(O_2BO_3)_2$ is less than the magnetic entropy. Taking into account that in $Co_6(O_2BO_3)_2$ and $Co_{4.76}Al_{1.24}(O_2BO_3)_2$ the magnetic ions occupy mainly sites 1, 2 and 3, and that this sites form planar substructures; the small entropy release at T_C could be related to this low dimensional arrangement of the magnetic ions. In $Co_5Sn(O_2BO_3)_2$, however, the magnetic atoms are not restricted to planar substructures, since Co^{2+} occupies 50% of site 4 and in this case, the value of the total entropy released is higher than the magnetic entropy.

Table 4-5: Magnetic entropy considering a LS Co^{3+} (S_M) state and the total entropy (S) released at T_C.

	S_M	$S(T_C)$
	J/mol K	J/mol K
$Co_6(O_2BO_3)_2$	46.1	27.4
$Co_{4.76}Al_{1.24}(O_2BO_3)_2$	46.1	13
$Co_5Sn(O_2BO_3)_2$	57.6	65.68

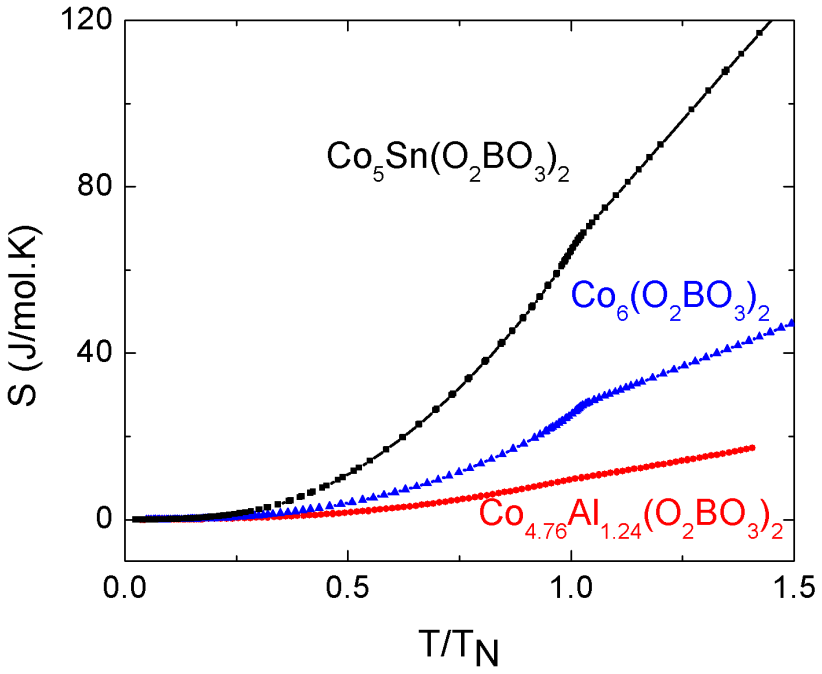

Figure 4-8: Entropy curves for $Co_6(O_2BO_3)_2$ [7], $Co_{4.76}Al_{1.24}(O_2BO_3)_2$ and $Co_5Sn(O_2BO_3)_2$ obtained from specific heat results as functions of temperature.

Chapter 5. Structural and magnetic studies in ludwigite $Ni_5SnB_2O_{10}$

5.1 Introduction

To extend the understanding of the complex magnetic behavior in oxyborates type ludwigite, we study the structural and magnetic properties of a Ni ludwigite. Ludwigites containing Ni atoms have a heterometallic composition: $Ni_2FeO_2BO_3$ [10], $Ni_2MnO_2BO_3$ [37, 38], $Ni_2VO_2BO_3$[39], $Ni_2CrO_2BO_3$ [39], Ni_2AlBO_5[40], $Ni_5SnB_2O_{10}$ [41], $Ni_5GeB_2O_{10}$ [42], Ni_2GaBO_3[43], $Ni_5TiB_2O_{10}$ [44]. Most of these ludwigites only have a structural characterization. The Ni ludwigites in which the magnetic properties were studied have shown: magnetic order of Fe ions at ~107 K and a spin freezing of the Ni ions at ~46 K in $Ni_2FeO_2BO_3$ [10], pole reversal magnetization in $Ni_2MnO_2BO_3$ [37] and a partial magnetic order or spin glass state in $Ni_5GeB_2O_{10}$ [42].

In this chapter, we study the structural and magnetic properties of the ludwigite $Ni_5Sn(O_2BO_3)_2$ through X-ray diffraction, ^{119}Sn Mössbauer spectroscopy, magnetization and specific heat techniques. Previously the crystalline structure of this compound was studied [41]. From reference [41], $Ni_5Sn(O_2BO_3)_2$ is known to belong to the space group *Pnma* and not to the usual *Pbam.* This is due to the periodical distribution of the Sn ions on site 4. However, in the present study, the Sn ions have a random distribution on site 4 and the ludwigite $Ni_5Sn(O_2BO_3)_2$ we synthesized belong to the space group *Pbam*.

From the study of the Co ludwigites with nonmagnetic ions, $Co_5Sn(O_2BO_3)_2$ stand out for having a magnetic order at the highest temperature (82K). In this study, ludwigite $Ni_5Sn(O_2BO_3)_2$ have exactly the same crystalline structure as $Co_5Sn(O_2BO_3)_2$, but now the spin of the Ni^{2+} is $S = 1$ instead of the spin $S = 3/2$ of the Co^{2+}. We are interested in understanding the role played by the spin size in the magnetic properties of the ludwigites. Preliminary results indicate a complex magnetic behavior with partial magnetic ordering close to 80 K, and a second magnetic order at ~6 K.

5.2 Experimental

5.2.1 Synthesis

The synthesis was performed at the laboratory facilities of the IF-UFF. Dark-green needle crystals of $Ni_5Sn(O_2BO_3)_2$ were obtained from a mixture of NiO_2: SnO_2: H_3BO_3 in 5: 1: 2 molar proportions respectively with an excess of borax. The mixture was heated at 1160 °C for 30 minutes and cooled down to 600 °C for 24 hours. Then the furnace was turned off. The resultant compound was dissolved in hot water and the crystals cleaned with diluted hydrochloric acid in an ultrasonic bath at 50 °C. The presence of Sn in the crystals was confirmed by ^{119}Sn Mössbauer Spectroscopy. X-ray powder diffraction confirms the a single phase corresponding to the $Ni_5Sn(O_2BO_3)_2$

5.2.2 Structural Characterization

A single needle crystal was used for x-ray diffraction experiments. The measurement was carried out on a D8 Venture Bruker diffractometer at room temperature, using IμS microfocus X-ray and MoKα radiation. The crystal was mounted on a Kappa goniometer, and data collection was performed using a PHOTON 100 detector. Data collection and cell index were performed with APEX2 v4.2.2 [45]. Data integration was carried out using SAINT[46]. Multiscan absorption correction was performed with the SADABS program [47]. The Fullmatrix least-squares refinements based on F^2 with anisotropic thermal parameters were carried using SHELXL-2013 program packages[48] with WINGX [49] and ShelXle [50] software interface. Crystallographic tables were generated by WINGX. Crystal data, data collection parameters, and structure-refinement data are shown in

Table 5-1.

.

Table 5-1: Crystal data and structure refinement of $Ni_5Sn(O_2BO_3)_2$.

Empirical formula from x-ray analisys	$Ni_{9.99}Sn_{2.01}B_4O_{20}$

Formula weight	1188.44
Temperature	293(2) K
Wavelength	0.71073 Å
Crystal size	$0.026 \times 0.058 \times 0.092$ mm^3
Crystal system	Orthorhombic
Space group	*P b a m*
Unit cell dimensions a=	9.2865(3) Å
b=	12.2664(4) Å
c=	3.04640(10) Å
Volume	347.02(2) Å^3
Z	1

Table 5-2 shows the fractional coordinates, site occupancy factor (SOF), normalized site occupancy (Occ.), and equivalent isotropic displacement parameters (Ueq.). Sites 1, 2 and 3 are exclusively occupied by Ni atoms. Site 4 is randomly occupied by Sn and Ni ions in the same proportion. The ^{119}Sn Mössbauer experiments shown that Sn atoms have oxidation number 4+. So, the charge balance ascribes oxidation number 2+ for all the Ni ions. Just for comparison, the lattice parameters, atomic occupation and interatomic distances of this compound are very similar to those of the $Co_5Sn(O_2BO_3)_2$.

Table 5-2: Fractional coordinates, site occupation factor (SOF), the normalized occupancy (Occ.) and the equivalent isotropic displacement parameters (Å^2×10^3) for $Ni_5Sn(O_2BO_3)_2$. U(eq) is defined as one-third of the trace of the orthogonalized Uij tensor. Multiplying the SOF factor by 8 gives the number of atoms in the unit cell [25].

Site	*x/a*	*y/b*	*z/c*	SOF	Occ.	U(eq)
Ni1(2a)	1.0	0	0	0.25	1	6(1)
Ni2(2d)	0.5	0	0.5	0.25	1	8(1)
Ni3(4g)	0.4975(1)	0.2177(1)	0	0.5	1	6(1)
Ni4(4h)	0.7600(10)	0.1152(8)	0.5	0.253	0.506	5(1)
Sn4(4h)	0.7600(5)	0.1156(4)	0.5	0.247	0.494	5(1)
O2	0.6488(2)	0.2633(2)	0.5	0.5	1	7(1)
O1	0.6125(2)	0.0777(2)	0	0.5	1	7(1)
O4	0.8509(2)	-0.0423(2)	0.5	0.5	1	7(1)
O3	0.3737(2)	0.1408(2)	0.5	0.5	1	7(1)
O5	0.8953(2)	0.1431(1)	0	0.5	1	5(1)
B1	0.7254(3)	0.3606(2)	0.5	0.5	1	7(1)

Table 5-3: Selected bond lengths (Å) for $Ni_5Sn(O_2BO_3)_2$.

Ni1-O5	2.0066(18)	Ni4-O1	2.100(7)
Ni1-O4	2.1228(12)	Ni4-O4	2.109(10)
Ni2-O1	2.0780(13)	O2-B1	1.389(4)
Ni2-O3	2.0877(18)	O4-B1	1.386(3)
Ni3-O5	1.9535(18)	O3-B1	1.377(4)
Ni3-O1	2.022(2)	Ni4-Ni2	2.797(10)
Ni3-O3	2.1282(13)	Ni3-Ni1	3.4634(4)
Ni3-O2	2.1469(13)	Ni3-Ni2	3.0739(4)
Ni4-O5	2.004(6)	Ni4-Ni3	3.135(5)
Ni4-O2	2.090(10)	Ni4-Ni1	3.049(5)

5.2.3 Magnetic measurements

The DC magnetization measurements were performed in both powder and oriented single crystals of $Ni_5Sn(O_2BO_3)_2$ using a commercial Quantum Design SQUID-VSM at UFSCar, with the assistance of the Ph.D. student Raphael Garcia. The results of the magnetic measurements are shown in Figure 5-1 to Figure 5-4.

Figure 5-1 shows magnetization measurements in oriented crystals with applied magnetic field of 100 Oe along (//) and perpendicular (⊥) to the c axis. The magnetic susceptibility response is compatible with an anisotropic compound with the easy magnetization direction on the *a*-*b* plane, as observed previously on Co ludwigites. In the inset of Figure 5-1 is observed an abrupt change of the derivative of the magnetization at $T_c = 80K$ which correspond to the magnetic ordering temperature. This Tc is very close to the magnetic ordering temperature found in $Co_5Sn(O_2BO_3)_2$ ($82\ K$). For lower temperatures, the ZFC and FC curves separate. From the linear fit of the inverse dc susceptibility above 120 K, we obtained the Curie-Weiss temperature $\theta_{CW} = -82.8$ K and the Curie constant $C = 6.12 \times 10^{-3}$ emu.K/g.Oe. The negative value of θ_{CW} indicates the predominance of antiferromagnetic interactions. From the Curie constant, the effective moment per f.u. $p_{eff} = 5.39\ \mu_B$ is determined. The spin only moment per f.u. of $Ni_5Sn(O_2BO_3)_2$ with $S = 1$ gives $p = 5.65\mu_B$. Then, the effective moment observed for the Ni is consistent with a null orbital contribution, characteristic of a $3d$ transition metal. This result contrast with the large orbital contribution observed for the Co ions in the ludwigite $Co_5Sn(O_2BO_3)_2$.

The ac-susceptibility measurements with were performed at UFES with a Quantum Design PPMS. Figure 5-2 shows the real part of the ac-susceptibility measurements for different frequencies as a function of temperature. The small peak observed at $T_c = 80$ K could be attributed to a partial magnetic order. Similar behavior was observed in $Fe_3O_2BO_3$ for the partial magnetic order of the 4-2-4 ladder at 112 K [8, 28]. The position of the peak barely moves to lower temperatures (less than 0.5K) for changes of two decades in the frequency. This result is consistent with a long range magnetic ordering of part of the Ni ions. A partial magnetic ordering is confirmed by specific-heat and Mössbauer spectroscopy experiments as will be shown forward. We remark the presence of steps in the ac susceptibility curve close to the peak at 80 K, which are also observed in the derivative of the dc magnetization (see inset Figure 5-1). These steps could be related with reorientations of the spins occurring below the temperature magnetic transition. At low temperatures a second and higher peak is observed at 5 K in the ac susceptibility curve. The position of this peak barely changes with frequency (2 K for two decades change in frequency). This peak temperature corresponds with a plateau in the dc magnetization, which is better seen in the inset of Figure 5-1, with a zero derivative value.

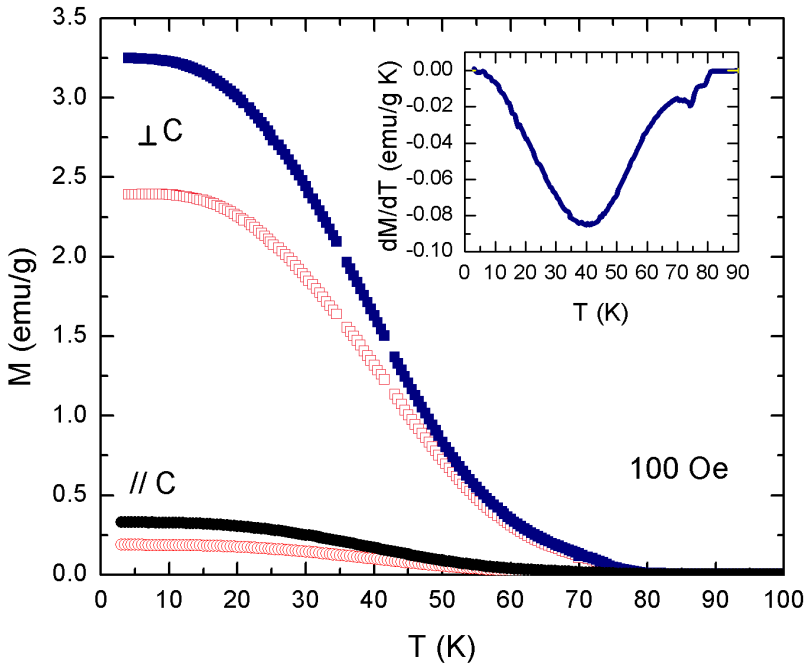

Figure 5-1: Magnetization versus temperature under an applied field of 100 Oe in both regimes: field cooled (FC: closed symbol) and zero-field cooled (ZFC: open symbol) for oriented crystals of $Ni_5Sn(O_2BO_3)_2$. The inset shows

the derivative of the FC curve with applied magnetic field perpendicular to the *c* axis.

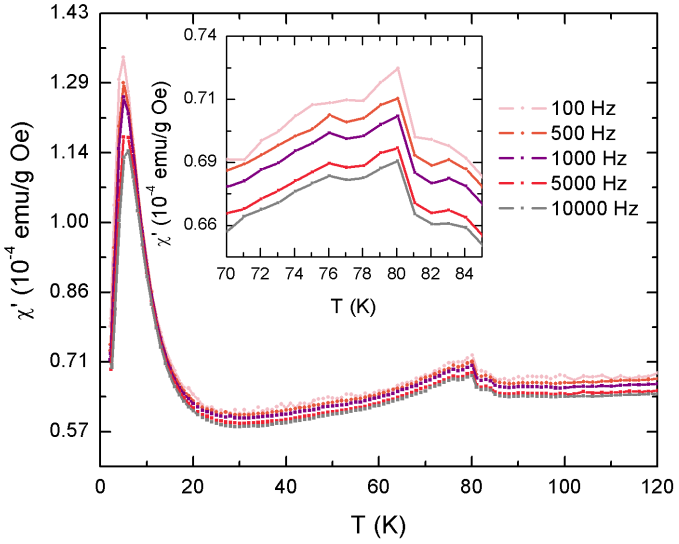

Figure 5-2: Real (χ') part of the ac magnetic susceptibility as functions of temperature of powder sample of $Ni_5Sn(O_2BO_3)_2$ for different frequencies. The amplitude of the oscillating magnetic field is 10 Oe.

Figure 5-3 shows the magnetic hysteresis loops at 3K and 50 K in oriented crystals of $Ni_5Sn(O_2BO_3)_2$. Measurements perpendicular to the *c* axis have open loops characteristics of compound with ferromagnetic, ferrimagnetic or weak ferromagnetic behavior. Considering that the interactions are of antiferromagnetic nature and all the ions involved have the same spin, a canted AFM structure resulting in a weak ferromagnetism probably occurs below the magnetic transition temperature. For low fields (less than 2T) the hysteresis loops are highly anisotropic showing that the easy magnetization direction is on the *a*-*b* plane (Figure 5-3), as also occurs in the Co ludwigites. However, for higher applied magnetic fields the anisotropy is strongly reduced, for instance at 9 T the value of the magnetization parallel to *c* axis is comparable to the value of the magnetization perpendicular to *c* axis (Figure 5-3). This result found for the $Ni_5Sn(O_2BO_3)_2$ is different from what happens in the Co ludwigites where the magnetization values at 9T is strongly dependent of the direction (Figure 3-7).

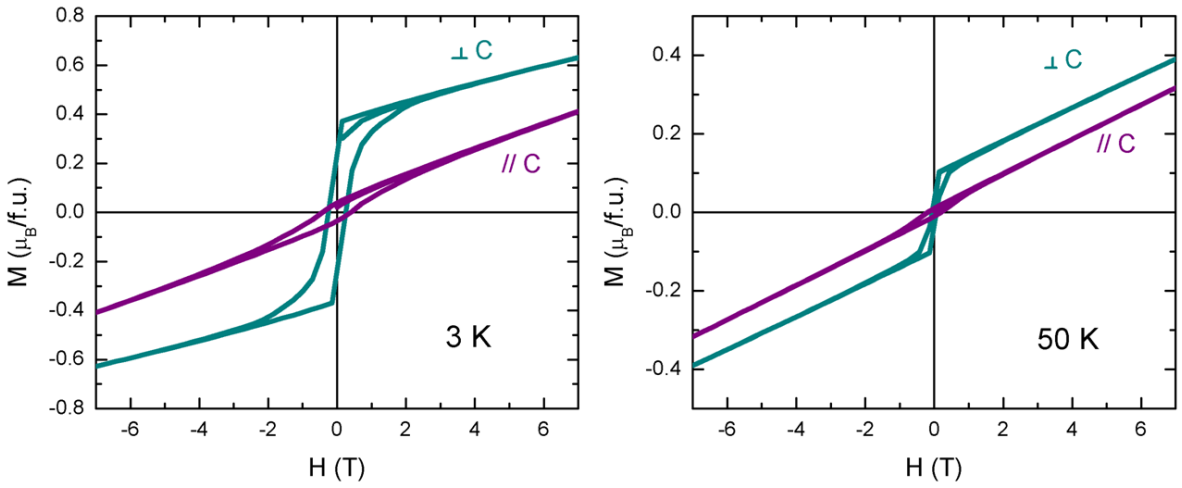

Figure 5-3: Magnetization versus applied magnetic fields for oriented crystals at 3 K (left) and 50 K (right).

Figure 5-4 shows the magnetic hysteresis loops of powder samples of $Ni_5Sn(O_2BO_3)_2$ for different temperatures. At 100 K the magnetization has a linear paramagnetic behavior. Below T_C it is observed open hysteresis loops down to the lowest reached temperatures. Applied fields of 7 T are not strong enough to saturate the magnetization, however, for comparison, we will be consider: $M_S(7\ T) = gS \approx 0.9\mu_B/f.u.$, considering $g = 2$, gives $S \approx 1/2$, this is half the spin value of one Ni^{2+}ion per f.u. Different from $Co_5Sn(O_2BO_3)_2$ that has a saturation moment with an effective spin moment equal to one Co^{2+} ion per f.u. Moreover, there are no signals of magnetic jumps found in powder measurements of $Co_5Sn(O_2BO_3)_2$.

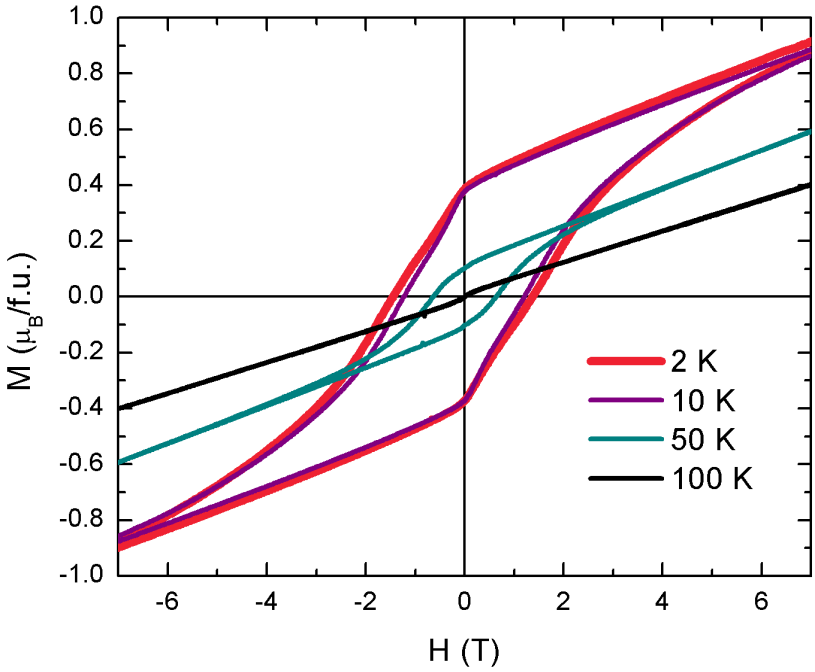

Figure 5-4: Magnetization versus applied magnetic fields of powder sample of $Ni_5Sn(O_2BO_3)_2$ for different temperatures.

5.2.4 Specific heat measurements

Specific heat measurements as a function of temperature and magnetic field were performed with randomly oriented needles crystals using a commercial Quantum Design Dynacool PPMS at CBPF. Results are shown in Figure 5-5 and Figure 5-6.

Figure 5-5 shows the specific-heat curves plotted as C/T versus T for applied magnetic fields of 0 and 5 T. As expected, the specific heat decrease with temperature, however at ~80 K a raise of the specific heat is observed, reaching a maxima at ~75 K. These temperatures correspond to anomalies observed in the dc and ac magnetic measurements. A second increase of the specific heat occurs at ~60 K reaching a maximum at ~52 K. The application of a magnetic field of 5 T slightly move the peaks to higher temperatures see inset of Figure 5-5). The two wide peak observed in $Ni_5Sn(O_2BO_3)_2$ contrast with only one sharp peak observed in $Co_5Sn(O_2BO_3)_2$.

Figure 5-6 shows the low temperature specific-heat curves plotted as C versus T for 0 and 9 T. There is no clear anomaly in the 0 T specific heat curve that could correspond to the peak observed at 5 K in the ac-susceptibility (Figure 5-2). The low temperature data were fitted with a temperature dependent equation $C = \gamma T + \alpha T^2$ (Figure 5-6).

For the 0 T curve the linear term is dominant. As mentioned in previous chapters, the linear term in ludwigites is related with a spin glass system or magnetic frustration, as in ludwigite $Co_5Ti(O_2BO_3)_2$. For an applied magnetic field of 9T, the T^2 term becomes dominant. This unexpected T^2 dependence in $Ni_5Sn(O_2BO_3)_2$ could indicate a 2D antiferromagnetic magnons or phonons as in $Co_{4.76}Al_{1.24}(O_2BO_3)_2$.The linear coefficient at 0 T, $\gamma(0\ \mathrm{T}) = 10.3$ mJ/mol K^2, is of the order of that observed on the $Co_5Ti(O_2BO_3)_2$, indicating a strong magnetic frustration. In $Ni_5Sn(O_2BO_3)_2$, the application of a magnetic field of 9 T reduce drastically this parameter ($\gamma(9\ \mathrm{T}) = 0$).

Figure 5-7 shows the temperature-dependent entropy in zero field obtained from the C/T vs T curve. At $T_c = 80$ K the entropy released is $S\ (T_C) = 66.2$ J/mol K, which is higher than the full magnetic entropy $S = 5\ R\ \ln(2(1) + 1) = 45.7$ J/mol K expected for five Ni^{2+} (S=1) per f.u. Those values are consistent with an entropy released due to lattice and magnetic contributions.

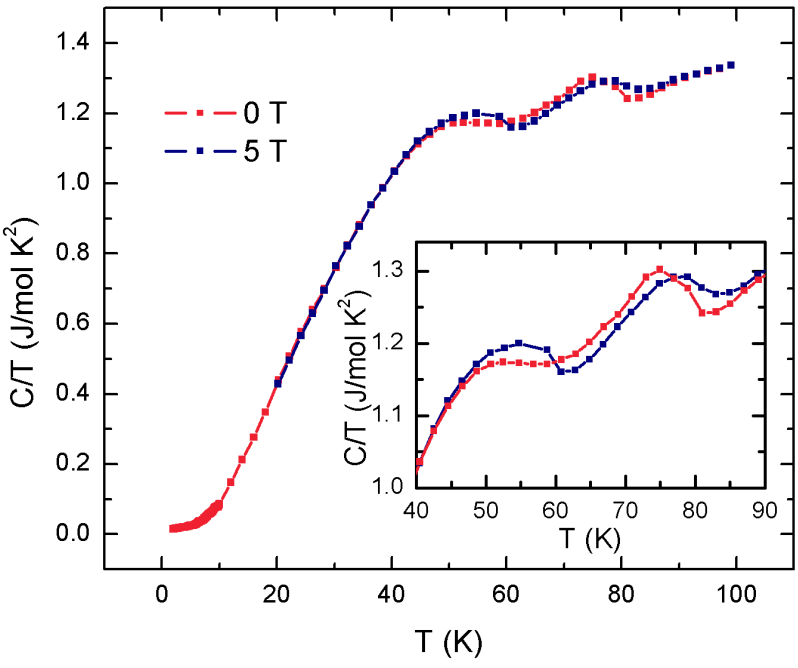

Figure 5-5: Specific heat of ludwigite $Ni_5Sn(O_2BO_3)_2$, plotted a C/T vs T for applied magnetic fields of 0 and 5 T. Inset: Entropy as a function of temperature obtained from the specific heat curves.

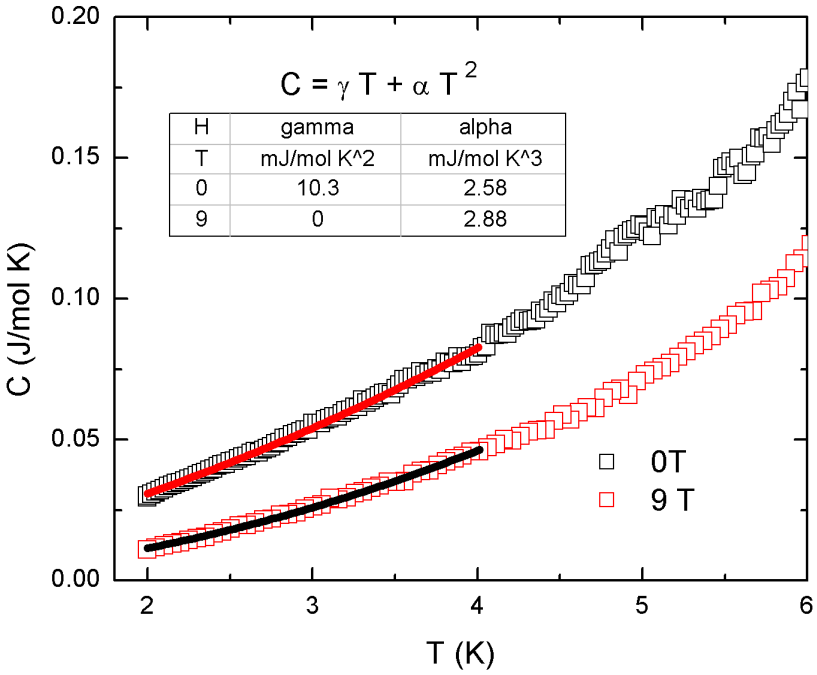

Figure 5-6: Low-temperature specific heat versus temperature for 0 and 9 T of ludwigite $Ni_5Sn(O_2BO_3)_2$. The lines through the data are fittings to a power-law $C = \gamma T + \alpha T^2$. The table inside shows the fitting parameters.

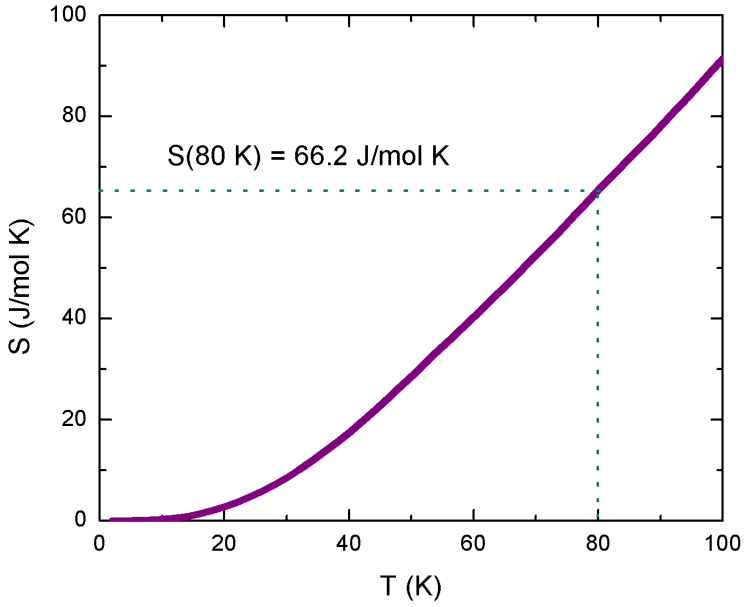

Figure 5-7: Entropy as a function of temperature for ludwigite $Ni_5Sn(O_2BO_3)_2$.

5.2.5 Mössbauer spectroscopy

The ^{119}Sn Mössbauer spectroscopy experiments were performed at CBPF. The spectra were taken with the ludwigite $Ni_5Sn(O_2BO_3)_2$ sample kept in a Montana variable temperature closed-cycle cryostat in the range temperature from 3 to 300 K. The ^{119}Sn:$CaSnO_3$ source was kept at room temperature, moving in a sinusoidal mode outside of the cryostat. To analyze the spectra the least-square fitting NORMOS program [51] was used. The ^{119}Sn Mössbauer spectra of $Ni_5Sn(O_2BO_3)_2$ as a function of temperature is shown in Figure 5-8. The hyperfine parameter obtained from the fit of the spectra are shown in Table 5-4.

As mention in previous chapters, the magnetic hyperfine field at the Sn nucleus is a transferred magnetic field from the magnetic moments of the neighboring Ni ions. Then, the magnitude and direction of the magnetic hyperfine field at the ^{119}Sn nuclei are determined by the resultant of the magnetic moments of the Ni atoms around the Sn ions [30]. To fit of the paramagnetic spectra between 200 and 75 K, only one paramagnetic doublet was used. The isomer shift (δ) values are in relation to $BaSnO_3$. The value of δ =0.26 mm/s at room temperature (RT) is consistent with an oxidation state 4+ for Sn [30]. The linewidth Γ=1 mm/s at RT indicates that Sn ions places at only one site, in agreement with the x-ray data presented above.

As we can see in Figure 5-8, below 75 K the spectra begin to broad magnetically, indicating the onset of magnetic interactions. This temperature is slightly lower than the temperature at which the susceptibility increases abruptly. The magnetic spectra were fitted with a single sextet indicating a static magnetism. The free fitting parameters wereδ, Γ, the hyperfine magnetic field (B_{hf}), the angle (θ) between the direction of B_{hf} and the principal axis of the electrical gradient field V_{ZZ}. Assuming no structural transitions the quadrupole splitting was left fixed to fit the low temperature Mössbauer spectra ($\Delta E_Q = -1.15$ mm/s) the value obtained at 200 K where the whole structure is paramagnetic. The other fitting parameters were left free. Figure 5-9 shows the temperature dependence of the hyperfine parameters B_{hf} and θ. The B_{hf} increases with decreasing temperature following a typical magnetization curve, reaching saturation at 30 K.

Table 5-4: Mossbauer hyperfine parameter of $Ni_5Sn(O_2BO_3)_2$ for temperatures between 200 and 4.2 K. The parameters are the temperature T, isomer shift δ, quadrupole splitting ΔE_Q, linewidth Γ, hyperfine magnetic field B_{hf} and angle θ between the B_{hf} and the principal axis of the electrical gradient field V_{ZZ}.

T(K)	δ (mm/s)	ΔE_Q (mm/s)	Γ (mm/s)	B_{hf} (T)	θ(°)
200	0.24	-1.15	1.11	-	-
90	0.26	-1.15	1.00	-	-
75	0.26	-1.15	2.54	0	-
70	0.26	-1.15	2.18	4.20	97
60	0.28	-1.15	1.30	6.75	77
50	0.27	-1.15	1.18	7.68	71
40	0.26	-1.15	1.10	8.14	66
30	0.26	-1.15	1.12	8.51	61
20	0.26	-1.15	1.14	8.58	59
3	0.26	-1.15	1.06	8.62	55

The presence of a single magnetic component could, in principle, indicate a relatively simple magnetic structure, $\theta \approx 55°$, could indicate disorder consistent with a spin glass system. Figure 5-10 shows the normalized $B_{hf}(T)/B_{hf}(3K)$ vs T/T_C of $Ni_5Sn(O_2BO_3)_2$, together with a normalized Brillouin function [29], for J=1/2 and J=1. The Brillouin function do not fit well the experimental data, as expected, indicating that the system is not a classical ferromagnet. In fact, the negative Curie Weis temperature indicate that AFM interactions are involved.

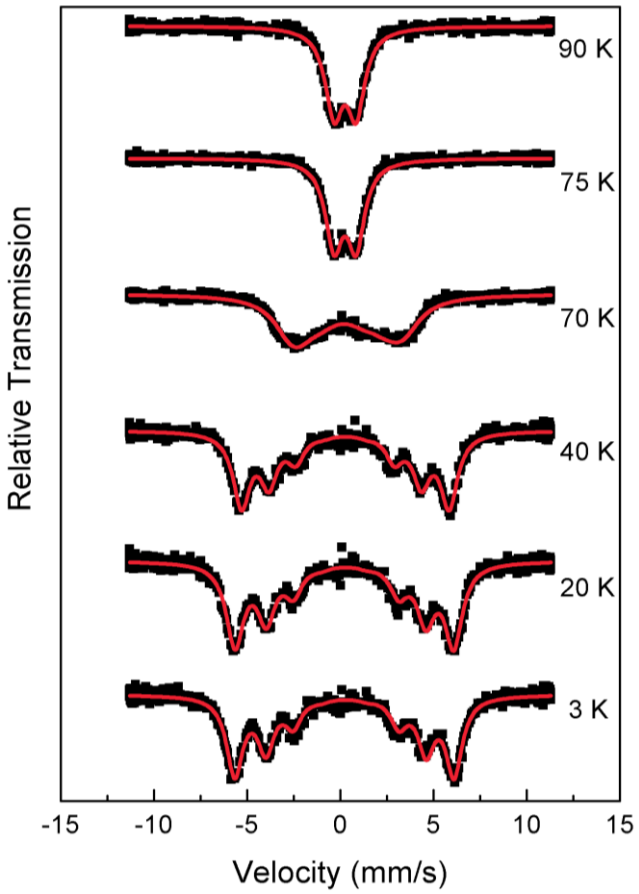

Figure 5-8: Some ^{119}Sn Mossbauer spectra of $Ni_5Sn(O_2BO_3)_2$ in the temperature range of $300 \geq T \geq 4.2$ K. Below 70 K the spectra were fitted with a single magnetic subspectra.

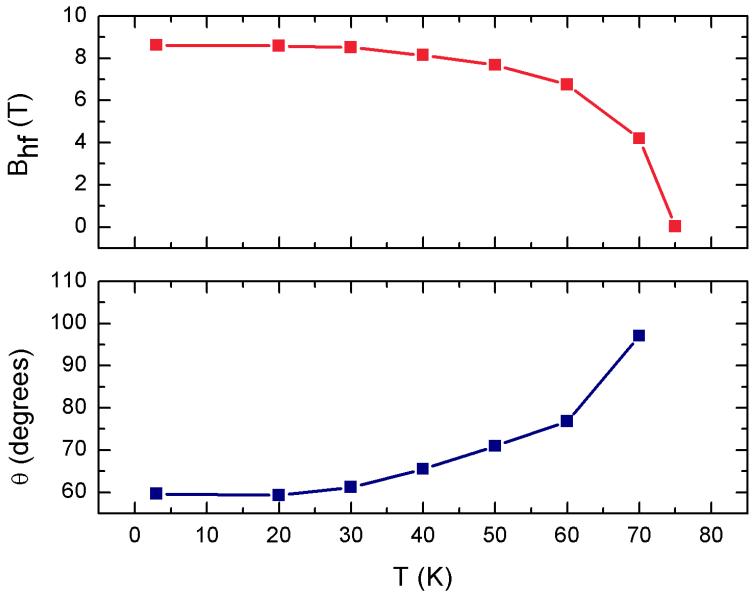

Figure 5-9: Temperature dependence of the ^{119}Sn Mössbauer fitting parameters B_{hf} and θ.

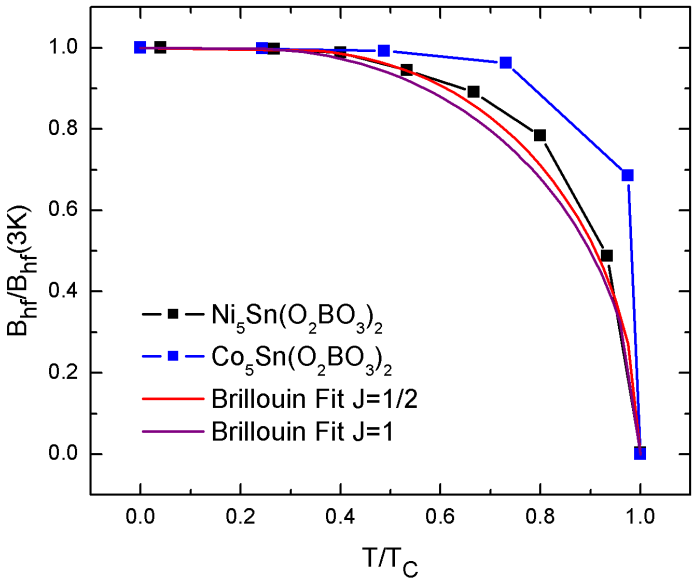

Figure 5-10: Normalized hyperfine magnetic field $(B_{hf}(T)/B_{hf}(4\ K))$ as a function of reduce temperature. Black square correspond to $Ni_5Sn(O_2BO_3)_2$, blue square to $Fe_3O_2BO_3$. Solid lines correspond to Brillouin fitting.

5.3 Discussion

The study of nonmagnetic dilution of Co ludwigite has shown that in $Co_5Sn(O_2BO_3)_2$ the 4+ oxidation state of the Sn ions, force the Co ions to adopt the 2+ oxidation state; as a result $Co_5Sn(O_2BO_3)_2$ has the biggest number of Co^{2+} per f.u. In addition, the preferential occupation of site 4 by Sn plays an important role to reduce magnetic frustration giving rise to high magnetic order temperatures. In $Ni_5Sn(O_2BO_3)_2$, nonmagnetic Sn ions occupy the site 4, the same place that it occupy in $Co_5Sn(O_2BO_3)_2$. $Ni_5Sn(O_2BO_3)_2$ and $Co_5Sn(O_2BO_3)_2$ have very similar lattice parameters and spin size, Ni with $S = 1$ and Co with $S = 3/2$. These similarities had suggested similar behaviors.

Surprisingly, the magnetic properties of $Ni_5Sn(O_2BO_3)_2$ are very different from that of $Co_5Sn(O_2BO_3)_2$. A partial magnetic ordering occurring in $Ni_5Sn(O_2BO_3)_2$ at 80K is consistent with a small peak on the susceptibility and a wide peak in the specific heat curves. Similar characteristic was observed on the partial magnetic order of $Fe_3O_2BO_3$ [5, 28]. A step like behavior of the magnetic order is also observed in $Ni_2MnO_2BO_3$ [38], which have similar inflection points at $T_O = 85$ K and $T = 71$K, the authors relate this behavior to the existence of several coupled magnetic subsystems being ordered

separately at different temperatures. For lower temperatures, below 10 K the dc-magnetization curve has a plateau, and the ac-susceptibility has a peak at 5 K, whose position is slightly affected by the frequency. At this temperature the specific heat curve does not have any signal of magnetic ordering, suggesting that this peak could be related with the establishment of a spin glass state. The spin glass state is supported by Mössbauer measurements where an angle of =55 is related with a random orientation of the magnetic moments. Finally, the high anisotropy observed for the low applied magnetic field is considerably reduced with high applied magnetic fields, behavior that has not been observed before in Fe and Co ludwigites, but was already observed in $Ni_{1.8}Mn_{1.2}O_2BO_3$ where the anisotropy is not only reduced but change the direction with applied magnetic fields along the *c* axis [37].

Chapter 6. Structural and magnetic studies of hulsite $Ni_{5.14}Sn_{0.86}(O_2BO_3)_2$

6.1 Introduction

Oxyborates with warwickite and ludwigite structures are known to present unconventional structural and magnetic properties with a strong unidimentional character. Those properties are related to their substructures in the form of ladder in ludwigites and ribbons in warwickites. It has been observed charge ordering transitions in ludwigite $Fe_3O_2BO_3$ and warwickite Fe_2OBO_3, partial magnetic order in ludwigites $Fe_3O_2BO_3$, $Co_2FeO_2BO_3$, and $Ni_2FeO_2BO_3$, and random singlet phase in warwickite $MgTiOBO_3$. On the other hand, oxyborates with hulsite structure are known to have a strong two-dimensional (2D) character related to planar substructures. They can be found in nature with an iron-based chemical composition; however, they are less explored because the difficulties found in the synthesis process.

Hulsite crystallizes in space group *P2/m* and have a general formula $M_{6-x}^{2+}M'^{5+}_{x}(O_2BO_3)_2$ where M and M' are metal ions that occupy five nonequivalent crystallographic sites in oxygen octahedral coordination that form two families of parallel sheets. Up to date, only two hulsites were synthesized, $Co_{5.52}Sb_{0.48}(O_2BO_3)_2$ and $Ni_{5.33}Sb_{0.67}(O_2BO_3)_2$, they were reported to present a conventional antiferromagnetic order of the whole structure at 42 K and 170 K respectively [35, 52], see .

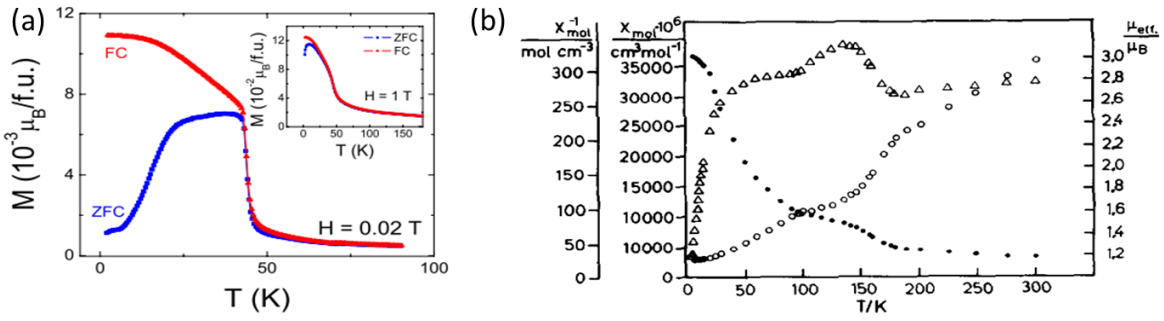

Figure 6-1: Magnetization as a function of temperature of (a) $Co_{5.52}Sb_{0.48}(O_2BO_3)_2$ [35] and (b) $Ni_{5.33}Sb_{0.67}(O_2BO_3)_2$ [52].

Here we synthesized a new hulsite with chemical formula $Ni_{5.14}Sn_{0.86}(O_2BO_3)_2$, and similar to their predecessors, $Co_{5.52}Sb_{0.48}(O_2BO_3)_2$ and $Ni_{5.33}Sb_{0.67}(O_2BO_3)_2$, it has a nonmagnetic ion in its structure. The advantage of studying $Ni_{5.14}Sn_{0.86}(O_2BO_3)_2$ is that it holds the Mössbauer Sn probe. Thus, the application of the Mössbauer spectroscopy technique, which has already been shown to be a very useful tool in the study of magnetism, will allow obtaining local information on the magnetic properties of this compound, information that is very difficult to get with the conventional techniques such as magnetization, specific heat and resistivity.

The magnetic transition temperature shown by this compound is one of the highest among oxyborates (≈180 K). The results point to a complex magnetic behavior consistent with two magnetic subsystems. A partial magnetic ordering of a subsystem formed by Ni ions located in a plane with a quadrangular arrangement occurs at 180K. On the other hand, the other subsystem formed by Ni ions located in a plane with a triangular arrangement does not order at temperatures as low as 3 K. The two subsystems coexist at low temperatures.

6.2 Experimental

6.2.1 Synthesis

The syntheses were performed at the laboratories of the IF-UFF. The synthesis of the crystals is from a 5: 1: 2 molar mixture of NiO_2: SnO_2: H_3BO_3 with an excess of borax. The mixture was heated at 1160 °C for 30 minutes and cooled down to 600 °C for 24 hours. Then the oven was turned off. The bath was clean with hot water and with diluted hydrochloric acid. The resulting crystals appear to be dark green and transparent in thin section. The planar-shaped crystals grow up to 2 mm length. X-ray powder and single crystal diffraction confirms the purity of the sample.

6.2.2 Structural Characterization

A planar shaped twin crystal was employed for data collection from x-ray diffraction. The measurement was carried out on a D8 Venture Bruker diffractometer at room temperature, using IμS microfocus X-ray, MoKα radiation. The crystal was mounted on a Kappa goniometer, and data collection was performed using a PHOTON 100 detector. Data collection was performed with APEX2 v4.2.2

[45]. CELL_NOW[53] was used for indexing two twin components generating a *p4p* file for integration. Data integration was carried out using SAINT[46]. Empirical numerical absorption correction was performed with the TWINABS program. The Fullmatrix least-squares refinements based on F^2 with anisotropic thermal parameters were carried using SHELXL-2013 program packages[48] with WINGX [49] and ShelXle [50] software interfaces. Crystallographic tables were generated by WINGX. Crystal data are displayed in Table 6-1.

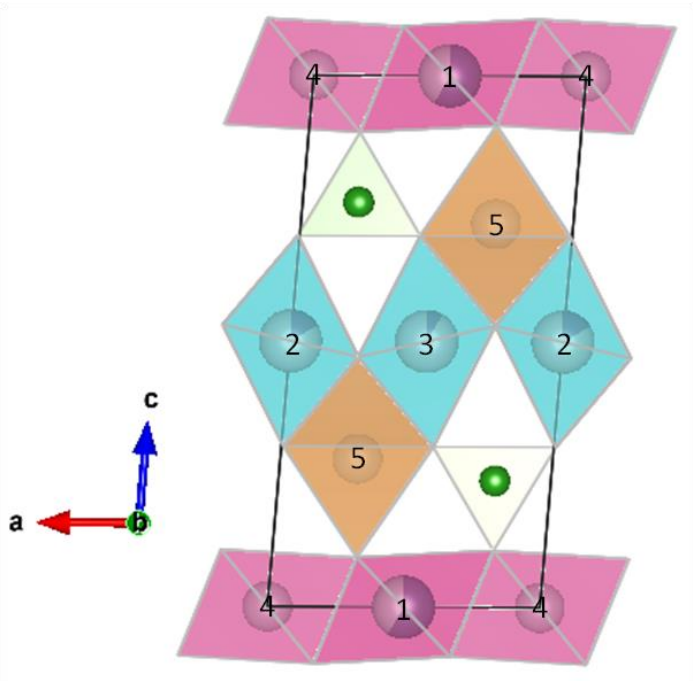

Figure 6-2: Schematic structure of a unit cell of hulsite $Ni_{5.14}Sn_{0.86}(O_2BO_3)_2$ formed by five metal sites within oxygen octahedra and boron in a triangular oxygen coordination. The structure is projected along the *b* axis. This figure was generated by Vesta 3.1.1 software[1].

Figure 6-2 shows a schematic structure of a unitary cell of hulsite $Ni_{5.14}Sn_{0.86}(O_2BO_3)_2$. The cell is composed of five metal sites within oxygen octahedra and boron in triangular oxygen coordination. Table 6-2 shows the fractional coordinates, the site occupation factor (SOF) and equivalent isotropic displacement parameters for $Ni_{5.14}Sn_{0.86}(O_2BO_3)_2$. The sites 1, 2 and 3 are occupied randomly by Ni and Sn ions, sites 4 and 5 are exclusively occupied by Ni atoms, see Figure 6-2. Oxidation numbers were obtained with XAFS experiments (not shown) for Ni ions that ascribe valence 2+ and Mössbauer experiments for Sn ions (shown later) that ascribe valence 4+. The main bond lengths in this compound are shown in Table 6-3. It is worth nothing the short distance between site 2 and 3 (~ 2.71 Å) compared with all other intermetallic distances that are higher than 3 Å.

Table 6-1: Crystal data of hulsite $Ni_{5.14}Sn_{0.86}(O_2BO_3)_2$.

Empirical Formula	$Ni_{5.14}Sn_{0.86}(O_2BO_3)_2$
Formula weight	585.16 g/mol
Wavelength	0.71073Å
Crystal Size	0.061 x 0.058 x 0.029 mm^3
Temperature	295(2) K
Crystal system	Monoclinic
Space group	*P2/m*
Unit cell dimension a =	5.4185(7) Å
b =	3.0504(4) Å
c =	10.6162(13) Å
β=	94.707 (4)°
Volume	174.81(4) $Å^3$
Z	1

The whole structure could be represented as formed by two planar substructures, one with rectangular arrangement of the Ni ions and the other with a triangular arrangement, which are linked by Ni atoms at sites 5. These sub-structures are represented in Figure 6-3, panels (a) and (b), the intermetallic coordination are

indicated by dark blue lines. Panel (a) shows the planar substructure with a rectangular coordination formed by metallic ions at sites 2 and 3 and we will refer in the following as "2–3–layer". In this layer, ~27% of the metallic ions are randomly occupied by nonmagnetic Sn^{4+} (see Table 6-2). Panel (b) shows the planar substructure with triangular coordination formed by sites 1 and 4 and we will name "1–4– layer". In this layer, 59% of the metallic ions at site 1 are randomly occupied by Sn^{4+} and the remaining by Ni^{2+}. The site 4 is occupied exclusively by Ni^{2+} ions.

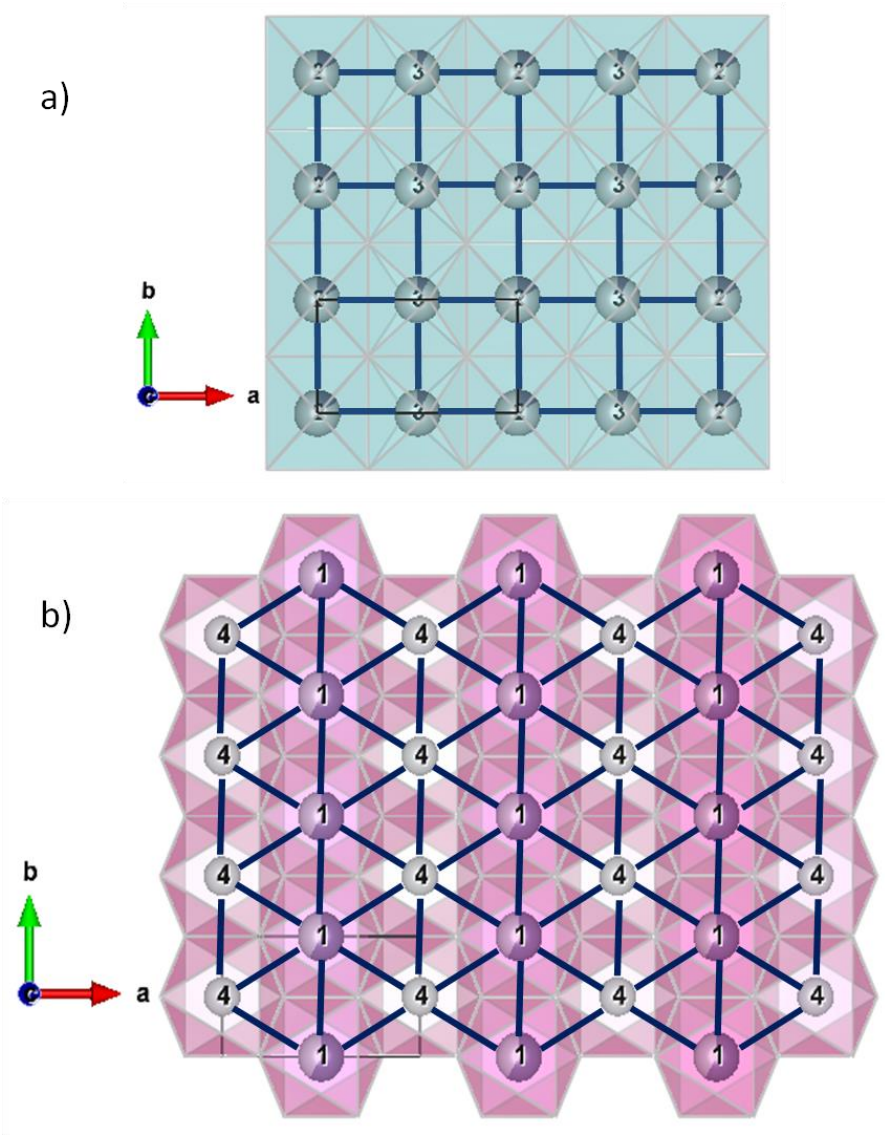

Figure 6-3: Schematic intermetallic coordinations in hulsite $Ni_{5.14}Sn_{0.86}(O_2BO_3)_2$. (a) Planar substructure formed by metal sites 2 and 3 in rectangular coordination (blue lines). (b) Planar substructure formed by metal sites 1 and 4 in triangular coordination (blue lines). These figures were generated by Vesta 3.1.1 software[1].

As we will see bellow, the principal physical properties of the hulsite $Ni_{5.14}Sn_{0.86}(O_2BO_3)_2$ are consistent with the presence of two magnetic subsystems which seem to be closely related with these two bidimensional substructures (5.0308 Å apart) which are linked by Ni at site 5. The site 5 is closer to 2–3 plane (2.32 Å) than from 1–4 plane (2.98 Å).

Table 6-2: Fractional coordinates, site occupancy factor (SOF), Occ. that is the occupation of atoms per site, normalized by the SOF factor and equivalent isotropic displacement parameters ($Å^2 \times 10^3$) for hulsite $Ni_{5.14}Sn_{0.86}(O_2BO_3)_2$. The SOF values must be multiplied by the factor 4 i to obtain the number of atoms in the unit cell. U(eq) is defined as one-third of the trace of the orthogonalized U_{ij} tensor [25].

Site	x/a	y/b	z/c	SOF	Occ.	U(eq)
Ni1	0.5	1	1	0.103	0.411	6(1)
Sn1	0.5	1	1	0.147	0.589	6(1)
Ni2	0	0	0.5	0.206	0.824	5(1)
Sn2	0	0	0.5	0.044	0.176	5(1)
Ni3	0.5	0	0.5	0.228	0.910	4(1)
Sn3	0.5	0	0.5	0.022	0.090	4(1)
Ni4	0	0.5	1	¼	1	5(1)
Ni5	0.2835(2)	0.5	0.72130(9)	½	1	5(1)
B	0.2057(14)	0	0.2384(9)	½		1(1)
O1	0.2539(10)	0.5	0.5298(6)	½		5(1)
O2	0.3127(11)	0.5	0.9068(5)	½		5(1)
O3	-0.0067(11)	0	0.3020(6)	½		5(1)
O4	0.8116(12)	1	0.8928(6)	½		6(1)
O5	0.4421(11)	0	0.3016(6)	½		7(1)

Table 6-3: Selected bond lengths in Å of hulsite $Ni_{5.14}Sn_{0.86}(O_2BO_3)_2$. The underline number correspond to the symmetry code: (10)-x+1,-y,-z+1.

M1 - O2	2.042(4)	M5 - O5	2.157(4)
M1 - O4	2.112(6)	M5 - O3	2.139(4)
M2 - O1	2.061(4)	B - O3	1.381(11)
M2 - O3	2.099(6)	B - O5	1.397(8)
M3 - O1	2.067(4)	B - O4	1.387(11)
M3 - O5	2.103(6)	M1 - M4	3.1091(3)
M3 - $O5_{(10)}$	2.104(6)	M2 - M3	2.7093(4)
M4 - O2	2.031(6)	M1 - M5	3.4468(9)
M4 - O4	2.115(4)	M4 - M5	3.4428(4)
M5 - O2	1.962(6)	M2 - M5	3.0999(3)
M5 - O1	2.026(6)	M3 - M5	3.1097(9)

6.2.3 Mössbauer Spectroscopy

The ^{119}Sn Mössbauer spectroscopy experiments were performed at CBPF. The experimental conditions are the same as described in chapter 5. To analyze the spectra the least-square fitting NORMOS program [51] was used. The ^{119}Sn Mössbauer spectra for different temperatures are shown in Figure 6-5. The room temperature spectrum shows a unique doublet with quadrupole splitting $\Delta E_Q = 1.12(1)$ mm/s, isomer shift $\delta = 0.2$ mm/s (relative to $BaSnO_3$ at RT) and linewidth $\Gamma = 0.98$ mm/s . The isomer shift value is characteristic of a Sn^{4+} oxidation state. The observed linewidth is somewhat larger than of 0.85 mm/s found for the related compound $Co_5Sn(O_2BO_3)_2$ ludwigite where the Sn occupy a unique site with an octahedral oxygen coordination [20]. The increase of the linewidth can be explained if we consider that Sn in $Ni_{5.14}Sn_{0.86}(O_2BO_3)_2$ occupy three sites in which are randomly distributed (1, 2 and 3) giving place to small variations in quadrupole splitting which is reflected as an increase of the linewidth.

Analogously, the Mossbauer spectra between 300 and 180 K were fitted with a unique doublet, characterized by a quadrupolar interaction between the electric quadrupolar moment of the Sn nucleus and the electric field gradient in Sn-O_6 octahedron bonds, with a slightly increased linewidth (see Figure 6-4) which may be caused by vibrations originating from the closed-cycle cryostat.

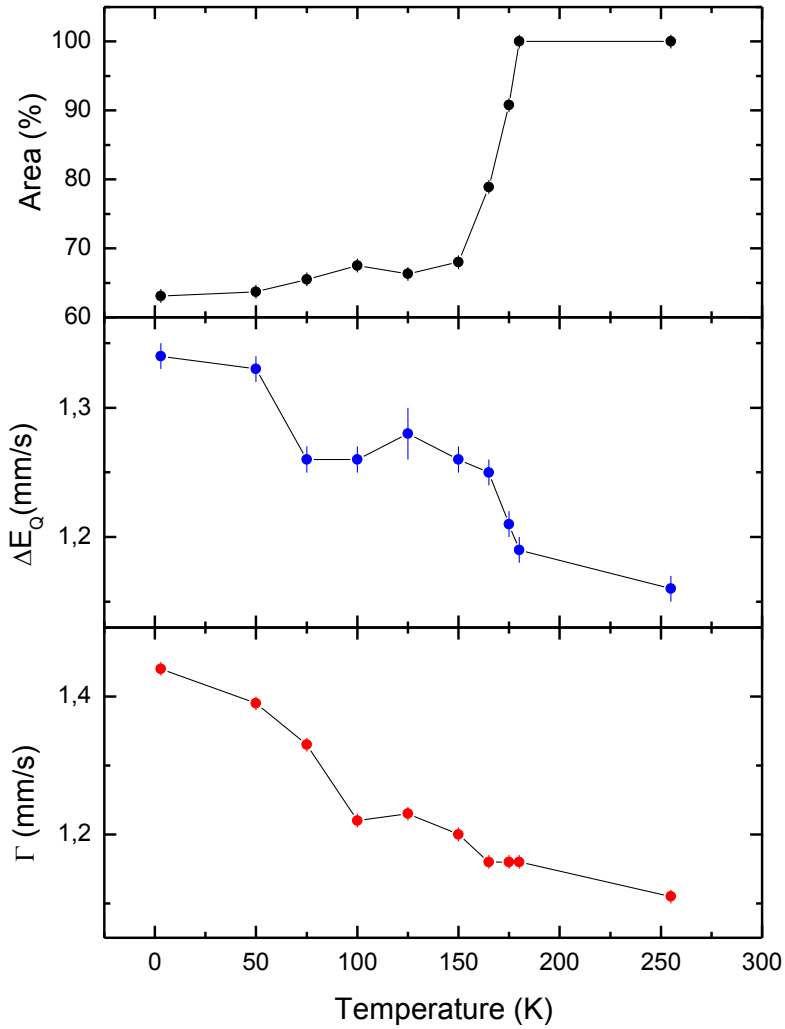

Figure 6-4: Temperature dependence of the hyperfine parameters of the doublet used to fit the spectra of hulsite $Ni_{5.14}Sn_{0.86}(O_2BO_3)_2$.

Below ~180 K the spectra begin to broad magnetically (see Figure 6-5 and Figure 6-6) indicating the onset of magnetic order. We want to mention at this point that, as Sn carries no local moment, the magnetic hyperfine field at the Sn nucleus is a transferred magnetic field due to the magnetic moments of the neighbor Ni ions. Then, the

magnitude and direction of the magnetic hyperfine field at the ^{119}Sn nuclei are determined by the resultant of the magnetic moments of the Ni atoms around [30]. Two subspectra are needed to resolve the spectra below 180 K, one of them corresponding to a quadrupole doublet and the other to a magnetic sextet. The magnetic subspectra have been fitted using the full hyperfine Hamiltonian, including electrical quadrupole and magnetic interaction whose eigenvalues of the $I = 3/2$ manifold for an arbitrary field orientation (with respect to which the principal axes system of the EFG is defined by the polar angle θ) is:

$$E_{M,Q}(I = 3/2, m_I) = -g_N B m_I + \mu_N (-1)^{|m_I|+\frac{1}{2}} (eQV_{zz}/8) \cdot (3cos^2\theta - 1)$$

Linewidth, quadrupole splitting ΔE_Q, isomer shift δ, magnetic hyperfine field B_{hf} and the angle θ were the free fitting parameters. Furthermore, we assumed the quadrupole asymmetry parameter $\eta = 0$ (for an axial symmetry), as it is expected for ^{119}Sn on a regular octahedral site. The hyperfine parameters as a function of temperature, obtained from the fitting procedure, are shown in Table 6-4.

The fitting procedure yield $\theta \approx 55^o$ for all the magnetic subspectra and a transferred magnetic hyperfine field B_{hf} which increases with decreasing temperature from B_{hf}(180 K)~0 T to B_{hf}(3 K)~20.1 T (Figure 6-6). The onset of magnetic ordering at 180 K is clearly seen. Below the ordering temperature the absorption area of the magnetic subspectra increases sharply down to ~150 K and for lower temperatures, this increase is much slower reaching 37 % of the total area at 3 K. The remaining 63 % of the absorption area at 3 K correspond to a slightly broad doublet indicating the absence of magnetic interaction. Relating this result with the single crystal XRD, where it is shown that 69% of the total ions of Sn go to site 1, we attribute the quadrupole doublet observed at low temperatures to Sn ions at site 1 where they do not feel a measurable transferred magnetic hyperfine field, even at 3 K. On the other hand, a pronounced line broadening of the doublet was observed as the temperature is reduced below the magnetic transition temperature. This line broadening could be related with a slow relaxation of the Ni^{2+} spins surrounding the Sn ion at sites 4 as will be discussed in the next section.

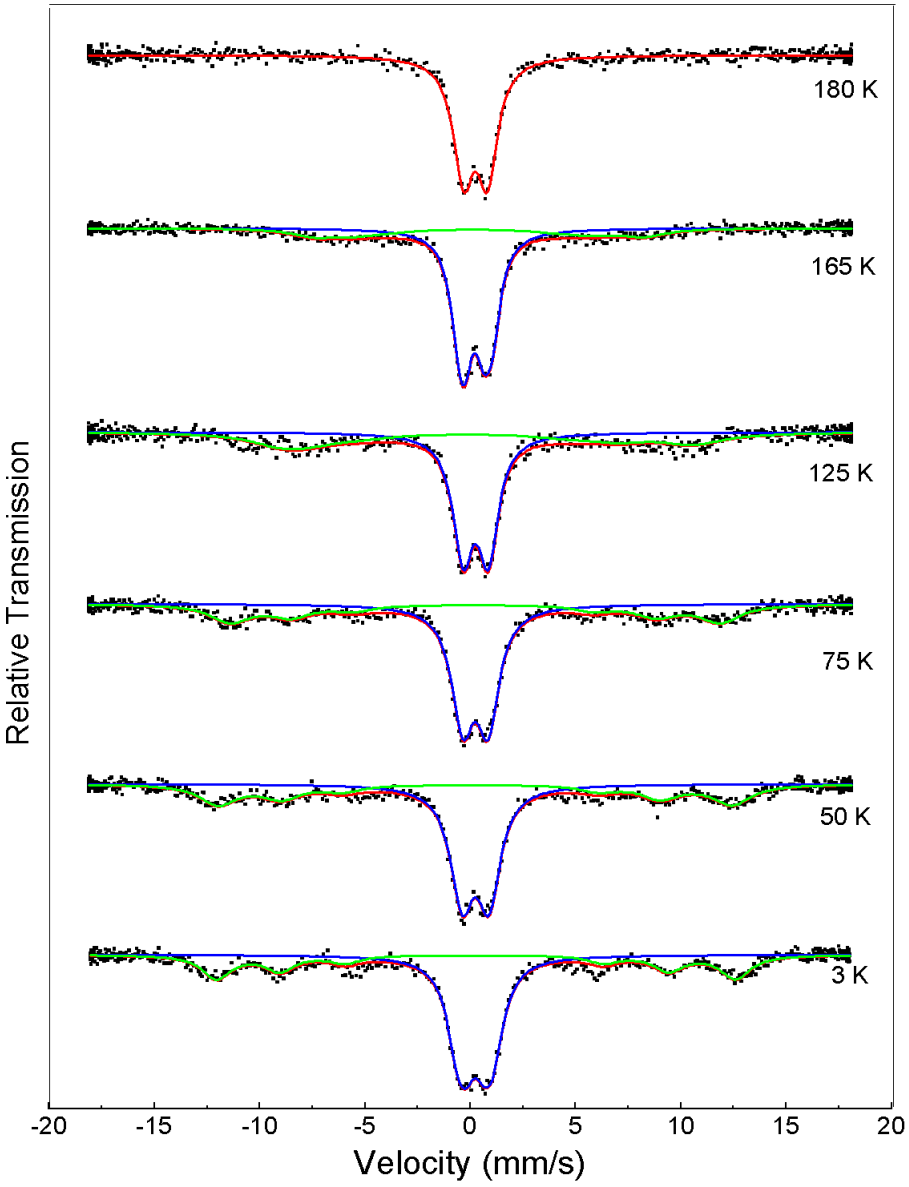

Figure 6-5: Some ^{119}Sn Mössbauer spectra of hulsite $Ni_{5.14}Sn_{0.86}(O_2BO_3)_2$ in the temperature range of 180 $< T <$ 3 K. For 180 K only one doublet was used to fit the spectra. Below 175 K all the spectra were fitted with two subspectra, one paramagnetic and one magnetic.

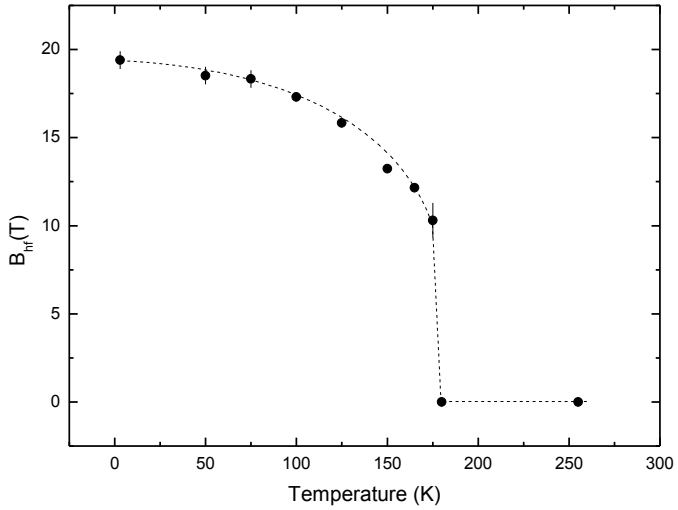

Figure 6-6: Temperature dependence of the transferred magnetic hyperfine field at Sn nucleus corresponding to the sextet used to fit the spectra of hulsite $Ni_{5.14}Sn_{0.86}(O_2BO_3)_2$.

Table 6-4: Mössbauer hyperfine parameters of hulsite $Ni_{5.14}Sn_{0.86}(O_2BO_3)_2$ for temperatures between 300 and 3 K. The parameters are the isomer shift δ, the quadrupole splitting ΔE_Q, linewidth , Γ , the hyperfine magnetic field B_{hf}, and the absorption area A.

T(K)	ΔE_Q (mm/s)	Γ (mm/s)	B_{hf} (T)	θ (°)	A (%)
300	1.12	0.98	-	-	100
255	1.16	1.11	-	-	100
200	1.16	1.11	-	-	100
180	1.19	1.16	-	-	100
175	1.21	1.16	-	-	91
	0.13	3.02	10.30	-	9
165	1.25	1.16	-	-	79
	0.12	3.20	11.4	-	21
150	1.26	1.2	-	-	68
	0.12	3.74	12.3	-	32
125	1.28	1.23	-	-	66
	0.19	3.92	14.7	-	34
100	1.26	1.22	-	-	68
	0.20	2.68	16.3	56	32
75	1.26	1.33	-	-	66
	0.20	2.42	17.4	55	34
50	1.33	1.39	-	-	64
	0.15	2.24	18.1	55	36
3	1.34	1.44	-	-	63
	0.22	1.66	18.5	70	37

6.2.4 Magnetic Measurements

The magnetic measurements were performed on powdered-single crystals of hulsite $Ni_{5.14}Sn_{0.86}(O_2BO_3)_2$ using a commercial Quantum Design PPMS at CBPF. Figure 6-6 shows the temperature dependence of magnetization curves for field-cooled (FC) and zero-field-cooled (ZFC) procedures, with applied magnetic fields of 0.01 T and 1 T. In all cases, lowering the temperature down to 2 K, the magnetization increases without reaching a maximum.

The magnetization rises sharply at ~180 K, which is more clearly observed in the derivative magnetization (inset) and for lower temperatures the ZFC and FC curves diverge. This temperature coincides with the beginning of the magnetic broadening of the Mössbauer spectra, so we can attribute this change in the magnetization to the onset of the magnetic ordering. As can see in the derivative magnetization curve subtle changes occurs at lower temperatures (see inset) as a maximum in ~20 K. Above the magnetic transition the magnetization decreases asymptotically with increasing the temperature and can be decribed by the Curie-Weiss law. The apropiate fit (of the 1T FC curve, Figure 6-7) leads to a Curie constant $C = 6.48 \times 10^{-3} emu \cdot \mathrm{K} \cdot g^{-1} Oe^{-1}$ with a Curie-Weiss temperature $\theta_{CW} = -26.8$ K indicating the predominance of antiferromagnetic interactions. From the Curie constant we determine the effective moment $p_{eff} = 5.51\ \mu_B$ per formula unit.

To get information on the spin state of Ni ions, we must consider that the Sn atoms have oxidation state 4+ (as indicated by Mössbauer spectroscopy experiments) and charge balance on $Ni_{5.14}Sn_{0.86}(O_2BO_3)_2$ leaves 4.86 atoms of Ni^{2+} and 0.28 atoms of Ni^{3+} per formula unit (f.u.). If we consider that all the Ni atoms are in the HS state, the spin only moment gives $p = 6.56\ \mu_B$. A second possibility is that Ni^{2+} are in the HS and Ni^{3+} in the LS state, in this case, the spin only moment gives $p = 6.30\ \mu_B$. But if all the magnetic atoms are Ni^{2+} in the HS state, then the spin only moment gives $p = 6.41\ \mu_B$. In any case, the effective experimental moment is lower than the expected value.

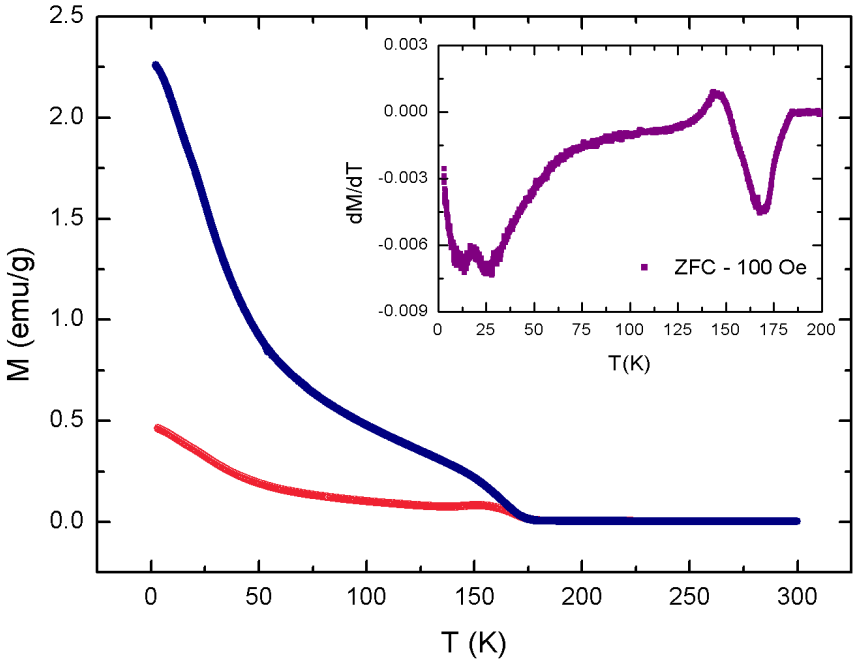

Figure 6-6: Magnetization versus temperature for hulsite $Ni_{.514}Sn_{0.86}(O_2BO_3)_2$ under an applied field of 100 Oe in both regimen: field cooled (blue) and zero field cooled (red). Inset: The derivative curve of the ZFC regime.

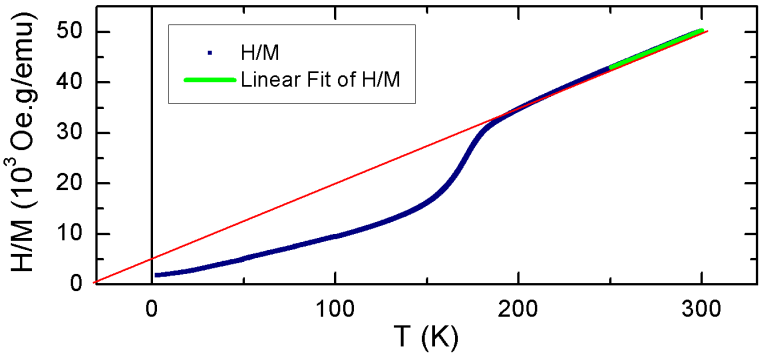

Figure 6-7: Inverse of the FC magnetization curve for an applied magnetic field of 1 T.

Figure 6-8 shows the real part of the ac-susceptibility (χ') for different frequencies as a function of temperature. It has increasing values below 300 K. Lowering the temperature, the susceptibility increase gradually and in ~180 K a sharp rise is observed reaching a maximum value at ~164 K and then decreases gradually down to 130K. The position of the peak does not change with frequency (see inset of Figure 6-8). For lower temperatures, the susceptibility increases again and at ~25 K a second drastic

rise is observed but this time without reaching a saturation down to 3 K, the lowest temperature of the experiment.

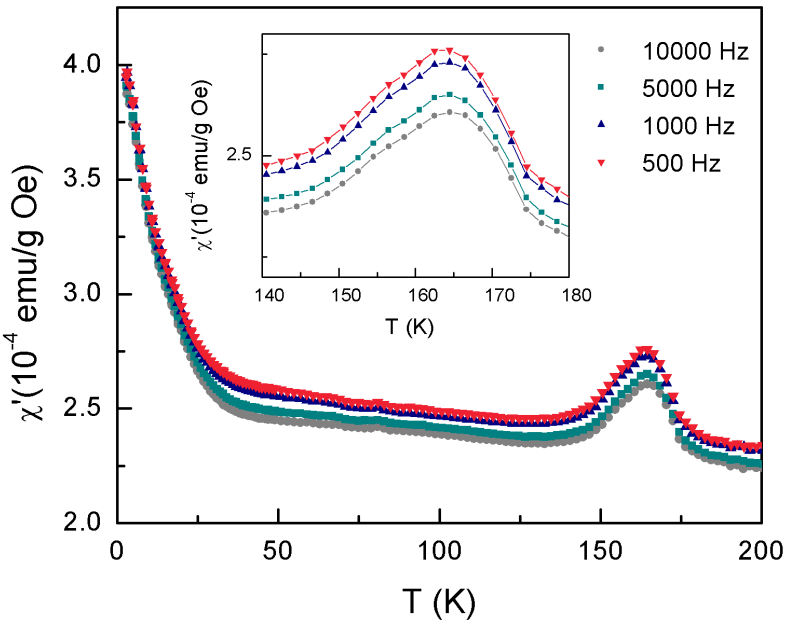

Figure 6-8: *AC*- susceptibility for hulsite $Ni_{5.14}Sn_{0.86}(O_2BO_3)_2$ as a function of temperature for 500 Hz,1 kHz, 5 kHz and 10 kHz.

Figure 6-9 shows the magnetization curves as a function of applied magnetic fields for different temperatures. Below 180 K hysteresis loop consistent with a ferromagnetic like order are observed. At 150 K the hysteresis loop is symmetric with a coercive field of 540 Oe and a remanent magnetization of $6.2 \times 10^{-2}\ \mu_B/f.u.$

A clear shift of the hysteresis loop (inset Figure 6-10) along the positive field axis is observed bellow 150 K indicating the occurrence of exchange bias (EB) effect in the system. The exchange bias field is calculated as $H_{EB} = (H^+ - H^-)/2$, where H^+ and $H^-$are the coercive fields for the ascending and descending curves. The temperature dependence of H_{EB} is shown in Figure 6-10. Large H_{EB} fields are observed for temperatures between $25 \lesssim T \lesssim 150$ K, however a significant reduction of this parameter is observed below ~25 K. Similar EB behaviour have been observed in $Ni_5Ge(O_2BO_3)_2$ ludwigite where the loop at 50K shows exchange bias but it vanishes for lower temperatures [42]. The exchange bias effects have also been observed in spin glass systems and some ferrimagnets [54, 55, 56, 57].

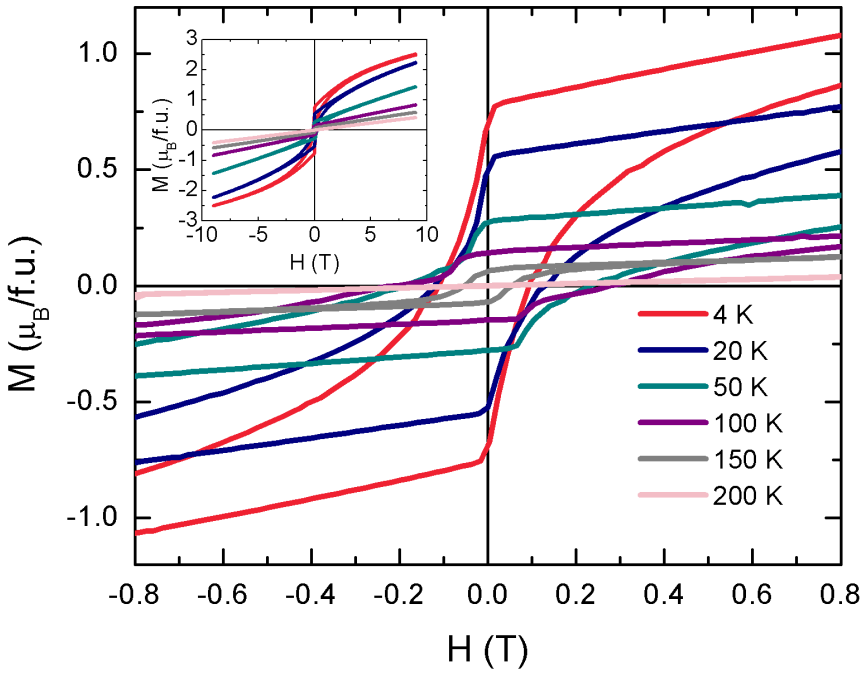

Figure 6-9: Hulsite $Ni_{5.14}Sn_{0.86}(O_2BO_3)_2$ magnetization versus smal applied magnetic field curves at 4, 20, 50, 100, 150, and 200 K. Inset: M vs H curves for applied field up to 7T.

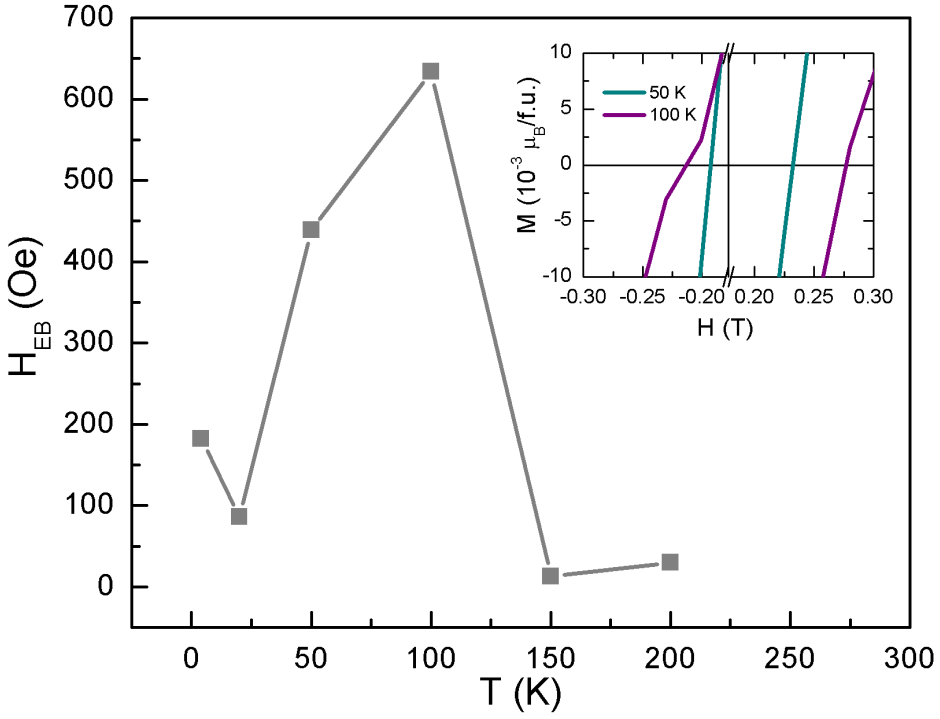

Figure 6-10: Temperature dependence of the exchange bias field (H_{EB}) of hulsite $Ni_{5.14}Sn_{0.86}(O_2BO_3)_2$.

6.2.5 Specific Heat Measurements

Specific heat measurements as a function of temperature and magnetic field were performed with randomly oriented needle crystals using a commercial Quantum Design PPMS at CBPF.

Specific-heat measurements of $Ni_{5.14}Sn_{0.86}(O_2BO_3)_2$ in the range of temperature $2 \leq T \leq 200$ K are shown in Figure 6-11 and Figure 6-12. Down to 50 K the zero field specific heat shows no obvious sharp features typical of structural or magnetic order. For lower temperatures, a rounded peak with a maximum at 20 K is observed. Its position does not change for applied magnetic fields as high as 9 T, only a slight flattening of the peak is observed at 9 T. The peak observed at 20 K in the specific heat measurements corresponds to slight changes in magnetic measurements, better seen in the derivative of magnetic curves (Figure 6-6-inset). The absence of significant changes in magnetic measurements could suggest a structural transition or a reduction of relaxation times.

On the other hand, in $NiGa_2S_4$, a two-dimensional Heisenberg triangular-lattice antiferromagnet, the specific heat display a peak at ~10 K whose position and amplitude is independent of applied magnetic fields (at least up to 7 T) and the susceptibility showed a broad maximum at the same temperature [58]. Early thermodynamic, neutron and muon spin spectroscopy (μSR) results have shown that despite strong antiferromagnetic (AF) interactions, it does not display a long-range magnetic ordering; only an incommensurate short-range order with a nanoscale correlation length and a spontaneous static interstitial magnetic field below $T_c = 9.2$ K and that its ground state is highly degenerate [59]. μSR results have demonstrated that there is a slowing down of magnetic fluctuations as the compound is cooled down through T_c rather than a spin freezing. The spin fluctuation rate decreases precipitously upon cooling towards $T_f = 8.5$ K, but fluctuations on the microsecond time scale then persist in an anomalous dynamical regime for lower temperatures[60]. Recent μSR and susceptibility data show a well-defined 2D phase transition at $T_f = 8.5$ K (leading to a disordered AFM ground state) below which the $NiGa_2S_4$ is neither a conventional magnet nor a singlet spin liquid [61]. On the other hand, it is less understood the fact that, while strong muon spin relaxation changes drastically with a magnetic field, the

entropy is almost not affected [61]. Several scenarios have been proposed to describe the experimental results, however, no theory so far is able to fully account for the unusual magnetism of this compound [59, 60, 61].

Another compound exhibiting field-independent specific heat is the frustrated kagomé lattice spin system $SrCr_8Ga_4O_{19}$ [62] but, different of the $NiGa_2S_4$, it does not exhibit spin freezing [63].

The specific heat exhibited power-law behavior at low temperatures (Figure 6-12). The zero field specific data between 2 and 3 K are well fitted by the relation $C = \gamma T + \alpha T^2$, with $\gamma = 171$ mJ mol^{-1} K^{-2}. Specific heat with linear temperature dependence is a characteristic of spin glass systems [27]. Among the oxyborates, the ludwigite $Co_{4.74}Ti_{1.26}(O_2BO_3)_2$ display a spin glass behavior and have a specific heat linear dependence in T with $\gamma = 15$ mJ mol^{-1} K^{-2} [21]. Linear temperature dependence of the specific heat is also a common feature among QSL candidates with considerably large values of γ [64, 65, 66]. For example, the quantum spin liquid candidate $Ba_3NiSb_2O_9$–6H-B, with planar triangular Ni^{2+} coordination, have a linear parameter $\gamma = 168$ mJ mol^{-1} K^{-2} [66]. This linear behavior in hulsite $Ni_{5.14}Sn_{0.86}(O_2BO_3)_2$ is different from hulsite $Co_{5.52}Sb_{0.48}(O_2BO_3)_2$ which shows a gapped T^2 dependence in the low-temperature range [35].

The low-temperature specific heat in hulsite $Ni_{5.14}Sn_{0.86}(O_2BO_3)_2$ depends strongly on applied magnetic fields as can be seen in Figure 6-12. Magnetic field reduces the specific heat and change its temperature dependence. The applied magnetic field specific heat data below 3 K are well fitted with a combination of a linear and quadratic temperature dependence $C = \gamma T + \alpha T^2$. Increasing the applied magnetic field the γ parameter decrease while the α parameter increases (see table in Figure 6-12). For high fields, the quadratic term is dominant indicating *gapless* two-dimensional excitations in $Ni_{5.14}Sn_{0.86}(O_2BO_3)_2$. Just for comparison, these results are somewhat different from that of the counterpart $Co_{5.52}Sb_{0.48}(O_2BO_3)_2$ hulsite where a clear T^2 behavior in the low-temperature range with a small gap of 0.75 K for an applied magnetic field of 9 T was found [35].

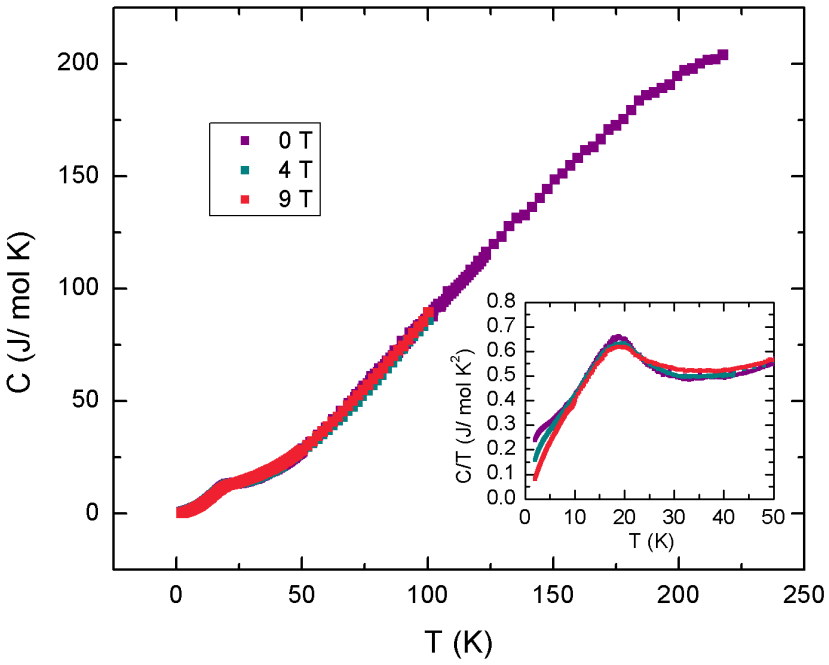

Figure 6-11: Hulsite $Ni_{5.14}Sn_{0.86}(O_2BO_3)_2$ specific heat plotted as C vs T for applied magnetic fields of 0, 4, and 9 T. The inset: Low temperature range plotted as C/T vs T.

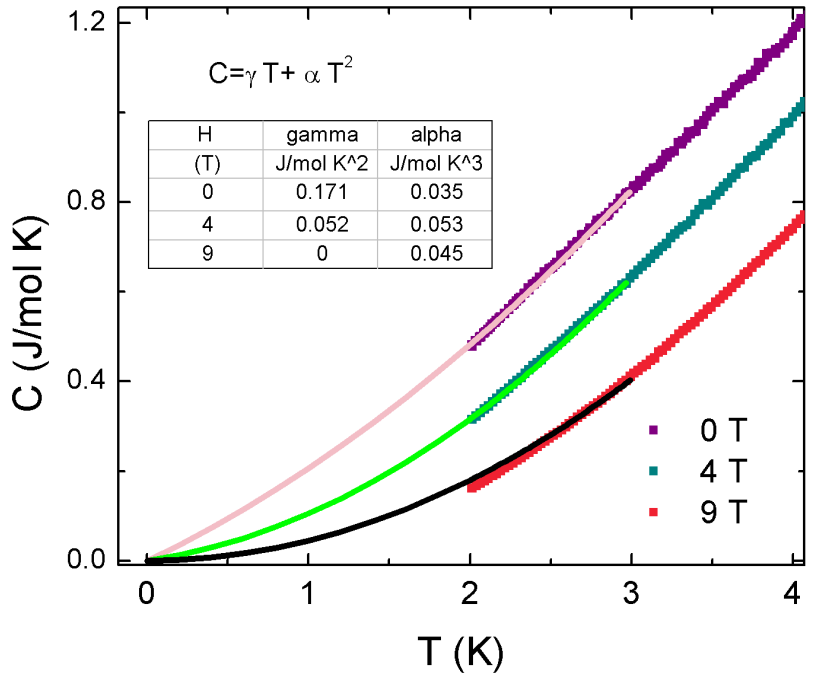

Figure 6-12: Low temperature specific heat of hulsite plotted as C versus T for 0 and 9 T. The solid lines are the fits described in the main text.

6.3 Discussion

Prior to this work, only two hulsites had been synthesized, the $Ni_{5.33}Sb_{0.67}(O_2BO_3)_2$ and the $Co_{5.52}Sb_{0.48}(O_2BO_3)_2$. The common characteristic of these compounds is that both of them have the nonmagnetic ion Sb^{5+} in their structures, occupying only one site (site 1), however they appear to have quite different magnetic properties. For the $Ni_{5.33}Sb_{0.67}(O_2BO_3)_2$, detailed information about the structural aspects can be found in the literature [52], however, the same cannot be said regarding its magnetic properties, the only available information is that a possible partial ordering occurs at ~170 K and that an antiferromagnetic ordering increases drastically below 40 K [52].

The $Co_{5.52}Sb_{0.48}(O_2BO_3)_2$ order magnetically below 42 K with an antiferromagnetic type structure. The specific-heat results at low temperatures are dominated by a gapped T^2 contribution and attributed to magnons with a linear dispersion relation propagating in planes [35]. These results give evidence of the two-dimensional nature of the magnetic ordering [35]. The possibility of studying two-dimensional phenomena in magnetic oxyborates opens new perspectives which are surely worth continuing to explore.

Here we sinthesized a new hulsite $Ni_{5.14}Sn_{0.86}(O_2BO_3)_2$ containing nonmagnetic Sn atoms. Different from the other hulsites, x-ray diffraction experiments in this compound show that the nonmagnetic ion Sn occupies more than one site. Sn ions are randomly distributed in sites 1, 2 and 3.

Before beginning a discussion of the magnetic properties of this compound, let us first look at some structural features. The compound consists of several layers composed of metal ions stacked along the *c*–axis. Sites 2 and 3 form a two-dimensional rectangular network, the 2–3 layer. The x-ray experiments show that this layer is predominantly composed of Ni^{2+} ions, with 27 % of their sites being occupied by Sn^{+4} ions randomly distributed at sites 2 and 3 (see Figure 6-3). The shortest distance between metallic ions is found in this plane and correspond to distance between site 2 and site 3 (d_{2-3} =2.71 Å).

The second layer formed by metallic ions at sites 1 and 4 is more interesting because they are arranged in a two-dimensional triangular lattice which is related with geometric frustration when AFM interactions between magnetic ions take place. The presence of nonmagnetic Sn ions at sites 1 do not destroy the triangular configuration of the Ni atoms as can be seen in Figure 6-13. Moreover, most of the magnetic ions are coordinated with four magnetic ions instead of six, as in a Kagome lattice, increasing geometric frustration, see appendix B. Thus, considering structural features, magnetic frustration is highly expected in 1–4 layer. The 1–4 and 2–3 layers are stacked along the c- axis, separated by Ni atoms at sites 5. The Ni atoms at site 5 are closer to 1–4 layer (2.32 Å) than to 2–3 layer (2.98 Å).

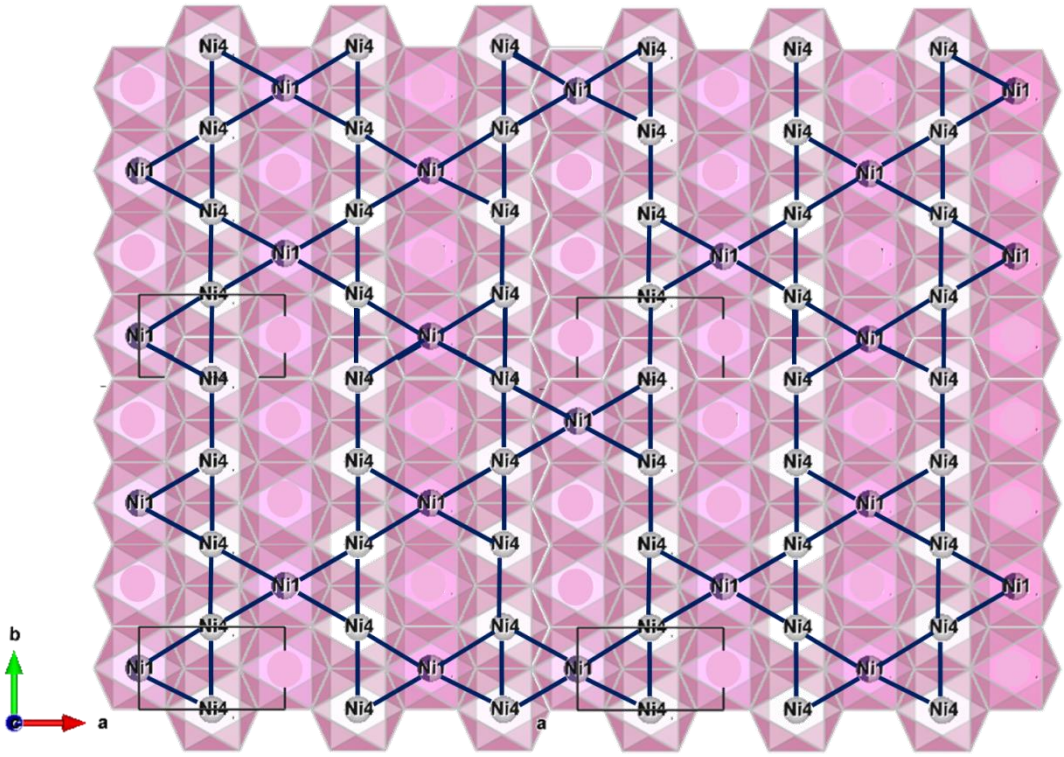

Figure 6-13: Magnetic interactions (black lines) in the 1-4 layer, considering randomly distributed nonmagnetic ions on site 1(light magenta circles). This figure was generated by Vesta 3.1.1 software[1].

The ^{119}Sn Mössbauer spectroscopy experiments confirm the oxidation state 4+ obtained for Sn, which in turn leads the Ni atoms to adopt a 2+ oxidation state to achieve a charge balance. The Mössbauer spectra in the temperature range between 300 and 180 K shows a unique doublet, typical for a paramagnetic regime and its slightly increased linewidth is consistent with the presence of three non-equivalent sites for the Sn as shown by x ray diffraction experiments. In the paramagnetic state, the three crystallographic sites for the Sn are indistinguishable in the Mössbauer spectra, however when the compound order magnetically are clearly distinguishable. When cooling down the sample below $T_M \leq 180$ K a complex ^{119}Sn Mössbauer spectrum split by magnetic hyperfine interactions appears indicating the onset of magnetic order, a temperature at which the magnetization and susceptibility rises drastically.

The Mössbauer experiments at low temperature show that only 37% of the Sn feel a static transferred magnetic hyperfine field, a fraction that is comparable with the fraction (31%) of the Sn ions in the rectangular 2–3 layer. So, is very reasonable to attribute the magnetic ordering observed at 180 K to a partial ordering of the 2–3 layer, where the shortest distance $\left(d_{2-3} = 2.71 \text{ Å}\right)$ between high spin Ni^{2+} $(S = 1)$ could give rise to strong *d*-*d* overlap and, consequently, direct exchange. Partial ordering has been already observed in $Fe_3O_2BO_3$ ludwigite [5], where the subsystem formed by Fe at sites 2 and 3 order at 110 K but the whole system ordered only at 70 K.

The negative θ_{CW} indicate antiferromagnetic interactions between high spin Ni^{2+} $(S = 1)$, however, the hysteresis loop below 180 K shown that a ferromagnetic type ordering takes place. On the other hand, Mössbauer results indicate a disordered or spin glass system below 180 K, which at first sight, seem to be in contradiction with a ferromagnetic type ordering. However, this apparent disagreement can be solved if we consider that the nonmagnetic Sn creates only local disorder. Thus the 2-3 layer would have regions with only Ni atoms which order ferromagnetically and regions with a local disorder where Sn is located. The assumption of a local disorder is supported by the fact that the position of the peak in the susceptibility data, corresponding to this transition, is slightly shifted with the increase of the frequency and by the fact that this magnetic transition does not show up in the macroscopic specific heat measurements.

The Mössbauer experiments show that at 3 K the Sn ions located at the 1-4 layer do not feel a measurable transferred magnetic hyperfine field indicating two possibilities: 1) the Ni ions in 1-4-layer are magnetically ordered in such a way that the transferred magnetic field of their magnetic moments to the Sn nucleus is zero, and 2) the Ni atoms in the 1-4-layer are magnetically frustrated. Taking into account that Ni forms a triangular two-dimensional lattice in the 1-4 layer and that Sn ions are randomly located at site 4 the first possibility is very unlikely and that these results are more consistent with a magnetic frustration in the 1-4 layer.

More difficult to explain is the peak observed at 20 K in the specific heat measurements since no corresponding visible changes are observed at the same temperature in the magnetization measurements. However, the Mössbauer spectroscopy can help us in its interpretation. The line broadening, corresponding to the doublet of the Sn in the 1-4 layer, is attributed to an unresolved hyperfine field at the Sn nucleus due to a supertransferred hyperfine interaction between the Sn nuclei and the surrounding Ni ions. The doublet below 180 K is believed to correspond to a situation where the Ni^{2+} ionic relaxation time is comparable with the Larmor precession time of the Sn nuclei. Below ~100 K a sharp increase of the linewidth is observed indicating an increase of the relaxation time. Other frustrated systems with two-dimensional triangular or Kagomé lattice have been shown a specific heat peak and related with a saturation decrease of the spin fluctuation rate [58, 63]. The frustrated Kagomé lattice spin system $SrCr_8Ga_4O_{19}$ [62] exhibit field-independent specific heat with a peak at ~3.5 K and a small cusp in the susceptibility data. Below this temperature a saturation of the spin fluctuation rate were observed but spin fluctuation persists down to 100 mK. No spin freezing was observed for this compound.

The $NiGa_2S_4$, a two-dimensional Heisenberg triangular-lattice antiferromagnet, the specific heat display a peak at ~10K whose position and amplitude is independent of applied magnetic fields and the susceptibility showed a broad maximum at the same temperature [58]. μSR results have demonstrated that there is a slowing down of magnetic fluctuations as the compound is cooled down through 9.2 K rather than a spin freezing [60]. More recent μSR and susceptibility studies have shown a well-defined 2D phase transition at $T_f = 8.5$ K (leading to a disordered AFM ground state) below which the $NiGa_2S_4$ is neither a conventional magnet nor a singlet spin liquid [61].

The Specific heat and Mössbauer results in hulsite $Ni_{5.14}Sn_{0.86}(O_2BO_3)_2$ are consistent with the assumption that magnetic frustration of the Ni spins occurs in the 1-4 layer which has a triangular lattice. Thus, magnetic ordering coexists with planes magnetically frustrated at low temperature.

At low temperatures (< 5 K) the linear dependence of the specific heat with the temperature was a new an unexpected result in oxyborates. The linear T dependent of the specific heat at low temperatures is unusual for a magnetic insulator having a 2D frustrated lattice. However, a linear dependence has been found in the 6H-B phase of $Ba_3NiSb_2O_9$ with a Ni^{2+} triangular lattice [66] and is a common feature among QSL candidates [64, 65, 67].

Thus the linear T dependent of the specific heat found in hulsite $Ni_{5.14}Sn_{0.86}(O_2BO_3)_2$ suggests a QSL behavior of the 1-4 layer. Evidently, a linear contribution with T due to local disorder in the 2–3 layer could also be included, but its contribution should not be dominant. The application of a magnetic field could lead to two-dimensional correlations in the 1–4 layer creating a T^2 dependence.

A possible scenario to describe the experimental results of our compound is as follows. hulsite $Ni_{5.14}Sn_{0.86}(O_2BO_3)_2$ could be separated in two subsystems: the 1-4 layers and the 2-3 layers coupled with Ni at site 5. At 180 K the 2-3 layer orders magnetically with a ferromagnetic type structure due to the strong d-d overlap of the Ni atoms, but local disorder is caused by the presence of Sn in this layer. Lowering the temperature Ni ions at site 5, which is closer to the 2-3 plane, order AFM generating an exchange bias effect. While, in the 1-4 layer, with a two-dimensional triangular lattice, the Ni spins stay magnetically frustrated and just a slowing down of magnetic fluctuations occurs down to 3 K.

Chapter 7. Conclusion

The study of nonmagnetic dilution of the Co ludwigites: $Co_3O_2BO_3$, $Co_5Sn(O_2BO_3)_2$ and $Co_{4.76}Al_{1.24}(O_2BO_3)_2$, have shown a gradual increase on the fraction of Co^{2+} at site 4 that is concomitant with an increase of magnetic ordering temperature (see Figure 7-1). This result suggest that HS Co^{2+} at site 4 couple magnetically the 1-2-3 planes enhancing the magnetic interactions and consequently, increasing the magnetic ordering temperature. To simplify the presentation of the structural and magnetic properties shown by the different Co ludwigites, they are presented with an equivalent f.u., it is $Co_6(O_2BO_3)_2$, $Co_5Sn(O_2BO_3)_2$ and $Co_{4.76}Al_{1.24}(O_2BO_3)_2$.

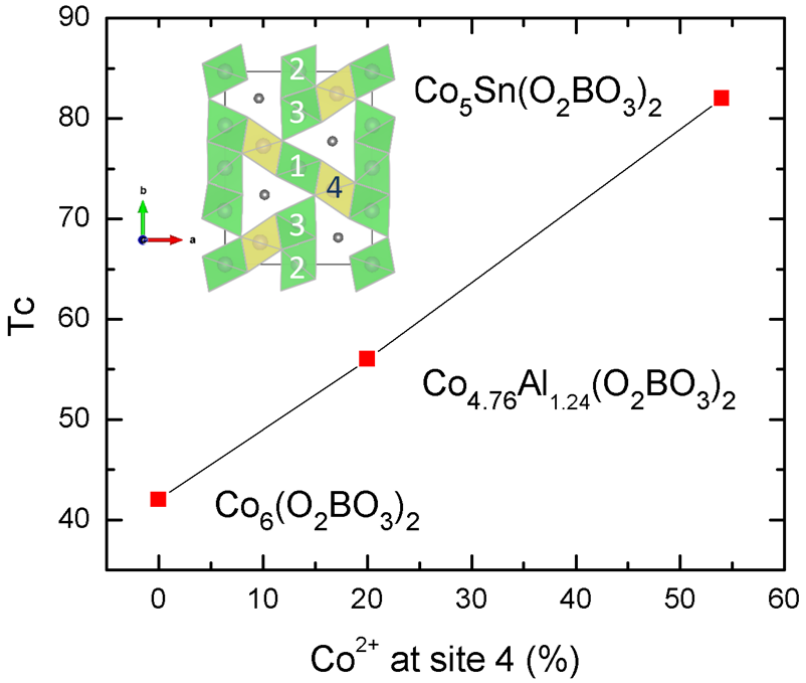

Figure 7-1: Magnetic ordering temperature T_C versus percentage of Co^{2+} at site 4.

In $Co_6(O_2BO_3)_2$ and $Co_{4.76}Al_{1.24}(O_2BO_3)_2$, with null and small content of HS Co^{2+} at site 4, respectively, the low-temperature specific heat data is characterized by a T^2 dependence and by small values of the entropy released at T_C indicating a 2D magnetic order. In $Co_5Sn(O_2BO_3)_2$ and $Co_{4.76}Al_{1.24}(O_2BO_3)_2$, with an amount of HS Co^{2+} at

site 4, the hysteresis magnetization curve are characterized by anomalies at ~4 T. In $Co_{4.76}Al_{1.24}(O_2BO_3)_2$ spin flop take place while in $Co_5Sn(O_2BO_3)_2$ magnetic jumps occurs.

The Co ludwigites have shown high magnetic anisotropy. The magnetic moments lie on the *a-b* plane, almost pointing along *b* axis, and are ferromagnetic coupled along the *c* axis. Taking into account the magnetic anisotropy, the saturation magnetization (Figure 7-2) and the magnetic structure of the $Co_6(O_2BO_3)_2$ obtained from NPD experiments see Figure 2-13, magnetic structures have been proposed for $Co_{4.76}Al_{1.24}(O_2BO_3)_2$ and $Co_5Sn(O_2BO_3)_2$ as shown in Table 7-1. The suggested models can serve as an incentive for the realization of NPD experiments, aiming to elucidate the magnetic structure of the nonmagnetic doped ludwigites.

Table 7-1: Suggested spin arrangement in the *ab* plane for some Co ludwigites. We assume a ferromagnetic coupling along the *c* axis. The dashed line encloses the magnetic ions in the plane formed by sites 1, 2 and 3.

Compound	H (T)	$M_o(\mu_B/f.u.)$	Model
$Co_6(O_2BO_3)_2$	9	6.6	$\frac{\uparrow}{3}\ \frac{\downarrow}{1}\ \frac{\uparrow}{3}\ \frac{\uparrow}{2}\ \frac{\times}{4}\ \frac{\times}{4}$
$Co_{4.76}Al_{1.24}(O_2BO_3)_2$	9	5.8	$\frac{\uparrow}{3}\ \frac{\downarrow}{1}\ \frac{\uparrow}{3}\ \frac{\uparrow}{2}\ \frac{\times}{4}\ \frac{\times}{4}$
$Co_{4.76}Al_{1.24}(O_2BO_3)_2$	0	~0	$\frac{\uparrow}{3}\ \frac{\downarrow}{1}\ \frac{\uparrow}{3}\ \frac{\downarrow}{2}\ \frac{\times}{4}\ \frac{\times}{4}$
$Co_5Sn(O_2BO_3)_2$	9	~3.3	$\frac{\uparrow}{3}\ \frac{\downarrow}{1}\ \frac{\uparrow}{3}\ \frac{\uparrow}{2}\ \frac{\downarrow}{4}\ \frac{\times}{4}$

In $Co_{4.76}Al_{1.24}(O_2BO_3)_2$ it is observed an antiferromagnetic coupling at low applied magnetic fields different from $Co_6(O_2BO_3)_2$ and $Co_5Sn(O_2BO_3)_2$, see Figure 7-2. The large substitution of site 2 with Al could be related to the antiferromagnetic coupling between site 2 and 3, that compensate the moments. Otherwise, if site 2 is completely occupied by Co^{2+} as in $Co_6(O_2BO_3)_2$ and $Co_5Sn(O_2BO_3)_2$ there is ferromagnetic like behavior. In $Co_6(O_2BO_3)_2$ is related to the ferromagnetic coupling between site 2 and 3, as observed in the NPD studies of $Co_6(O_2BO_3)_2$, see Figure 2-13.

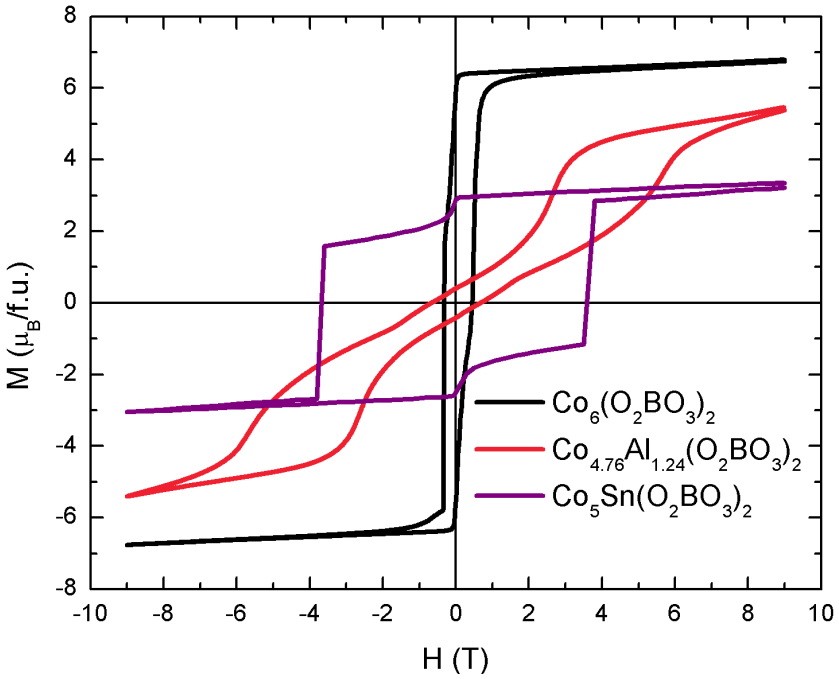

Figure 7-2: Magnetization as function of applied magnetic fiels for $Co_6(O_2BO_3)_2$, $Co_{4.76}Al_{1.24}(O_2BO_3)_2$ and $Co_5Sn(O_2BO_3)_2$ at ~5 K.

The oxyborates ludwigite $Ni_5Sn(O_2BO_3)_2$ and hulsite $Ni_{5.14}Sn_{0.86}(O_2BO_3)_2$ are novel compounds and synthesized by the first time. Despite having the same chemical formula, both structurally and magnetically are quite different. These compounds have shown partial magnetic orders coexisting with magnetic frustration, evidencing that magnetic interactions in Ni oxyborates, with Ni^{2+}in a HS state (S=1), are more complex than in their Co oxyborates (S=3/2) counterparts, despite the structural similarities of both families. As a consequence, linear T dependence of the specific heat data, with large coefficient, have been observed at low-temperatures. A small T^2 contribution is also present which is enhanced by the application of a magnetic field. For comparison, Table 7-2 presents the main magnetic parameters as long with the fitting parameters of the low-temperatures specific heat of the studied oxyborates.

The principal characteristics found in each compound are described below:

1. Ludwigite $Co_3O_2BO_3$.

The study of the ludwigite $Co_3O_2BO_3$ based on NPD results gives an approach to a better understanding why the only two know homometallic ludwigites, $Fe_3O_2BO_3$ and $Co_3O_2BO_3$, have different physical properties despite their similarities. In $Fe_3O_2BO_3$, all the Fe ions (Fe^{2+} and Fe^{3+}) have a spin moment $S>0$. These ions have a charge sharing instability between sites 4 and 2, which hold the shortest intermetallic distance. These two sites have predominant magnetic interactions also, giving to $Fe_3O_2BO_3$, 1D structural and magnetic properties. In $Co_3O_2BO_3$, on the contrary, there is charge stability of Co^{3+} at site 4. These ions have a LS state $S=0$, favored by the high symmetry of the oxygen octahedral environment and short Co-O distances at site 4. Then, even with the shortest distance between sites 4 and 2, the magnetic interactions are restricted to sites 1, 2, and 3 giving rise to 2D magnetic structure.

2. Ludwigite $Co_5Sn(O_2BO_3)_2$

The unexpected increase of the magnetic ordering temperature from 42 K in $Co_6(O_2BO_3)_2$ to 82 K in $Co_5Sn(O_2BO_3)_2$ after a nonmagnetic dilution is due to an increase of the magnetic ions at sites 4. The Sn doping increase the number of Co^{2+} in a HS state going from 4 atoms in $Co_6(O_2BO_3)_2$ to 5 in $Co_5Sn(O_2BO_3)_2$. The increase of the magnetic ordering temperature relies on the preferential occupation of the Sn ions at site 4 and to the absence of double exchange interaction.

3. Ludwigite $Co_{4.76}Al_{1.24}(O_2BO_3)_2$

In $Co_{4.76}Al_{1.24}(O_2BO_3)_2$ there is a long range magnetic order of the whole compound at 57 K. Like in $Co_5Sn(O_2BO_3)_2$, the magnetic transition temperature is raised by the presence of nonmagnetic ions. Magnetic and thermal results for $Co_{4.76}Al_{1.24}(O_2BO_3)_2$ indicate a ferrimagnetic order. Magnetic measurements under applied magnetic fields revealed the presence of magnetically frustrated spins leading to metamagnetic transitions. The critical field at which the metamagnetic transitions occur is temperature dependent, and a magnetic phase diagram can be constructed showing three regions, PM, FIM, and spin-flop phases with first- and second-order transitions among them. Heat-capacity measurements show magnetocaloric effects.

4. Ludwigite $Ni_5Sn(O_2BO_3)_2$

The study of ludwigite $Ni_5Sn(O_2BO_3)_2$ had shown a complex magnetic behavior. The magnetic properties are completely different of that shown by their counterpart $Co_5Sn(O_2BO_3)_2$ (where the Co^{2+} are in the HS state with S=3/2) which show only one transition of the whole system at 82 K. These results show that the spin of the involved ions play an essential role in determining the magnetic properties of the ludwigites.

5. Hulsite $Ni_{5.14}Sn_{0.86}(O_2BO_3)_2$

Combining macroscopic and local experimental techniques, the results shown that $Ni_{5.14}Sn_{0.86}(O_2BO_3)_2$ can be separated in two magnetic subsystems. At 180K the first subsystem formed by 2–3 layers, where strong d–d overlap are expected, order magnetically with a ferromagnetic type structure. Mössbauer spectroscopy gives evidence for local disorder caused by the presence of nonmagnetic Sn ion in this layer. Exchange bias effect take place below 180 K, which are probably due to the coupling of the FM 2-3 layer with the AFM ordered Ni spins at sites 5. On the other hand, Mössbauer spectroscopy shown that Ni at 1-4 layer do not feel a measurable transferred magnetic hyperfine interaction, indicating that this layer do not order magnetically down to 3K. The absence of magnetic ordering in this layer could be related with the magnetic frustration originated by the triangular arrangement of the Ni atoms. Just a decreasing of the magnetic fluctuations is observed at low temperatures. Thus, this is a compound with a complex magnetic structure where magnetic ordering coexists with magnetic frustration at low temperatures. Our results suggest also a spin liquid behavior for the subsystem with magnetic frustration.

Table 7-2: Principal magnetic and specific heat parameters values.

	$Co_6B_2O_{10}$	$Co_{4.76}Al_{1.24}B_2O_{10}$	Co_5SnBO_{10}	$Ni_5SnB_2O_{10}$	$Ni_{5.14}Sn_{0.86}B_2O_{10}$
Oxyborate Type	Ludwiguite	Ludwiguite	Ludwiguite	Ludwiguite	Hulsita
T_C	[a] 42 K	57 K	82 K	80 K	180 K
Peak $\chi'(T)$	[a] 42 K	57 K	82 K	80, 76 and 5 K	~164 K
Peak dM/dT	[a] 42 K	57 K	82 K	80, 75 and 40 K	175 K
[1] M_R	[a] ~6.6	0.4	3.0	0.4	0.76
[1] Ms	[a] ~6.6	5.8	3.3	--	--
H_C	[a] 0.7 T	0.8 T	4 T	1.4 T	0.1 T
θ_{cw}	-25 K	-4.8 K	-32.5 K	-82.8 K	-26.8 K
[2] p_{eff}	4.16	5.2	4.91	2.41	2.46
[2] p_S	3.87	3.55	3.87	2.82	2.82
[3] $\gamma(H = 0T)$	1.18	0	0.54	10.3	171
[3] $\gamma(H = 9T)$	--	0	0	0	0
[4] $\alpha(H = 0)$	3.06	2.95	0	2.58	35
[4] $\alpha(H = 9T)$	--	1.94	0	2.88	45
[5] $\beta(H = 0)$	1.02	0	0.650	0	0
[5] $\beta(H = 9T)$	--	0	0.656	0	0
[6] S_M	46.1	46.1	57.6	45.7	--
[6] $S(T_C)$	27.4	13	65.7	66.2	--

[a]Data from reference [7]

[1] $\mu_B/\ f.u.$, [2] $\mu_B/(Co\ or\ Ni)$

[3] $mJ/mol\ K^2$, [4] $mJ/mol\ K^3$, [4] $mJ/mol\ K^4$

[6] $mJ/mol\ K$

Appendix A- AFM Magnons and Phonons in 2D

Considering ($\hbar = 1$) the dispersion relation is given by:

$$\omega_D = v k_D \tag{3}$$

Then, density of states in two dimensions could be written as:

$$\rho(\omega) = \frac{A}{(2\pi)^2} \cdot \frac{2\pi k}{\left|\frac{\partial \omega}{\partial k}\right|}$$

$$= \frac{A}{2\pi} \cdot \frac{\omega / v}{v}$$

$$\rho(\omega) = \frac{A}{2\pi} \cdot \frac{\omega}{v^2} \tag{4}$$

On the other hand, the number o magnetic ions can be find as:

$$N = \frac{A}{(2\pi)^2} \int_0^{k_D} 2\pi k \, d(k)$$

$$\frac{N}{A} = \frac{{k_D}^2}{4\pi} \tag{5}$$

And the energy as:

$$E = \int \frac{\omega \rho(\omega)}{e^{\beta\omega} - 1} d\omega \tag{6}$$

With $\beta = 1/k_B T$, where k_B is the Boltzmann constant.

Replacing (4) in (6)

$$E = \frac{A}{2\pi v^2} \int_0^{\omega_D} \frac{\omega^2}{e^{\beta\omega} - 1} d\omega \tag{7}$$

Changing the variable of integration by $x = \beta\omega$ in (7), one may write

$$E = \frac{A}{2\pi v^2} \cdot \frac{1}{\beta^3} \int_0^{\omega_D / k_B T} \frac{x^2}{e^x - 1} dx$$

For low temperatures $T \ll T^*$,

where

$$T^* = \omega_D / k_B \tag{8}$$

and

$$E = \frac{A}{2\pi v^2} \cdot (k_B T)^3 \int_0^\infty \frac{x^2}{e^x - 1} dx$$

With the numerical value of the integral

$$\xi = \int_0^\infty \frac{x^2}{e^x - 1} dx = 2.40$$

One has

$$E = \frac{A}{2\pi v^2} \cdot (k_B T)^3 \cdot \xi$$

The energy per magnetic ion is given by

$$E' = E/N = \frac{(k_B T)^3}{2\pi v^2 (N/A)} \cdot \xi \tag{9}$$

by substituting eq. (5) in (9), one has

$$E' = \frac{2(k_B T)^3}{v^2 {k_D}^2} \cdot \xi \tag{10}$$

by using eq. (3) and (8), the equation (10) can be rewritten as

$$E' = \frac{2{k_B}^3 T^3}{{k_B}^2 T^{*2}} \cdot \xi$$

Then, the specific heat is given by

$$C = \frac{\partial E'}{\partial T} = \frac{6{k_B}^3 T^2}{{k_B}^2 T^{*2}} \cdot \xi = 6 \cdot \xi \cdot k_B (\frac{T}{T^*})^2$$

Finally one finds that for one mole

$$C = 6 \cdot Na \cdot \xi \cdot k_B (T/T^*)^2$$

$$C = 14.4\, R (T/T^*)^2$$

Appendix B – Geometrical Frustration

Geometric frustration in a magnetic system is related to antiferromagnetic interactions that cannot be simultaneously satisfied, resulting in a large degeneracy of ground states [68]. For example, on a triangular lattice with Ising antiferromagnetic spin interactions, three neighboring spins cannot be all antiparallel and instead of the two ground states (up and down) in a square lattice, there are six ground states, see Figure 0-1.

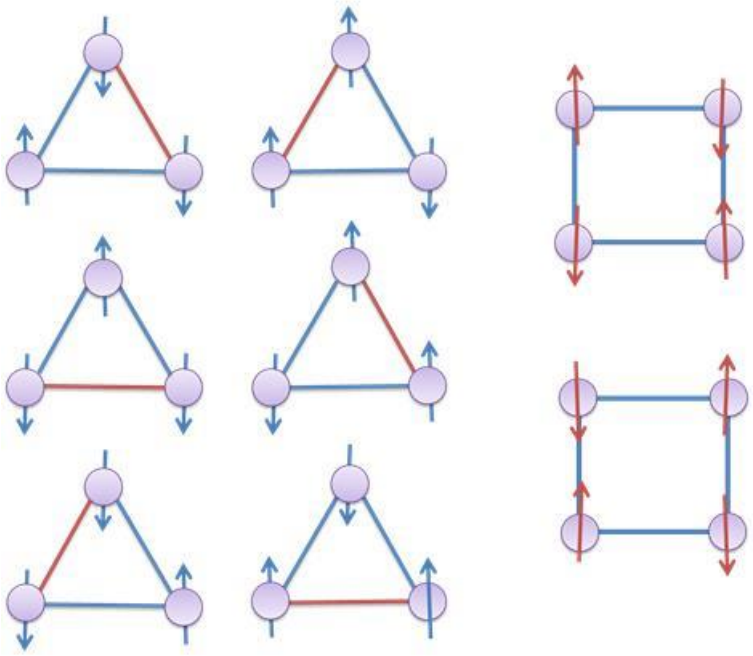

Figure 0-1: Schematic representation of spin arrangement. Left: The six ground states of three antiferromagnetic Ising spins in a triangular coordination. Right: the two ground states of four antiferromagnetic Ising spins in a square coordination.

"*For a Heisenberg model, an idea of the size of degeneracy can be given by a simple counting (Maxwellian counting) argument: The number of degrees of freedom in the ground state, is estimated to be* $D - K$, *where D is the total number of degrees of freedom of the spins and K the number of constrains that must be satisfied to put the system into a ground state*" [69]. Then to have a larger number of degrees of freedom it is necessary to reduce the number of constrains. Lattices that are made up of vertex sharing do that. In a triangular lattice each site belongs to six triangles, but in a two-dimensional Kagome lattice each site belongs to only two triangles, then the Kagome lattice is more frustrated. In a three dimensional lattice, vertex sharing clusters reduce

the number of constrains. Then, it is not surprising that in three dimensions, pyrochlore is the most frustrated lattice, see Figure 0-2.

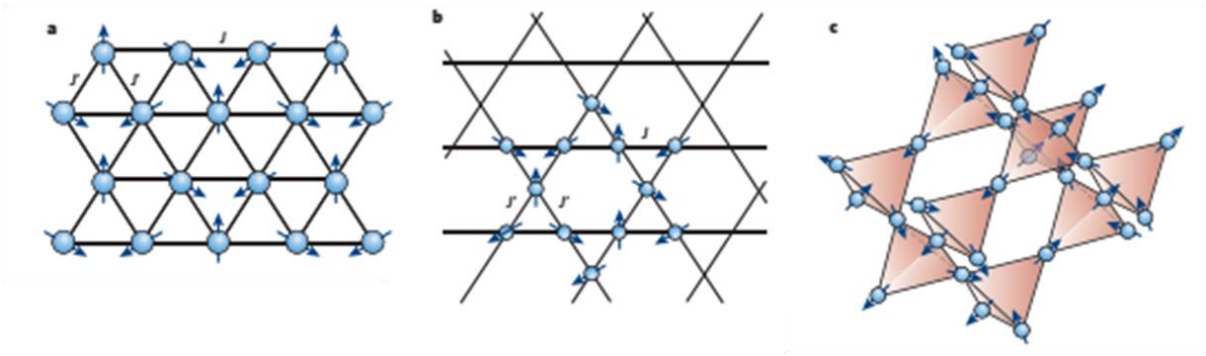

Figure 0-2: Geometrical frustrated lattices. In two dimensions: a) triangular lattice and b) Kagomékagomé lattice. In three dimensions: c) pyroclore lattice. Ref. [68].

Chapter 8. Bibliography

[1] Koichi Momma and Fujio Izumi. *VESTA3* for three-dimensional visualization of crystal, volumetric and morphology data. *Journal of Applied Crystallography*, 44(6):1272–1276, Dec 2011.

[2] DC Freitas, CPC Medrano, DR Sanchez, M Nuñez Regueiro, JA Rodrguez-Velamazán, and MA Continentino. Magnetism and charge order in the ladder compound $Co_3O_2BO_3$. *Physical Review B*, 94(17):174409, 2016.

[3] C. P. C. Medrano, D. C. Freitas, E. C. Passamani, C. B. Pinheiro, E. Baggio-Saitovitch, M. A. Continentino, and D. R. Sanchez. Field-induced metamagnetic transitions and two-dimensional excitations in ludwigite $Co_{4.76}Al_{1.24}(O_2BO_3)_2$. *Physical Review B*, 95(21):214419, 2017.

[4] Mt Mir, RB Guimarães, JC Fernandes, MA Continentino, AC Doriguetto, YP Mascarenhas, J Ellena, EE Castellano, RS Freitas, and L Ghivelder. Structural transition and pair formation in $Fe_3O_2BO_3$. *Physical review letters*, 87(14):147201, 2001.

[5] Pierre Bordet and Emmanuelle Suard. Magnetic structure and charge ordering in Fe_3BO_5: A single-crystal x-ray and neutron powder diffraction study. *Physical Review B*, 79(14):144408, 2009.

[6] J Bartolome, A Arauzo, NV Kazak, NB Ivanova, SG Ovchinnikov, Yu V Knyazev, and IS Lyubutin. Uniaxial magnetic anisotropy in $Co_{2.25}Fe_{0.75}O_2BO_3$ compared to $Co_3O_2BO_3$ and Fe_3O_2BO ludwigites. *Physical Review B*, 83(14):144426, 2011.

[7] DC Freitas, MA Continentino, RB Guimaraes, JC Fernandes, Javier Ellena, and L Ghivelder. Structure and magnetism of homometallic ludwigites: $Co_3O_2BO_3$ versus $Fe_3O_2BO_3$. *Physical Review B*, 77(18):184422, 2008.

[8] RB Guimaraes, M Mir, JC Fernandes, MA Continentino, HA Borges, G Cernicchiaro, MB Fontes, DRS Candela, and E Baggio-Saitovitch. Cation-mediated interaction and weak ferromagnetism in $Fe_3O_2BO_3$. *Physical Review B*, 60(9):6617, 1999.

[9] NB Ivanova, NV Kazak, Yu V Knyazev, DA Velikanov, LN Bezmaternykh, SG Ovchinnikov, AD Vasiliev, MS Platunov, J Bartolomé, and GS Patrin. Crystal structure and magnetic anisotropy of ludwigite $Co_2FeO_2BO_3$. *Journal of Experimental and Theoretical Physics*, 113(6):1015–1024, 2011.

[10] DC Freitas, MA Continentino, RB Guimaraes, JC Fernandes, EP Oliveira, RE Santelli, Javier Ellena, GG Eslava, and L Ghivelder. Partial magnetic ordering and crystal structure of the ludwigites $Co_2FeO_2BO_3$ and $Ni_2FeO_2BO_3$. *Physical Review B*, 79(13):134437, 2009.

[11] NV Kazak, NB Ivanova, OA Bayukov, SG Ovchinnikov, AD Vasiliev, VV Rudenko, J Bartolome, A Arauzo, and Yu V Knyazev. The superexchange interactions in mixed Co–Fe ludwigite. *Journal of Magnetism and Magnetic Materials*, 323(5):521–527, 2011.

[12] PM Raccah and JB Goodenough. First-order localized-electron collective-electron transition in $LaCoO_3$. *Physical Review*, 155(3):932, 1967.

[13] MA Senars-Rodrguez and JB Goodenough. $LaCoO_3$ revisited. *Journal of Solid State Chemistry*, 116(2):224–231, 1995.

[14] MA Korotin, S Yu Ezhov, IV Solovyev, VI Anisimov, DI Khomskii, and GA Sawatzky. Intermediate-spin state and properties of $LaCoO_3$. *Physical Review B*, 54(8):5309, 1996.

[15] Paolo G Radaelli and S-W Cheong. Structural phenomena associated with the spin-state transition in $LaCoO_3$. *Physical Review B*, 66(9):094408, 2002.

[16] Robert A Bari and J Sivardiere. Low-spin-high-spin transitions in transition-metal-ion compounds. *Physical Review B*, 5(11):4466, 1972.

[17] M. A. Continentino, J. C. Fernandes, R. B. Guimarães, B. Boechat, and Saguia A. *Magnetism in highly anisotropic borates: experiment and theory*. Frontiers in Magnetic Materials, 2005. pp.385-410.

[18] Jung-Fu Lin, Alexander G Gavriliuk, Viktor V Struzhkin, Steven D Jacobsen, Wolfgang Sturhahn, Michael Y Hu, Paul Chow, and Choong-Shik Yoo. Pressure-induced electronic spin transition of iron in magnesiowustite-(Mg, Fe) o. *Physical Review B*, 73(11):113107, 2006.

[19] Jin-Ming Chen, Yi-Ying Chin, Martin Valldor, Zhiwei Hu, Jenn-Min Lee, Shu-Chih Haw, Nozomu Hiraoka, Hirofumi Ishii, Chih-Wen Pao, Ku-Ding Tsuei, et al. A complete high-to-low spin state transition of trivalent cobalt ion in octahedral symmetry in $SrCo_{0.5}Ru_{0.5}O_{3-\delta}$. *Journal of the American Chemical Society*, 136(4):1514–1519, 2014.

[20] Cynthia P Contreras Medrano, DC Freitas, DR Sanchez, CB Pinheiro, GG Eslava, L Ghivelder, and MA Continentino. Nonmagnetic ions enhance magnetic order in the ludwigite $Co_5Sn(O_2BO_3)_2$. *Physical Review B*, 91(5):054402, 2015.

[21] DC Freitas, RB Guimaraes, DR Sanchez, JC Fernandes, MA Continentino, Javier Ellena, A Kitada, H Kageyama, A Matsuo, K Kindo, et al. Structural and magnetic properties of the oxyborate $Co_5Ti(O_2BO_3)_2$. *Physical Review B*, 81(2):024432, 2010.

[22] NB Ivanova, MS Platunov, Yu V Knyazev, NV Kazak, LN Bezmaternykh, EV Eremin, and AD Vasiliev. Spin-glass magnetic ordering in $CoMgGaO_2BO_3$ ludwigite. *Low Temperature Physics*, 38(2):172–174, 2012.

[23] NB Ivanova, MS Platunov, Yu V Knyazev, NV Kazak, LN Bezmaternykh, AD Vasiliev, SG Ovchinnikov, and VI Nizhankovskii. Effect of the diamagnetic dilution on the magnetic ordering and electrical conductivity in the $Co_3O_2BO_3$: Ga ludwigite. *Physics of the Solid State*, 54(11):2212–2221, 2012.

[24] Richard M Wood and Gus J Palenik. Bond valence sums in coordination chemistry. a simple method for calculating the oxidation state of cobalt in complexes containing only Co- O bonds. *Inorganic chemistry*, 37(16):4149–4151, 1998.

[25] Peter Paufler. International tables for crystallography. vol. a. 5th edition. Edited by Th. Hahn. pp. xx + 911. Dordrecht: Kluwer Academic Publishers, 2002. ISBN 0-7923-6590-9. *Acta Crystallographica Section A*, 60(6):641–642, Nov 2004.

[26] J.M.D. Coey. *Magnetism and Magnetic Materials*. Magnetism and Magnetic Materials. Cambridge University Press, 2010.

[27] K.H. Fischer and J.A. Hertz. *Spin Glasses*. Cambridge Studies in Magnetism. Cambridge University Press, 1993.

[28] JC Fernandes, RB Guimarães, MA Continentino, L Ghivelder, and RS Freitas. Specific heat of $Fe_3O_2BO_3$: Evidence for a wigner glass phase. *Physical Review B*, 61(2):R850, 2000.

[29] C. Kittel. *Introduction to Solid State Physics*. Wiley, 2004.

[30] N.N. Greenwood and T.C. Gibb. *Mössbauer spectroscopy*. Chapman and Hall, 1971.

[31] Yu V Knyazev, NB Ivanova, NV Kazak, MS Platunov, LN Bezmaternykh, DĐ Velikanov, ĐD Vasiliev, SG Ovchinnikov, and G Yu Yurkin. Crystal structure and magnetic properties of mn substituted ludwigite $Co_3O_2BO_3$. *Journal of Magnetism and Magnetic Materials*, 324(6):923–927, 2012.

[32] NB Ivanova, NV Kazak, Yu V Knyazev, DA Velikanov, AD Vasiliev, LN Bezmaternykh, and MS Platunov. Structure and magnetism of copper-substituted cobalt ludwigite $Co_3O_2BO_3$. *Low Temperature Physics*, 39(8):709–713, 2013.

[33] Tapas Samanta, I Das, and S Banerjee. Giant magnetocaloric effect in antiferromagnetic ErRu2Si_2 compound. *Applied Physics Letters*, 91(15):152506, 2007.

[34] RD Dos Reis, LM Da Silva, AO Dos Santos, AMN Medina, LP Cardoso, and FCG Gandra. Anisotropic magnetocaloric effect in $ErGa_2$ and $HoGa_2$ single-crystals. *Journal of Alloys and Compounds*, 582:461–465, 2014.

[35] DC Freitas, RB Guimarães, JC Fernandes, MA Continentino, CB Pinheiro, JALC Resende, GG Eslava, and L Ghivelder. Planar magnetic interactions in the hulsite-type oxyborate $Co_{5.52}Sb_{0.48}(O_2BO_3)_2$. *Physical Review B*, 81(17):174403, 2010.

[36] N Tristan, V Zestrea, G Behr, R Klingeler, B Büchner, HA Krug von Nidda, A Loidl, and V Tsurkan. Spin frustration and magnetic exchange in cobalt aluminum oxide spinels. *Physical Review B*, 77(9):094412, 2008.

[37] LN Bezmaternykh, EM Kolesnikova, EV Eremin, SN Sofronova, NV Volkov, and MS Molokeev. Magnetization pole reversal of ferrimagnetic ludwigites $Mn_{3-x}Ni_xBO_5$. *Journal of Magnetism and Magnetic Materials*, 364:55–59, 2014.

[38] Evgeniya Moshkina, Svetlana Sofronova, Alexey Veligzhanin, Maxim Molokeev, Ilya Nazarenko, Evgeniy Eremin, and Leonard Bezmaternykh. Magnetism and structure of Ni_2MnBO5 ludwigite. *Journal of Magnetism and Magnetic Materials*, 402:69–75, 2016.

[39] R Norrestam, M Kritikos, K Nielsen, I Søtofte, and N Thorup. Structural characterizations of two synthetic ni-ludwigites, and some semiempirical EHTB calculations on the ludwigite structure type. *Journal of Solid State Chemistry*, 111(2):217–223, 1994.

[40] JA Hriljac, RD Brown, AK Cheetham, and LC Satek. The synthesis and crystal structures of the related series of aluminoborates: $Co_{2.1}Al_{0.9}BO_5$, ni2albo5, and Cu_2AlBO_5. *Journal of Solid State Chemistry*, 84(2):289–298, 1990.

[41] Karsten Bluhm and Hanskarl Müller-Buschbaum. Eine neue verbindung vom $M_5TiB_2O_{10}$-typ mit geordneter metallverteilung: $Ni_5SnB_2O_{10}$. *Monatshefte für Chemie/Chemical Monthly*, 120(2):85–89, 1989.

[42] S.N. Sofronova, L.N. Bezmaternykh, E.V. Eremin, I.I. Nazarenko, N.V. Volkov, A.V. Kartashev, and E.M. Moshkina. The superexchange interactions and magnetic ordering in low-dimentional ludwigite $Ni_5GeB_2O_{10}$. *Journal of Magnetism and Magnetic Materials*, 401:217 – 222, 2016.

[43] K Bluhm and Hk Müller-Buschbaum. Ein beitrag über oxometallate mit trigonal planaren bo3-polyedern Ni_2MBO_5 (M= Ga, Fe, Al, Cr). *Zeitschrift für anorganische und allgemeine Chemie*, 582(1):15–20, 1990.

[44] CGF Stenger, GC Verschoor, and DJW Ijdo. The crystal structure of $Ni{=}TiB_2O_{10}$. *Materials Research Bulletin*, 8(11):1285–1292, 1973.

[45] Bruker. Apex3. Bruker AXS Inc., Madison, Wisconsin, USA, 2012.

[46] Bruker. Saint. Bruker AXS Inc., Madison, Wisconsin, USA, 1999.

[47] G. M. Sheldrick. Sadabs. Program for Empirical Absorption Correction of Area Detector Data, University of Göttingen, Germany, 1996.

[48] George M. Sheldrick. Crystal structure refinement with *SHELXL*. *Acta Crystallographica Section C*, 71(1):3–8, Jan 2015.

[49] Louis J. Farrugia. *WinGX* and *ORTEP for Windows*: an update. *Journal of Applied Crystallography*, 45(4):849–854, Aug 2012.

[50] Christian B. Hübschle, George M. Sheldrick, and Birger Dittrich. *ShelXle*: a Qt graphical user interface for *SHELXL*. *Journal of Applied Crystallography*, 44(6):1281–1284, Dec 2011.

[51] R. A. Brand. Normos mössbauer fitting program. Univ. Dortmund, 2002.

[52] K Bluhm, Hk Müller-Buschbaum, and L Walz. Eine synthetische variante des hulsit-typs: Ni5, 33sb0, 67b2o10. *Journal of the Less Common Metals*, 158(2):339–345, 1990.

[53] G. M. Sheldrick. CELLNOW. University of Göttingen, Germany, 2008.

[54] J NoguÃ©s and Ivan K Schuller. Exchange bias. *Journal of Magnetism and Magnetic Materials*, 192(2):203 – 232, 1999.

[55] Bibhuti B. Dash and S. Ravi. Magnetization reversal and tunable exchange bias in $GdCr_{1-x}Mn_xO_3$ (x=0-0.50). *Journal of Magnetism and Magnetic Materials*, 429:281 – 286, 2017.

[56] L.T. Coutrim, E.M. Bittar, E. Baggio-Saitovitch, and L. BufaiÃ§al. Spin glass-like properties and exchange bias in $La_{1.5}Sr_{0.5}CoIrO_6$. *Journal of Magnetism and Magnetic Materials*, 441:243 – 247, 2017.

[57] L.T. Coutrim, E.M. Bittar, E. Baggio-Saitovitch, and L. BufaiÃ§al. The influence of temperature and applied magnetic field on the exchange bias effect of $La_{1.5}Sr_{0.5}CoIrO_6$. *Journal of Magnetism and Magnetic Materials*, 428:70 – 72, 2017.

[58] Satoru Nakatsuji, Yusuke Nambu, Hiroshi Tonomura, Osamu Sakai, Seth Jonas, Collin Broholm, Hirokazu Tsunetsugu, Yiming Qiu, and Yoshiteru Maeno. Spin disorder on a triangular lattice. *Science*, 309(5741):1697–1700, 2005.

[59] A Yaouanc, P Dalmas de Réotier, Y Chapuis, C Marin, G Lapertot, A Cervellino, and A Amato. Short-range magnetic ordering process for the triangular-lattice compound $NiGa_2S_4$: A positive muon spin rotation and relaxation study. *Physical Review B*, 77(9):092403, 2008.

[60] Yusuke Nambu, Jason S. Gardner, Douglas E. MacLaughlin, Chris Stock, Hitoshi Endo, Seth Jonas, Taku J. Sato, Satoru Nakatsuji, and Collin Broholm. Spin fluctuations from hertz to terahertz on a triangular lattice. *Phys. Rev. Lett.*, 115:127202, Sep 2015.

[61] D. E. MacLaughlin, Y. Nambu, S. Nakatsuji, R. H. Heffner, Lei Shu, O. O. Bernal, and K. Ishida. Unconventional spin freezing and fluctuations in the frustrated antiferromagnet $NiGa_2S_4$. *Phys. Rev. B*, 78:220403, Dec 2008.

[62] AP Ramirez, B Hessen, and M Winklemann. Entropy balance and evidence for local spin singlets in a kagome-like magnet. *Physical review letters*, 84(13):2957, 2000.

[63] YJ Uemura, A Keren, K Kojima, LP Le, GM Luke, WD Wu, Y Ajiro, T Asano, Y Kuriyama, M Mekata, et al. Spin fluctuations in frustrated kagomé lattice system $SrCr_8Ga_4O_{19}$ studied by muon spin relaxation. *Physical review letters*, 73(24):3306, 1994.

[64] Satoshi Yamashita, Yasuhiro Nakazawa, Masaharu Oguni, Yugo Oshima, Hiroyuki Nojiri, Yasuhiro Shimizu, Kazuya Miyagawa, and Kazushi Kanoda. Thermodynamic properties of a spin-1/2 spin-liquid state in a κ-type organic salt. *Nature Physics*, 4(6):459–462, 2008.

[65] Satoshi Yamashita, Takashi Yamamoto, Yasuhiro Nakazawa, Masafumi Tamura, and Reizo Kato. Gapless spin liquid of an organic triangular compound evidenced by thermodynamic measurements. *Nature communications*, 2:275, 2011.

[66] JG Cheng, G Li, L Balicas, JS Zhou, JB Goodenough, Cenke Xu, and HD Zhou. High-pressure sequence of $Ba_3NiSb_2O_9$ structural phases: New S= 1 quantum spin liquids based on Ni_{2+}. *Physical review letters*, 107(19):197204, 2011.

[67] HD Zhou, ES Choi, G Li, L Balicas, CR Wiebe, Yiming Qiu, JRD Copley, and Jason S Gardner. Spin liquid state in the s= 1/2 triangular lattice $Ba_3CuSb_2O_9$. *Physical review letters*, 106(14):147204, 2011.

[68] Leon Balents. Spin liquids in frustrated magnets. *Nature*, 464(7286):199–208, 2010.

[69] Roderich Moessner and Arthur P Ramirez. Geometrical frustration. *Phys. Today*, 59(2):24, 2006.